Benefits to Processor Load for Quadrature Baseband versus Radio Frequency Demodulation Algorithms

LUSUNGU NDOVI

Thesis presented in partial fulfilment of the requirements for the degree of Master of Science in Electronic Engineering

At Stellenbosch University

SUPERVISOR: Prof. J.G. LOURENS
Co-SUPERVISOR: Dr. R. WOLHUTER

December 2008

Declaration

By submitting this thesis electronically, I declare that the entirety of the work contained therein is my own, original work, that I am the owner of the copyright thereof (unless to the extent explicitly otherwise stated) and that I have not previously in its entirety or in part submitted it for obtaining any qualification.

Date: December 2008

Abstract

Keywords: Quadrature baseband, QBB, Radio frequency, RF, Beamforming, Multipath compensation, Doppler shift compensation, Software-defined radio, SDR, Matched filter detection.

The continued advancement and improvement of software-defined radio technology has been a key factor in furthering research into the implementation of most signal processing algorithms at baseband. Traditionally, these algorithms have been carried out at RF, but with the coming of SDR, there has been a need to shift the processing down to baseband frequencies which are more compatible with the fast developing software radio technology.

The study looks at selected demodulation algorithms and investigates the possibility and benefits of carrying them out at QBB. The study ventures into the area of beamforming, multipath compensation, Doppler shift compensation and matched filter detection. The analysis is carried out using Matlab simulations at RF and QBB. The results obtained are compared, not only to evaluate the possibility but also the benefits in terms of the processing load. The results of the study showed that indeed, carrying out the selected demodulation algorithms at QBB was not only possible, but also resulted in an improvement in the processing speed brought about by the reduction in the processing load.

Opsomming

Kernwoorde: Kwadratuur basisband, QBB, Radiofrekwensie, RF, Bundelvorming Multi-pad kompensasie, Dopplerskuif kompensasie, Sagteware gedefineerde radio, SDR, aangepaste filter deteksie.

Die aangaande vooruitgang en verbetering in sagteware gedefineerde radio tegnologie was ‘n groot faktor om die implementasie van meeste sein verwerkings algoritmes by basisband verder na te vors. Tradisioneel, was hierdie algoritmes by RF gedoen, maar met die ontwikkeling van SDR was daar 'n behoefte om die verwerking by basisband te doen wat meer versoenbaar is met vinnige groeiende sagteware radio tegnologie

Die studie kyk na geselekteerde demodulasie algoritmes en ondersoek die moontlikheid en voordele daarvan om dit by QBB uit te voer. Die studie kyk verder na bundelvorming, multi-pad kompensasie, Doppler skuif en aangepaste filters deteksie. Die analise word uitgevoer deur van Matlab implementasies gebruik te maak by RF en QBB. Die resultate word vergelyk om nie net die moontlikheid nie, maar ook die voordele in terme van verwerkingslas te ordersoek. Die resultate van die studie het gewys dat die demodulasie algoritmes by QBB nie net moontlik is nie, maar ook’ n die verbetering in prossesserings-spoed veroorsaak het, deur die verwerkingslas te verminder.

Acknowledgements

I would like to thank the following:

- My supervisor, Prof Johan Lourens for his support, supervision and guidance during the whole course of my studies.
- My co-supervisor Dr Riaan Wolhuter for his support, supervision and guidance in finalising my studies.
- Dr G-J van Rooyen for his support.
- My friends and colleagues in the DSP lab.
- The Copperbelt University (CBU) in Zambia for their financial support.
- My mom and sisters Suzyo and Lushomo for their encouragement.
- Above all GOD the creator.

Contents

List of Figures

List of Tables

Nomenclature

Acronyms

AM	Amplitude Modulation
LSB	Lower Sideband
LO	Local Oscillator
RF	Radio Frequency
QBB	Quadrature Baseband
SDR	Software Defined Radio
AM DSB-SC	Amplitude Modulated Double Side Band-Suppressed Carrier
AM DSB-LC	Amplitude Modulated Double Side Band-Large Carrier
FM	Frequency Modulation
QAM	Quadrature Amplitude Modulation
LPF	Low Pass Filter
MIMO	Multiple Input Multiple Output
FFT	Fast Fourier Transform
DFT	Discrete Fourier Transform
IFFT	Inverse Fourier Transform
SDMA	Space Division Multiple Access
MAX	Maximum
DSP	Digital Signal Processor
I/Q	In-phase and Quadrature Components
MF	Matched Filter

Variables

Symbol	Description
f(t)	Modulating input for AM
m(t)	Modulated signal input for AM
f_c	Carrier frequency
f_m	Modulating signal frequency
ω	Instantaneous frequency
ω_c	Carrier angular frequency
ω_m	Modulating signal angular frequency
θ	Phase angle
Φ	Phase angle delay
$F(\omega)$	General frequency domain signal
λ	Wave length
c	Speed of light
dt	Time delay
t	Continuous time
T	Discrete time period
AF	Antenna array factor
$f(\psi)$	Normalized array factor
P_e	Probability of error

Chapter 1

Introduction

1.1 Motivation

Modulation shifts a signal up to much higher frequencies than its original span. This often results in doubling of the bandwidth. However, baseband frequencies are much lower than radio frequencies and therefore, signal processing at baseband presents this key advantage of working at much *lower frequencies* [2]. Processing at the lower QBB enables more sub-sampling to take place than at RF and this in turn results in a reduction in the number of samples being processed entailing a reduction in the processor load and subsequently an improvement in processing speed. However, one cannot substantiate the advantages of working at QBB without firstly carrying out the study and then producing results that will justify the purpose of the research.

1.2 Objectives

The primary objective of the study was to investigate the possibility and benefits in terms of processor load of carrying out beamforming, multipath compensation, Doppler shift compensation, multiple compensation for multipath and Doppler shift, and matched filter detection at quadrature baseband for selected modulation schemes. The study showed the expected benefits of carrying out these techniques at quadrature baseband and the advantages of QBB over RF were seen by comparing and discussing the results from the RF and QBB simulations. Noiseless transmissions and narrowband signals were assumed.

1.3 Thesis overview

The structure of the thesis is as follows:

Chapter 2: Background theory and literature review

This chapter outlines software defined radio and its development in relation to the advancement of baseband processing. Quadrature baseband is explained and its

role in the advancement of software radio technologies is also discussed. A general general for the beamforming, multipath, Doppler shift, multiple compensation and matched filter detection is given. The QBB demodulation of the modulation schemes that were used in the simulations are summarised and the reciprocity that exists between a channel and compensator is discussed. The mode of accessing the benefits in terms of processor load and speed of QBB over RF implementation of the techniques and demodulation algorithms under discussion is also given.

Chapter 3: Beamforming

This chapter investigates beamforming for AM DSB-SC, AM DSB-LC and FM modulation schemes and simulation results obtained from the RF and QBB beamforming are given and discussed. Firstly, the possibility of beamforming at QBB is proved as well as the benefits and outcome of beamforming at QBB. The benefits of working at QBB in terms of processor load will be seen in terms of simulation runtime and number of calculations done for the simulations at RF and QBB. It should be noted that the analogue and digital ways of generating QBB will be both considered in the comparison process. It is shown from the results obtained that the processing load does increase when beamforming at QBB as compared to RF for the simulation case in which the QBB signals are generated digitally. However, when considering the real life case in which the QBB signals are generated using analogue method, QBB emerged more superior to RF in terms of processing load which in turn resulted in a reduction in the processing time required.

Chapter 4: Multipath compensation

This part of the study investigated multipath compensation at RF and QBB for QAM and FM modulation schemes. Similarly, the simulation results from the multipath compensation analysis for the two modulation schemes are discussed and the benefits of compensating at QBB compared to their RF counterparts. It is shown that the compensation process is possible at QBB coupled with the expected benefits that come along with doing so in terms of the processing time and load.

Chapter 5: Doppler shift compensation

This chapter investigates Doppler shift compensation at RF and QBB for QAM and FM modulation schemes. The simulation results from the Doppler shift compensation analysis for the two modulation schemes are given and discussed. The possibility of compensating for Doppler shift at QBB is shown and the benefits of working at QBB in comparison to RF will be evaluated. Similarly, the simulation runtime and sample processing results show why QBB is more advantageous than RF implementation of the compensation process.

Chapter 6: Multiple signal compensation

The study in this chapter considers a special case where we have multiple inputs but with a signal output. This part of the study investigates the possibility and benefits of compensating for multipath and Doppler shift compensation at QBB as compared to RF in the case of multiple signal reception. The simulation results are given, analysed and discussed. The analysis considers QAM modulated signals. The chapter shows the possibility of multiple compensation RF and QBB and if not, the reasons for the simulation outcome are outlined and discussed. For the possible compensation scenario, the benefits in terms of processing load and time of QBB against RF are shown and reasons why it is more advantageous to work at QBB.

Chapter 7: Matched filter detection

The study moves to the digital processing arena by investigating matched filter detection of a chirp signal at RF and QBB. It considers cases of the direct path, multipath, Doppler shift and multiple signal input situation. The simulation results are given and discussed as done for the previous chapters. The chapter firstly considers noiseless transmissions and then considers two cases of noisy channel transmissions with the matched filter detection taking place at RF and QBB. The processing load and simulation run times are analysed for the noiseless and noisy transmission cases and the results show that it is more advantageous in terms of processing load to carry out the

matched filter detection process at QBB as compared to doing so at RF.

Chapter 8: Conclusion, M-Files

The study is concluded in this chapter and a summary of the findings from the study is given and discussed. It will be interesting to see the variations in results obtained from the various simulations carried out. The M-Files which were created are also given.

The study results show that carrying out the selected demodulation algorithms at quadrature baseband is not only possible but does also result in an improvement in processing speed caused by the reduction in processing load when sub-sampling is carried out. Interesting results are seen for the beamforming case where the processor load is more at QBB than at RF for the simulated QBB but when the real life analogue down-mixed QBB case is considered, there is a much bigger reduction in the amount of computation required at QBB.

Chapter 2

Background theory: Quadrature baseband, beamforming, compensation and demodulation algorithms

The chapter gives a background of the main components of the study. The concept of quadrature baseband is explained in detail giving an insight into the reasons for carrying out the study. The selected demodulation algorithms that were analysed in the study are outlined and the general simulation flow structures are given so as to have a preview of the actual simulation analysis to be carried out in later chapters. The mode of measuring the simulation runtime and amount of computation so as to see the benefits of working at quadrature baseband is explained.

2.1 Software defined radio and baseband processing

Software radio technology advancement has been a factor in promoting research into baseband signal processing. Baseband signal processing technology is experiencing a period of radical change [16, 17]. This has prompted the need to investigate more about baseband processing in order to implement most functions that were traditionally implemented at RF so as to utilise the benefits that come with working at baseband.

2.2 Quadrature baseband

Quadrature baseband is a term that refers to the generation of in-phase and quadrature components of a signal at baseband. **Baseband** is an adjective that describes signals and systems whose range of frequencies is measured from 0 to a maximum bandwidth or highest signal frequency [15]. Usually, it is considered as a synonym to lowpass and an antonym to passband. The simplest definition is that a signal's baseband bandwidth is its bandwidth before modulation and multiplexing, or after demultiplexing and demodulation. The figure on the next page illustrates the comparison between radio frequency and baseband.

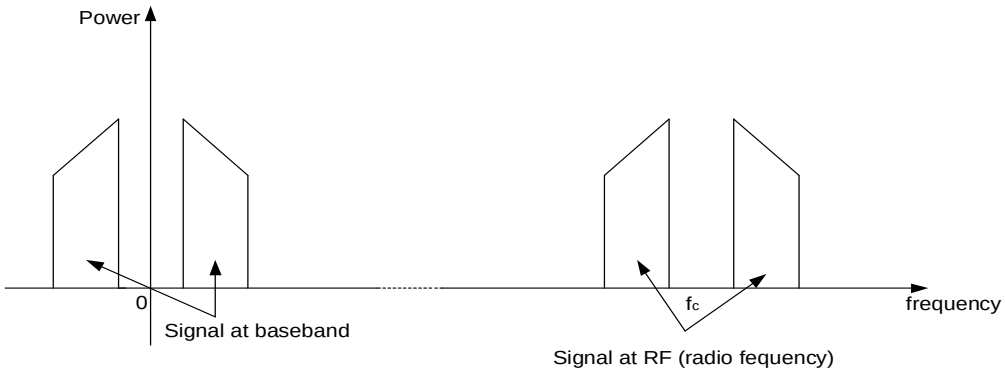

Figure 2.1: *Comparison of the baseband version and RF version of an AM modulated signal. The RF signal sits at the carrier frequency f_c.*

Quadrature baseband modulation/demodulation basically processes baseband signals which is basically a signal having in-phase and quadrature phase components [1, 15]. Before undertaking the study in depth, it is necessary to define and distinguish clearly the various components of software defined radio. These are defined below [6]:

- *Baseband modulation*:- refers to the generation of I and Q signals containing modulated information (digital).
- *Quadrature upmixing*:- refers to the multiplication of the I(t) and Q(t) signals with quadrature shifted carriers which are subtracted from each other to produce the RF signal (analogue).
- *Quadrature modulation*:- refers to the combination of the baseband modulation and quadrature upmixing and in its entirety represents the conversion from the modulating to modulated signal.
- *Baseband demodulation*:- refers to the DSP method of recovering a modulated signal from I and Q signals (digital).
- *Quadrature downmixing*:- refers to the multiplication of the received RF signal (analogue) with quadrature shifted carriers resulting in two baseband signals I(t) and Q(t).
- *Quadrature demodulation*:- refers to the combination of the baseband demodulation and quadrature downmixing and in its entirety represents the conversion from the modulated to the demodulated signal [6].

- *Sampling*:- refers to the conversion of analog signals into discrete impulses or samples so as to be easily processed using digital technology.

The conversion of an RF signal to quadrature baseband is carried out by the following steps:

- The RF signal is multiplied with a complex carrier in what is referred to as down-mixing.
- The complex down-mixed signal is then lowpass filtered resulting in the quadrature baseband version of the RF signal. The expressions given below illustrate these steps.

Let ω_c be the carrier frequency of the modulated RF signal, it follows that the complex carrier used in the down-mixing process is a complex exponential with the same carrier frequency ω_c.

$$f(t)_{downmixed} = f(t) \bullet e^{-j\omega_c t} \tag{2.1}$$

The low pass filter then eliminates the high frequency component of the spectrum resulting in the complex baseband signal.

$$f(t)_{qbb} = [\, f(t)_{downmixed} \,]_{LPF} \tag{2.2}$$

The real part of the lowpass filtered signal corresponds to the inphase quadrature component of the baseband signal [1]. The figure below illustrates the process outlined above. The spectral changes resulting from the conversion from RF to baseband are also shown in Figure 2.3 on the next page.

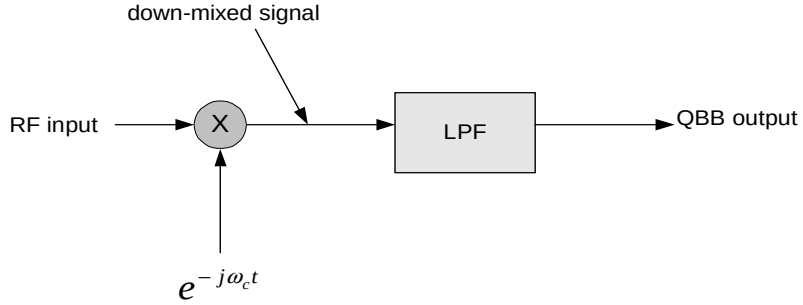

Figure 2.2: *Conversion of an RF carrier to quadrature baseband.*

The spectral changes resulting from the conversion to QBB are shown and discussed below.

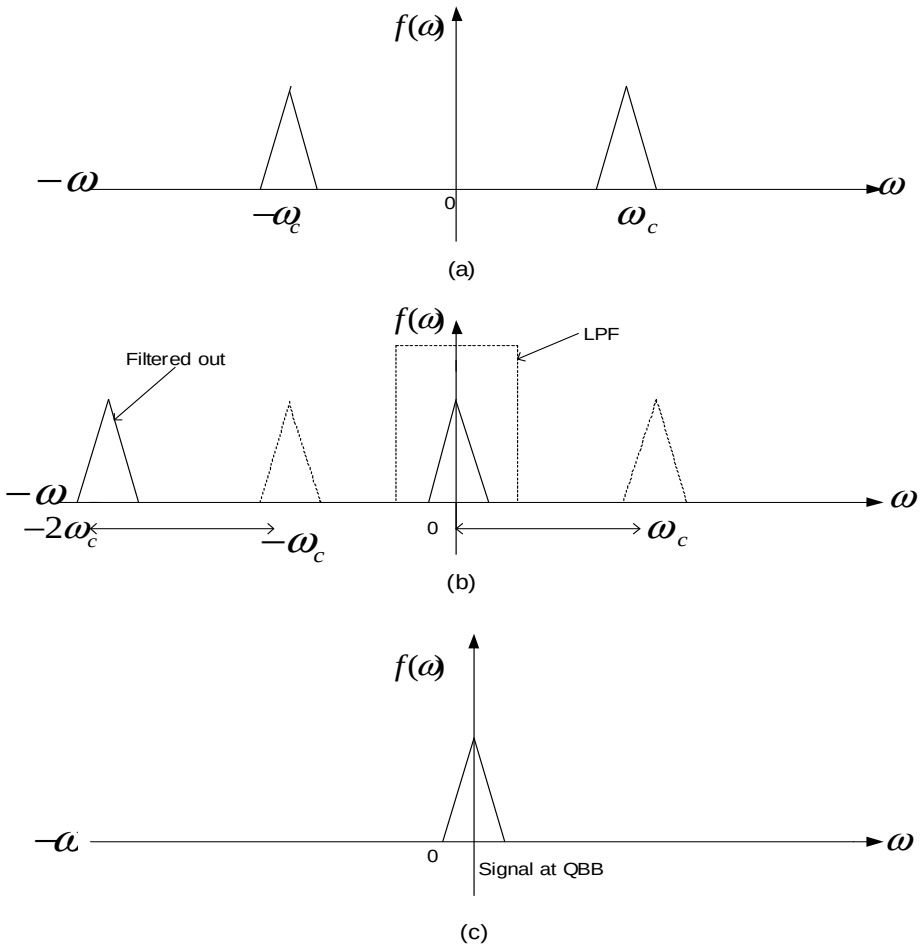

Figure 2.3: *Spectral changes* **(a)** *RF signal spectrum* **(b)** *Spectrum of down-mixed signal:-the spectrum shifts down by* ω_c **(c)** *Spectrum of QBB signal.*

Figure 2.3(a) shows the RF carrier spectrum before down mixing. The down-mixing process shifts down the spectral components by ω_c as shown in Figure 2.3(b). The down-mixed signal is then lowpass filtered and this eliminates the higher frequency component of the spectrum. This resulting spectrum shows the low frequency carrier component which now sits at zero IF or baseband [1, 6, 15]. For our simulations, the QBB signal generation was done in the digital domain as will be shown in Chapter 3. The alternative real life situation involves generating the QBB signal in the analogue domain by carrying out analogue down-mixing and lowpass filtering. In this case, the analysis assumes that the received signals are already at QBB and hence the comparisons in terms of the amount of computation in the simulations will overlook the

down-mixing and lowpass filtering stage. Chapter 3 will gives more details about this process.

2.3 Beamforming

Beamforming is a signal processing technique that is widely used to enhance signal strength. It enables the reuse of the same carrier frequency by signals from other directions. It also enhances antenna sensitivity so as to improve the signal to noise ratio especially in the event of receiving weak signals [9]. Through beamforming, smart antennas offer low co-channel interference and large antenna gain to the desired signals which leads to more improved performance than conventional antenna systems. Implementing beamforming in DSP enables arrays to benefit from a single steerable antenna with a narrow gain pattern. SDR enables the beamforming to be performed using software and hence formation of several beams is possible by simply reusing the array output. This entails the possible usage of these software techniques in MIMO systems. Smart antennas have brought about significant benefits to latest wireless technologies [16]. The coming of software defined radio is a key advancement in enabling smart antenna base stations to be realized by utilizing *baseband beamforming* [16]. The study carries out beamforming at RF and QBB and compares the results. Sections 2.3.1 and 2.3.2 outline beamforming at RF and QBB respectively.

The study will be carried out using MatLab analysis and then, comparisons will be made between the beam patterns produced by the two beamforming methods. It involves carrying out beamforming upon the reception of 4 input signals for each of the modulation methods under investigation. The 4 input signals for both the RF and QBB case are aligned at an angle theta `θ' to the antenna array. The weighting coefficient of the antennas was assumed to be unity for simplicity sake. The first signal has no input delay whilst the other three signals have a delay `Δt' determined by 'θ' and other parameters. The analysis is to be done by varying 'θ' from 0 to 2π. Therefore, the results of our analysis in MatLab will justify the possibility of carrying out beamforming at quadrature baseband.

2.3.1 Beamforming at RF

Simple beamforming at RF involves summing up the 4 input signals at RF before demodulating the summed-up signal. The beam pattern is produced from the output signal by plotting the amplitude of the output signal against theta. The antenna weighting coefficients are assumed to be equal to 1 for simplicity.

2.3.2 Beamforming at QBB

The procedure under QBB involves mixing down the incoming signals to quadrature baseband. The beamforming process now takes place at QBB. The processing in an SDR (real life case) assumes the processing of the signals already at QBB. Therefore, comparisons will be made between the simulated QBB beamforming and the simulated RF beamforming. The real life analogue down-mixed QBB scenario was considered for merely showing the benefits of QBB over RF in terms of processing load and was thus not simulated. In the chapters that follow, it will be interesting to see why working at QBB is more beneficial in terms of the simulation runtime and the amount of numerical processing as compared to RF. The main reason that will be seen that makes working at QBB superior to RF in terms of processor load reduction is the fact that working at QBB facilitates for further downsampling [32] to take place which inturn reduces the number of samples being processed. Does this entail a definite reduction in the simulation runtime too? The simulation results given in the next chapters will answer this question since comparisons between the runtimes and number of calculations in the simulation code at RF and QBB will be compared. Working at RF does have a limitation in the downsampling process with aliasing more likely to occur resulting in signal distortion. The analogue down-mixing process is illustrated in the Figure 2.4 on the next page. In our simulations, the processing time was measured using inbuilt MatLab commands and the amount of processing was depicted by the number of numerical calculations taking place in the codes that executed the processes being analyzed. It should be emphasised that the simulation runtime and numerical processing measurements that were carried out in the study were carried out using *relative methods.*

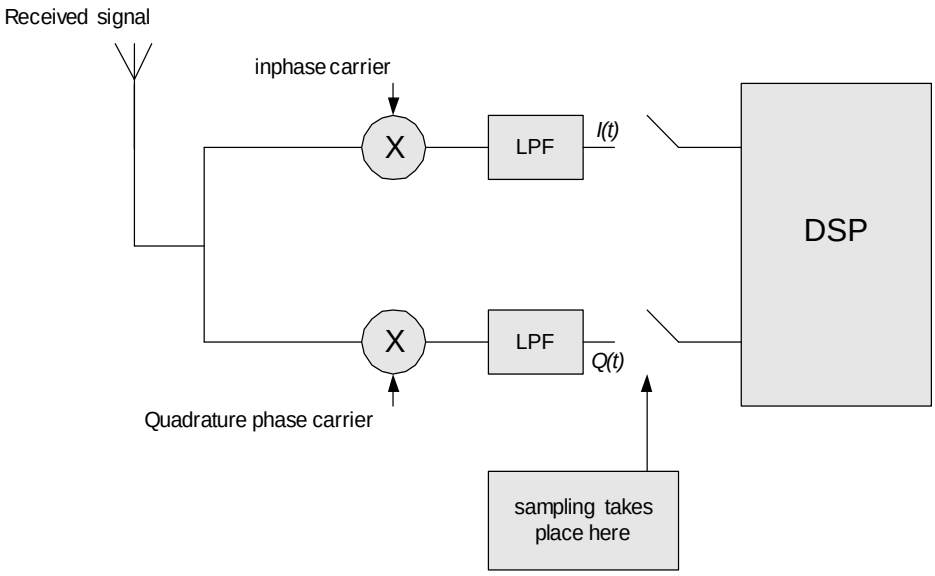

Figure 2.4: *Analogue down-mixing and QBB signal generation. In the DSP block, further processing can take place which represents the real life scenario.*

The figure above shows that the received signal is multiplied with an inphase and quadrature phase carriers after which low pass filtering is done resulting in the quadrature phase components. The resulting signal can then be converted to digital form and further processing can be done [6]. Therefore, the real life scenario assumes the reception of the signals baseband in readiness for further processing by a DSP. For the analysis, we have to simulate the baseband signals before the processing can commence. Thus the real life case would be void of this step. It will now be relied upon the simulation results to verify the possibility and benefits of beamforming at quadrature baseband. This will be done for AM DSB-SC, AM DSB-LC and FM and the results will be observed and discussed.

2.4 Multipath

Multipath is a form of *interference* and therefore it is undesired in radio propagation. Some of the effects of multipath distortion include data corruption, increased signal amplitude (constructive interference), reduced signal amplitude (destructive interference), unwanted frequency response, co-symbol interference, etc [21]. In order to mitigate the effects of multipath, a signal processing technique called '*multipath compensation*' is used. This implies that a receiver should be equipped with a compensator that will eliminate the multipath effects and allow for the processing of the desired direct-path signal only.

Multipath propagation plays a vital role in determining the nature of communication channels. This implies determination of the impulse, or frequency response of radio channels [20]. However, this study does not consider other channel factors in detail but focuses on the compensation aspect of multipath. We will also ignore angular spread and constriction effects since the main purpose of the study is to investigate the possibility and benefits of compensating for multipath at QBB. It should also be noted that we are using narrow band signals and noiseless channels are assumed. It is required by this study to find out the possibility of compensating at baseband frequencies as compared to the traditional RF methods and analyzing the benefits of compensating at QBB.

2.4.1 Spectral changes due to time-shift in a signal

Time delay in a signal causes a linear phase shift in its spectrum. It does not change the amplitude spectrum [3]. Suppose $f(t)$ is being synthesized by its fourier components, which are sinusoids of certain amplitudes and phases. It is seen that the delayed signal $f(t-t_o)$ can be synthesized by the same sinusoidal components, each delayed by t_o seconds [27]. The amplitudes of the components remain unchanged. Therefore, the amplitude spectrum of $f(t-t_o)$ is identical to that of $f(t)$. The time delay t_o in each sinusoid does however change the phase of each component. It is therefore, seen that a time delay t_o in a sinusoid frequency ω manifests as a phase delay of ωt_o. This is a linear function of ω, which entails that higher-frequency components must undergo proportionately higher phase shifts to achieve the same time delay. Let us now consider

the unit impulse response for the multipath channel. The response is expected to have the direct path and delayed echo components. The mathematical expressions and graphical plot for a delayed unit impulse are shown below.

$$
\begin{aligned}
& f(t-\tau) \leftrightarrow F(\omega)e^{-j\omega\tau} \\
& H = (1+ke^{-j\omega\tau}) \\
& \therefore f(t)*H = f(t)*(\delta(t)+k\delta(t-\tau)) = f(t)+kf(t-\tau)
\end{aligned}
\tag{2.1}
$$

The plot below illustrates the results above expressions.

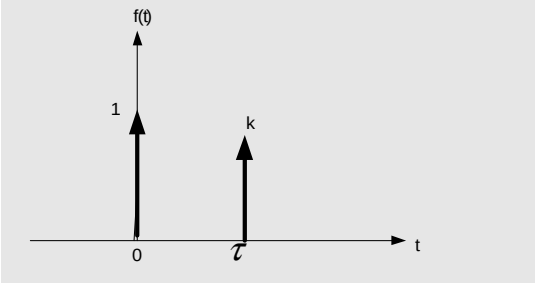

Figure 2.5: *Channel impulse response.*

From the expressions above and assuming that the unit impulse is transmitted through a multipath channel, it is seen that the convolution [27] between the unit impulse and the channel *H* results in the direct path signal and an echo which is a delayed and scaled down version of the direct path signal. In this case, the delayed signal is scaled down by a factor ` k'.

2.4.2 RF and QBB Multipath compensation

In this part of the study as was explained for the beamforming case, the compensation process is done at RF and then shifts to quadrature baseband in view of compensating for multipath at QBB and utilising the benefits that come along with it. For the multipath analysis, noiseless transmissions and narrow band signals were assumed.

2.5 Doppler shift

Doppler shift is another form of interference encountered in wireless communications. Its effects are immense and the final result is that the received signal is distorted and hence the need to compensate for the Doppler shift arising from motion between the transmitting and receiving ends [25]. Doppler shift compensation restores the frequency spectrum of the received signal by undoing the effects caused by the Doppler shift. The simulations for this case will similarly be run at RF and QBB.

Frequency shifting

The frequency shift property of the Fourier transform forms the basis for our modeling of a Doppler signal and its spectrum in MatLab. The duality between the time and frequency domains does enable the frequency translation of a time domain signal by a given value by multiplying the time domain signal with an exponent whose frequency is equal to the required frequency shift [3]. The above statement is illustrated below:

$$f(t) \Leftrightarrow F(\omega) \tag{2.2}$$

Multiplying a time function with the $e^{jw_d t}$ yields the required frequency shift 'ω_d'.

$$\begin{aligned} & f(t)e^{j\omega_d t} \Leftrightarrow F(\omega - \omega_d) \\ & or \\ & f(t)e^{-j\omega_d t} \Leftrightarrow F(\omega + \omega_d) \end{aligned} \tag{2.3}$$

The expressions above thus entail the possibility of simulating the Doppler shift signal by use of the frequency shifting property.

2.6 Multiple compensation

The study also looks at a scenario where multiple signals are received and summed up together. The signals comprise the direct path signal, multipath signal, Doppler shift signal and a signal that has been subjected to both multipath and Doppler shift effects. It is required to compensate for the multipath and Doppler shift effects simultaneously.

This need not be confused with a MIMO system which has multiple inputs and multiple outputs [36]. For the beamforming case, the presence of multiple antennas at the transmitting and receiving ends creates a MIMO channel which offers significant diversity [34]. The simulation results in Chapter 6 will show whether it is possible to carry out multiple compensation.

2.7 Matched filtering :- Chirp signal

The study also carries out matched filter detection at RF and investigates the possibility of doing so at QBB. A chirp signal will be used in the simulations. A chirp is a signal whose frequency either increases or decreases with time [30]. A linear chirp is one whose frequency varies linearly with time as shown in the expression on the next page.

$$f(t) = f_0 + kt \tag{2.4}$$

where f_0 represents the starting frequency (at time t=0), and k represents the rate of frequency increase. k is thus a frequency interval over a period of time. The frequency interval is referred to as the 'deviation frequency' and is shown in the equation below.

$$f(t) = f_0 + f_d \frac{t}{T} \tag{2.5}$$

Now it is well known that the phase is the integral of the instantaneous frequency *f(t)*.

Therefore, integrating the above equation gives us:

$$phase(\varphi) = 2\pi(f_0 t + f_d \frac{t^2}{2T}) \tag{2.6}$$

The sinusoidal chirp signal is thus given as

$$x(t) = \sin 2\pi t(f_0 + f_d \frac{t}{2T}) \tag{2.7}$$

Matched filter detection of a chirp signal

A matched filter keeps a copy of the time reversed version of the expected signal. Intuition behind matched filtering is that by convolving the matched filter impulse

response with the received signal (chirp), you are basically sliding across your time reversed h(t) across your received signal doing a point wise multiplication and then integrating over the area of that product [31]. Thus, the peak in the real part of the output is only going to occur when the chirp in h(t) is exactly lined up with a chirp in the received signal. In other words, the spike output corresponds to the point where the greatest area underneath the curve is produced from the point-wise multiplication. The location of the spike itself corresponds to the location of where the right most edge of a chirp is located in the received signal [10]. The block diagram below summarizes the RF matched filter detection processes. Its QBB counterpart is also below.

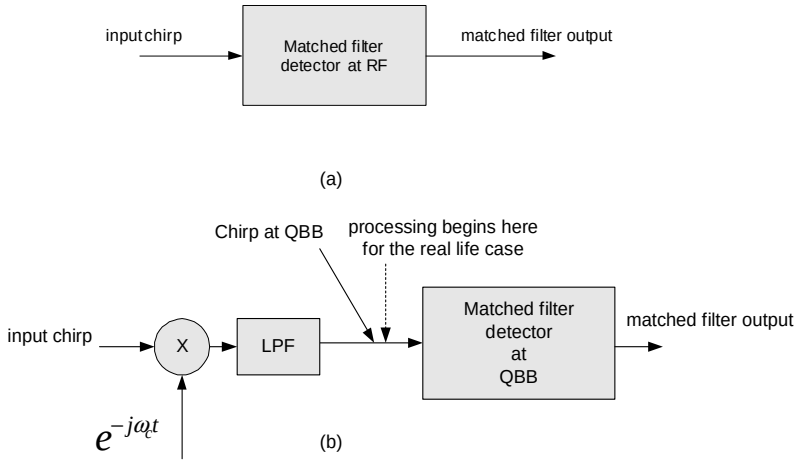

Figure 2.6: *Matched filter detection flow structure* **(a)** *Matched detection of a chirp signal at RF* **(b)** *Matched filter detection of a chirp signal at QBB.*

From the Figure 2.6(b), it is seen that the chirp is mixed-down and lowpass filtered to quadrature baseband before being fed into the matched filter which has a time-reversed copy of the QBB input chirp. The output does have its peak at t=T as in the previous RF analysis. The simulation results in Chapter 7 will give a more detailed comparison of the graphical results obtained from the RF and QBB simulations. The simulations/analysis will also consider the case of a noisy transmission channel.

2.8 AM DSB-SC, AM DSB-LC, FM and QAM

A brief summary of the 4 modulation schemes used in the simulations is given in the following sub-sections. The focus is on carrying out the processing at QBB and hence the demodulation at QBB for the selected modulation schemes is outlined.

2.8.1 AM DSB-SC

An Amplitude Modulated Double Sideband signal with Suppressed Carrier can be represented by the equation shown below.

$$m(t) = f(t)\cos\omega_c t \tag{2.8}$$

where $f(t)$ is the message signal [3,4,12]. The modulated signal is then transmitted and at the receiving end, the signal has to be demodulated.

QBB demodulation:- DSB-SC

Consider the figure shown below:

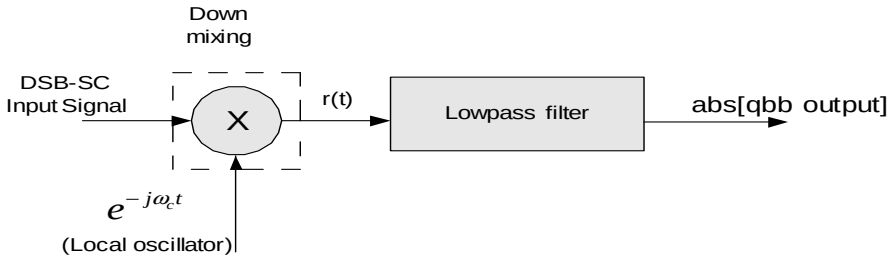

Figure 2.7: *QBB demodulation block diagram.*

The figure above shows that the demodulation of a DSB-SC quadrature baseband signal is done by simply taking real part of the QBB signal and this gives the demodulated signal. The QBB signal output is complex with the imaginary part being neglected and hence taking the real part of this complex signal does give us the demodulated signal.

2.8.2 AM DSB-LC

The second modulation method that will be used in the simulations is AM DSB-LC. The demodulation of a DSB-LC signal is done either coherently or non-coherently. The non-coherent method being used here is envelope detection. A DSB-LC modulated signal is given by the following expression [3, 12]:

$$m(t)=(A_c + mf(t))cos(\omega_c t) \tag{2.9}$$

where m= modulation index,

A_c= carrier amplitude,

Normalizing the carrier amplitude results in the following expression:

$$m(t)=(1 + mf(t))cos(\omega_c t) \tag{2.10}$$

AM DSB-LC QBB demodulation

For the QBB demodulation, the coherent and non coherent methods are used with the coherent QBB demodulation method being similar to the DSB-SC method. For the analysis, only the coherent QBB method was simulated.

2.8.3 FM

Unlike AM, FM is a non-linear type of modulation [8]. In our analysis, we will look at a single-tone modulated FM signal. Assuming the modulating signal is a unit amplitude sinusoid of the form $m(t)=cos(\omega_m t)$, the FM modulated signal can be expressed as

$$y(t) = A\cos(\omega_c t + m.\sin(\omega_m t)) \tag{2.11}$$

where m represents the modulation index and is the ratio of the maximum frequency deviation to the particular modulating frequency, f_c is the carrier frequency (Hz), and Φ_c is the initial phase (rads). $\theta(t)$ is the modulation phase, which changes with the amplitude of the input $m(t)$. The expression for $\theta(t)$ is given as

$$\theta(t) = K_o \int_0^t m(t)dt \tag{2.12}$$

where K_o is the sensitivity factor, which represents the gain of the integrator output [8].

FM demodulation at QBB

On the other hand, FM QBB demodulation is done by unwrapping of the phase angle using a MatLab command 'unwrap' followed by differentiating so as to give the demodulated signal. The equation below illustrates this.

$$theta = unwrap(atan2(imag[s_4], Real[s_4])) \tag{2.13}$$

where s_4 is the QBB FM signal. The unwrapped angle is the differentiated as shown in the equation on the next page.

$$s_5 = diff(theta) \tag{2.14}$$

2.8.4 QAM (analogue)

The beamforming analysis modulation schemes that will be used are AM DSB-SC and AM DSB-LC and FM. However, under multipath and Doppler shift we consider QAM and FM. Before getting into the study of multipath compensation for QAM, it is necessary to have a brief background about this modulation method. QAM modulates an in-phase signal $m_I(t)$ and a quadrature signal $m_Q(t)$ using the expression shown below:

$$y(t) = m_I(t).c\cos\omega_c t + m_Q(t)\sin(\omega_c t) \tag{2.15}$$

Alternatively, a QAM signal may also be represented on the next page.

$$y(t) = m(t)\cos(\omega_c t) + \hat{m}(t)\sin(\omega_c t) \tag{2.16}$$

where $m(t)$ represents a message signal and $\hat{m}(t)$ is the Hilbert transform of m(t). It should be noted that the expression above is for single side band QAM [22].

QAM demodulation at QBB

The QBB demodulation process is summarised by the block diagram below.

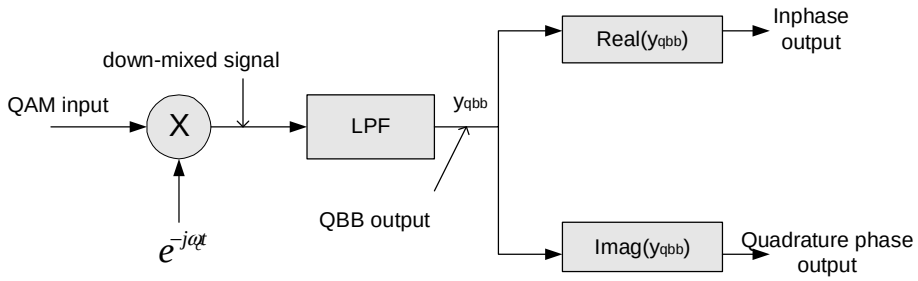

Figure 2.8: *QAM demodulation at QBB. After the mixing down process and lowpass filtering, the real and imaginary parts of the resulting signal are taken resulting in the inphase and quadrature phase outputs corresponding to the original inputs.*

2.9 Channel / Compensator reciprocity

The study will carry out compensation for multipath, Doppler shift and also considers multiple compensation. The aim of compensation is basically to retrieve the original signal from the distorted received signal. A layman would say "the solution to a problem lies in knowing the cause of the effect". An engineer would paraphrase this statement for the compensation case at hand and say "finding the compensator lies in knowing characteristics of the channel". By this is meant that in order to compensate for an effect, the transfer function (channel) that caused the effect must be known. This leads us to the reciprocity relationship between the channel and compensator illustrated in the figure which follows. Thus, the compensator is seen as the inverse of the channel transfer function. The simulations will verify this relationship. Will this relationship hold for the multiple signal input case too? Chapter 6 adequately analyses and answers this question. The block diagram on the next page illustrates this.

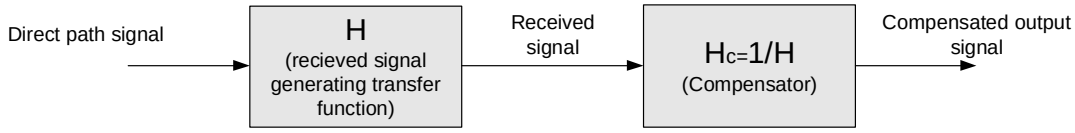

Figure 2.9: *Channel/Compensator reciprocity structure.*

2.10 Benefits of working at Quadrature baseband:- processor load

The focus of the study as mentioned earlier aims to verify possibility and the benefits of working at QBB as compared to working at RF for selected demodulation algorithms and compensation methods. The study will accomplish this by comparing two parameters of the simulations run in MatLab. The main benefit of working at QBB compared to RF is that the operating and sampling frequency is reduced. The other benefit is derived from the sub-sampling carried out for the QBB case and for the simulations, it will be assumed that the sub-sampling factor chosen would cause limitations for the RF brought about by aliasing. Therefore, relative methods were employed in order to quantify the sample processing. Chapter 3 illustrates how this was done in the study. The processing time was also estimated using in-built Matlab commands which measure the elapsed time between relevant parts of the simulation code. This does not represent the true processing time that would take place in a DSP. It is just a relative way of consolidating the processing load results as it expected that a reduction in the processing load should result in a reduction in the processing time.

2.11 Conclusion

The chapter introduced the quadrature baseband theory and gave a brief overview of the algorythms under investigation in this study. The modulation schemes used in the analysis were also outlined. Flow diagrams were given so as to have an overview of the general flow of the analysis that was carried out using MatLab simulations. The procedure for finding out the benefits of working at QBB as compared working at RF were also explained and as mentioned, Chapter 3 will give a more detailed outline of this procedure. With this background theory discussed in this chapter, the analysis and discussion of the simulations results takes place in the chapters that follow.

Chapter 3

Beamforming- simulation results

The MatLab simulation results for beamforming at RF and QBB for the selected modulation schemes are given and discussed in this chapter. The theoretical analysis for each method is given and the RF and QBB results compared, discussed and a summary of the results is given. The study does indeed show the possibility of beamforming at QBB. The chapter concludes by comparing the RF and QBB simulations in terms of simulation runtime and number of processing calculations for the signal samples processed by the simulations. Does QBB come out advantageous in this case? The latter part of the chapter should answer this question.

3.1 RF beamforming

In this analysis, four input signals are summed up together and the summed up signal is demodulated and then a beam pattern is produced. Earlier in Chapter 2, the RF and QBB beamforming processes where outlined.

Theoretical Analysis

A theoretical summary of the RF beamforming process is given below. The reference signal is the non-delayed sinusoidal input s_0. The reference signal in this case is the AMDSB-SC/AMDSB-LC or FM input depending on which modulation scheme is being analyzed. Therefore, taking s_0 as the reference signal, we generate 3 other signals with a fixed delay separation in between each signal.

$$\begin{aligned} s_1 &= s_0(t-\Delta t) \\ s_2 &= s_0(t-2\Delta t) \\ s_3 &= s_0(t-3\Delta t) \end{aligned} \tag{3.1}$$

The 4 signals were summed up to give the signal s_4. This represents a simple beamforming stage of the analysis.

$$s_4 = s_0 + s_1 + s_2 + s_3 \tag{3.2}$$

The beamformed signal is then demodulated using the demodulation method for each modulation scheme as outlined in Chapter 2 resulting in the demodulated signal which is denoted as s_5. The size of the demodulated signal is then determined so as to get the beam pattern. The figure below summarises the theoretical analysis beam forming at RF.

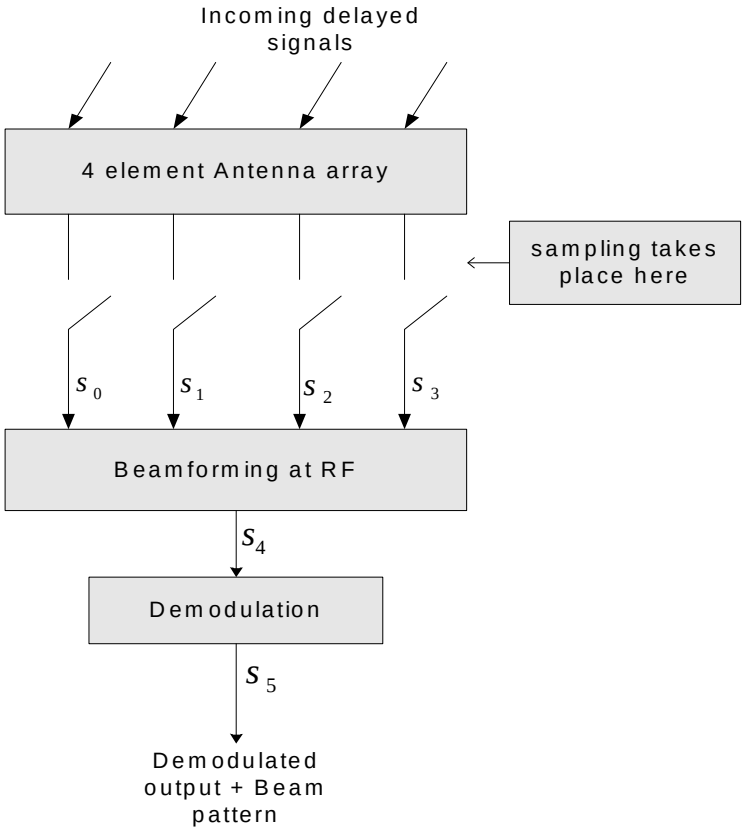

Figure 3.1: *RF Beamforming theoretical analysis block diagram.*

The block diagram above basically illustrates the processing of the signal from the input up to the final stage of forming the beam pattern. The delayed signals are thus arriving at the antenna array from a range of angles and the result of the signal size is stored up to the last value of theta. For the simulations carried out, the incoming signals were sampled before the beamforming stage. The beam pattern is then produced by taking the maximum signal size and making a polar plot against theta.

3.2 Quadrature Baseband (QBB) Beamforming

The idea of quadrature baseband beamforming involves carrying out beamforming at quadrature baseband frequencies. The procedure under QBB involves mixing down the four incoming signals to baseband and then lowpass filtering to get their quadrature baseband equivalents. The beamforming takes place at quadrature baseband after which demodulating the summed signal follows from which the maximum value of the output signal is taken so as to make a polar plot. For the simulations carried out, the four incoming signals are mixed down to baseband using a local oscillator having an exponential complex and then lowpass filtered to convert our down-mixed signals to quadrature baseband signals. Sub-sampling is done followed by QBB demodulation from which the beam pattern was derived.

Theoretical Analysis

A theoretical summary of the QBB beamforming process is given below. The four signals being fed into the antenna array as shown earlier in Figure 3.1 are mixed down by multiplication with a local oscillator LO which is a complex exponential ($e^{-j\omega_c t}$). Each of the 4 signals is down-mixed as shown by the expressions below:

$$\begin{aligned} s_{0dm} &= s_0 \cdot (LO) \\ s_{1dm} &= s_1 \cdot (LO) \\ s_{2dm} &= s_2 \cdot (LO) \\ s_{3dm} &= s_3 \cdot (LO) \end{aligned} \tag{3.3}$$

where the subscript ‘dm’ denotes down-mixed and s_0,s_1,s_2 and s_3 are as defined earlier under the RF process. The next step involves the lowpass filtering of each of the 4 individual signals so as to convert them into QBB signals. These expressions for the 4 QBB signals are given on the next page.

$$s_{0qbb} = [s_{0dm}]_{LPF}, s_{1qbb} = [s_{1dm}]_{LPF}$$
$$s_{2qbb} = [s_{2dm}]_{LPF}, s_{3qbb} = [s_{3dm}]_{LPF} \quad (3.4)$$

At this stage we have four QBB signals and the downsampling process can take place at this stage. This is done by taking every n^{th} sample of the signal where n represents the downsampling factor. The downsampled version of s_{0qbb} is obtained as follows in MatLab:

$$s_{0qbbds} = s_{0qbb}(1:n:end), s_{1qbbds} = s_{1qbb}(1:n:end)$$
$$s_{2qbbds} = s_{2qbb}(1:n:end), s_{3qbbds} = s_{3qbb}(1:n:end) \quad (3.5)$$

Beamforming can now take place at this stage.

$$s_4 = s_{0qbbds} + s_{1qbbds} + s_{2qbbds} + s_{3qbbds} \quad (3.6)$$

To get our demodulated output signal, the absolute value of s_4 is taken and this gives us our quadrature baseband demodulated out put signal.

$$s_5 = abs[s_4] \quad (3.7)$$

The maximum of s_5 is then taken and a polar plot is done to give us the required beam pattern. The block diagram on the next page summarizes the theoretical analysis for beamforming at QBB. As was mentioned earlier in Chapter 2, the QBB signals are generated by the simulation before the beamforming can take place. As explained earlier in Chapter 2, representing the real-life analogue processing is basically the same as that for the simulated representation but with the down-mixing and lowpass filtering stages skipped which precede the sampling process. Figure 3.2 on the next page summarises the QBB beamforming process.

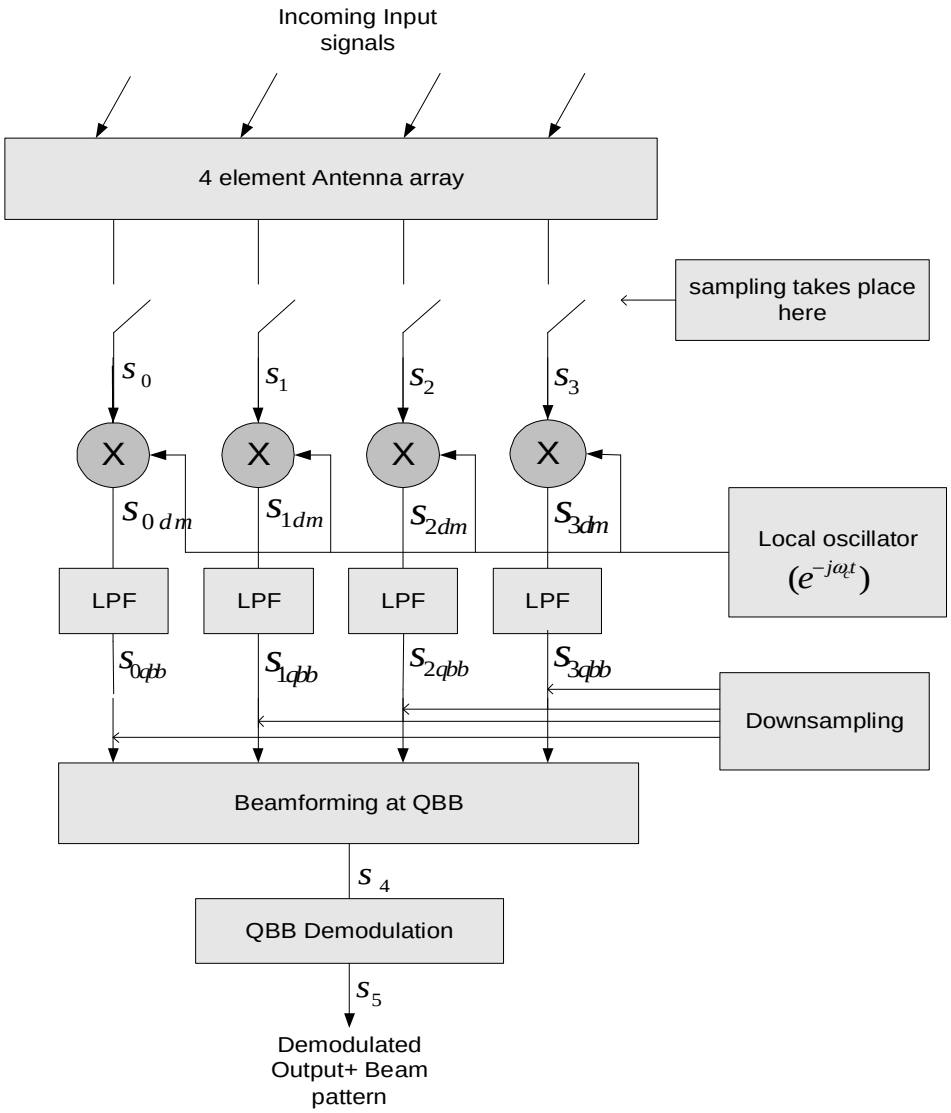

Figure 3.2: *Quadrature baseband beamforming theoretical analysis block diagram. It is seen from the diagram that the signal outputs at each stage have been shown. The figure above represents the beamforming process for the simulated QBB signals. The real life scenario representation would skip the generation stage and proceed with the processing of the analogue down-mixed QBB signals. It will be seen when analysing the benefits in terms of processor load of how the simulated and real life scenario QBB method compare with the simulated RF results.*

3.3 Simulation results – AM DSB-SC

This chapter analyses and discusses the actual simulation results of the MatLab analysis of RF and QBB beamforming. The beam pattern shapes are also controlled by factors like the antenna spacing and array factor [11, 19]. For the analysis, parameters like the antenna weight were normalised for simplicity's sake.

Simulation results: - RF Beamforming

The graphical results below result from RF beamforming simulations.

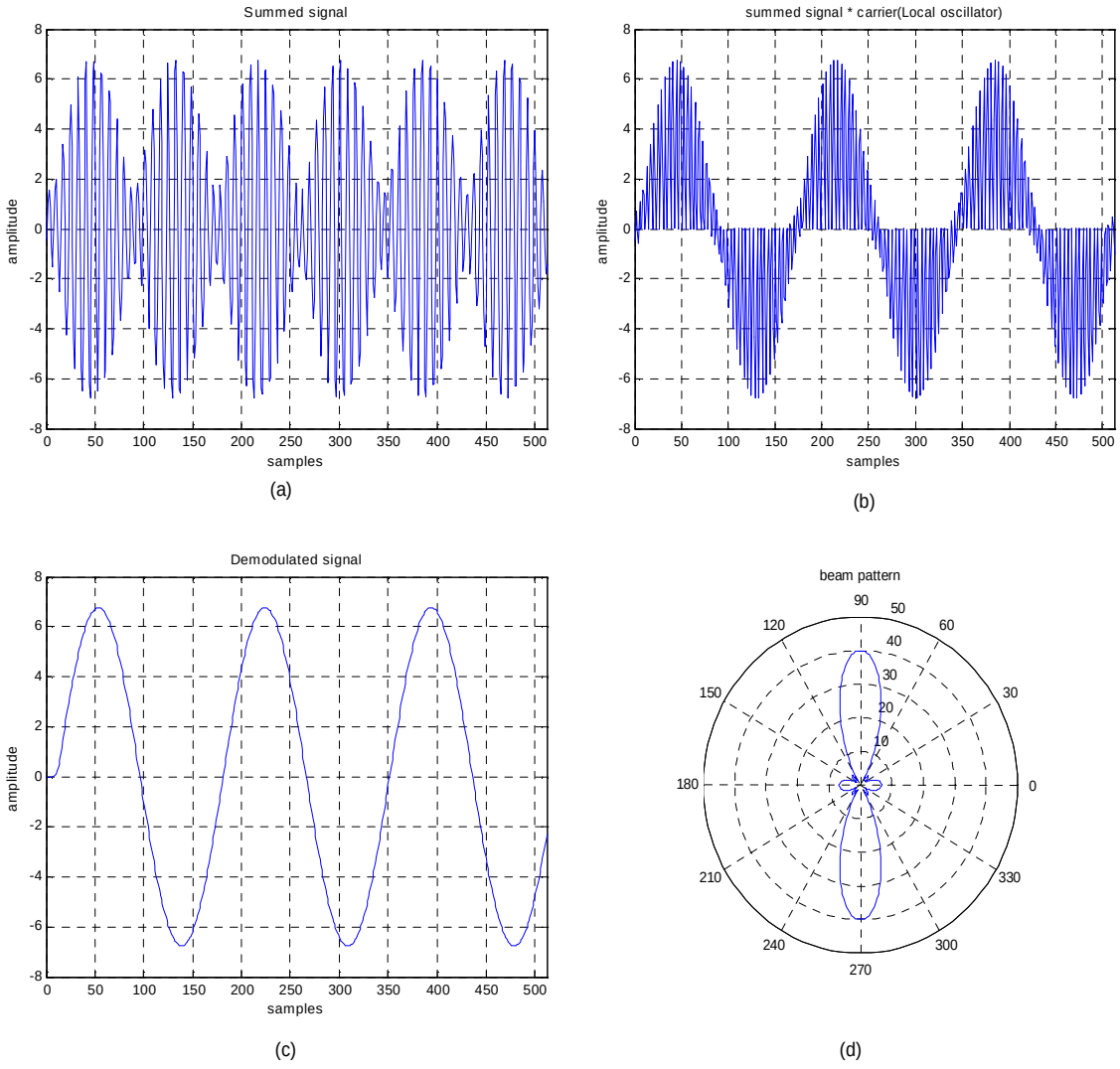

Figure 3.3: *Simulation results.* **(a)** *Summed signal* **(b)** *Summed signal multiplied with carrier* **(c)** *Demodulated output* **(d)** *Beam pattern.*

The simulation results obtained for RF beamforming for the signals being received by the antenna array are now analyzed. In Figure 3.3(a) it seen that there are three cycles for the 512 samples of the summed up signal. The local oscillator translates the frequency of the summed signal to $2f_c$ on the frequency spectrum where f_c represents the carrier frequency. This is done in order to facilitate for the demodulation of the summed signal using the AMDSB-SC demodulation method outlined earlier in Chapter 2. The resulting demodulated output is shown in Figure 3.3(c). Plotting the maximum of the demodulated output against theta yields the beam pattern shown in Figure 3.3(d) and consists of the main beam and side lobes. It is a well known fact that side lobes are undesirable in any beam pattern because they reduce the energy in the main beam. The resulting beam pattern has a maximum value of approximately 40 and has 6 sidelobes. The study is yet to come to its fulfilment because, we now have to carry out beamforming at quadrature baseband and compare the two results.

3.3 Simulation results - QBB Beamforming

The analysis moves down to quadrature baseband where beamforming will now take place. The signals now sit at QBB facilitating for beamforming at QBB. Sub-sampling which takes place before the beamforming and in this particular simulation, the sub-sampling factor was 4. Therefore, as can be seen from the demodulated output, there is a 4-fold reduction in the number of samples down to 128 samples as compared to the initial 512 samples that the input signals had. It is seen that this does not affect the demodulated output as well as the beam the resulting pattern. In actual fact, this presents an advantage of the beamforming at QBB in that the same results as at RF can be produced but with fewer samples. The beamformed signal is then demodulated using QBB demodulation by taking the real part of the QBB signal resulting in the demodulated output shown in Figure 3.4(a) on the next page and the corresponding beam pattern shown in Figure 3.4(b).

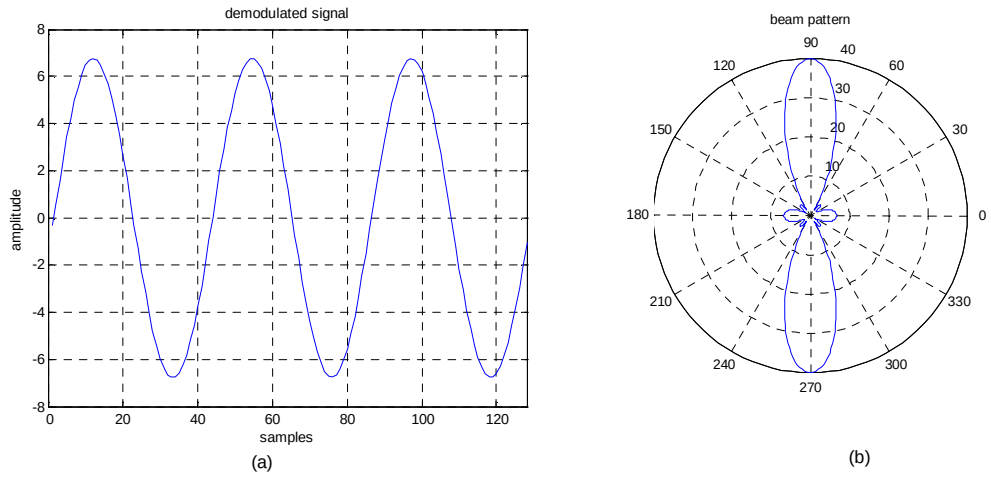

Figure 3.4: *Simulation plots* **(a)** *Demodulated signal* **(b)** *Beam Pattern.*

Are there any changes in the results obtained at QBB as compared to its RF counterpart? The beam pattern produced should answer the question. Compared to the RF demodulated signal output, it is seen that the two signals are the 'same' having the same amplitude and frequency characteristics and therefore, we expect to have similar beam patterns. However, the visual similarity can not be substantiated unless it accompanied by numerical backing. Therefore, the next section will verify the similarity between the RF and QBB beam patterns by plotting the numerical difference between them.

3.4 Beam pattern comparisons

The beam patterns are now shown together in Figure 3.5 on the next page for easy analysis and comparison of the patterns. In order to numerically prove the similarity of the two beam patterns, a MatLab program was created to carry out the numerical comparison. The program incorporates the two beamforming codes (RF and QBB) and then gets the difference between the normalized beam patterns is shown in figure 3.6(b) on the next page.

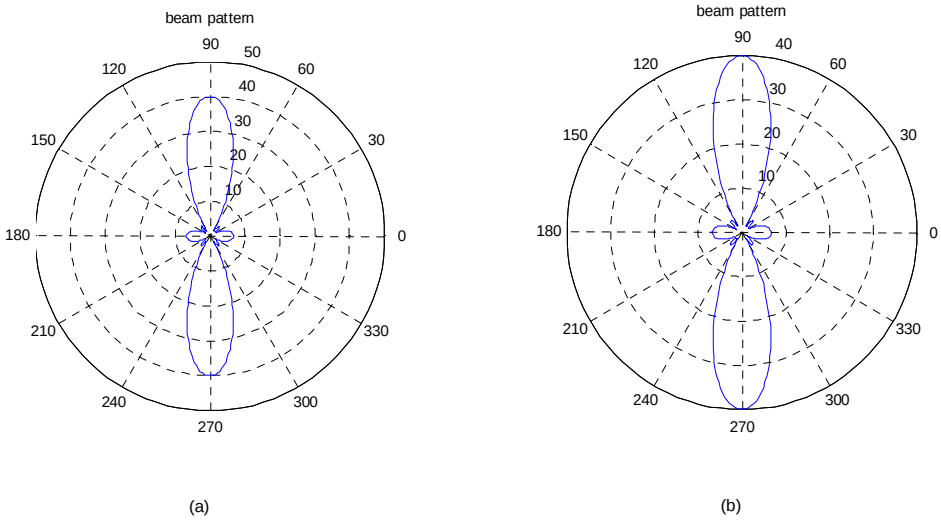

Figure 3.5: *Beam pattern comparisons* **(a)** *RF beam pattern* **(b)** *QBB beam pattern.*

The error/difference plot is given below.

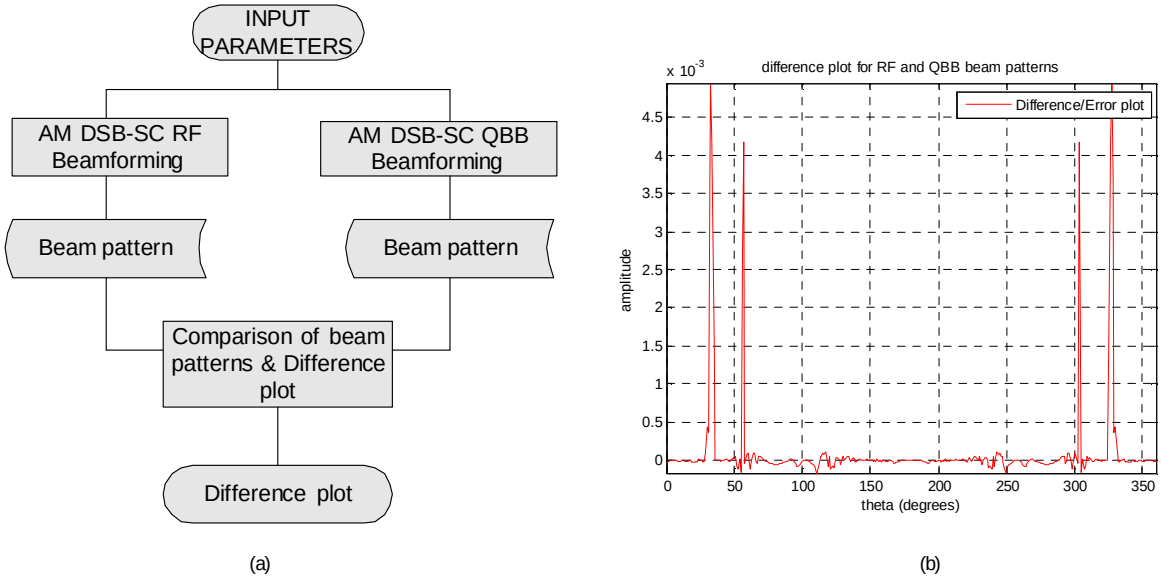

Figure 3.6: (a) *Difference plot flow diagram* **(b)** *Difference plot.*

It is clearly seen that the difference between the two plots is minimal and therefore, it suffices to say that the two beam patterns are similar and that it has been verified that beamforming at QBB gives a similar beam pattern to its RF counterpart. Therefore, suffices to say that beamforming at quadrature baseband is possible and this comes with

its main advantage of working at *lower sampling frequencies* unlike for the high RF frequencies.

3.6 MatLab Analysis Simulation Results: –AM DSB-LC

3.6.1 Beamforming: AM DSB-LC

This part of the study analyses RF beamforming for another AM modulation technique AM DSB-LC. The two methods being considered are the Coherent method and the Envelope detector (non-coherent). The MatLab analysis results are also shown and discussed in this chapter. The modulation method being analyzed is AM DSB-LC. There is a difference in the way an AM DSB-SC and AM DSB-LC signal is represented which is evidenced by the expressions given in Chapter 2. The demodulation of a DSB-LC signal is done either coherently or non-coherently. The non-coherent method being used here is envelope detection.

3.6.2 Coherent and Non-Coherent (Envelope) detection methods

As mentioned already in Chapter 2, two methods will be used to carry out our RF analysis of the beamforming process for the AMDSB-LC signals so as to see any changes that take place in the beam pattern shape when the detection process is done coherently and non-coherently. We have the coherent and the non-coherent method of which the latter is also referred to as the envelope detector. The flow diagram on the next page is a structural summary of the whole RF analysis that was used in the MatLab simulations.

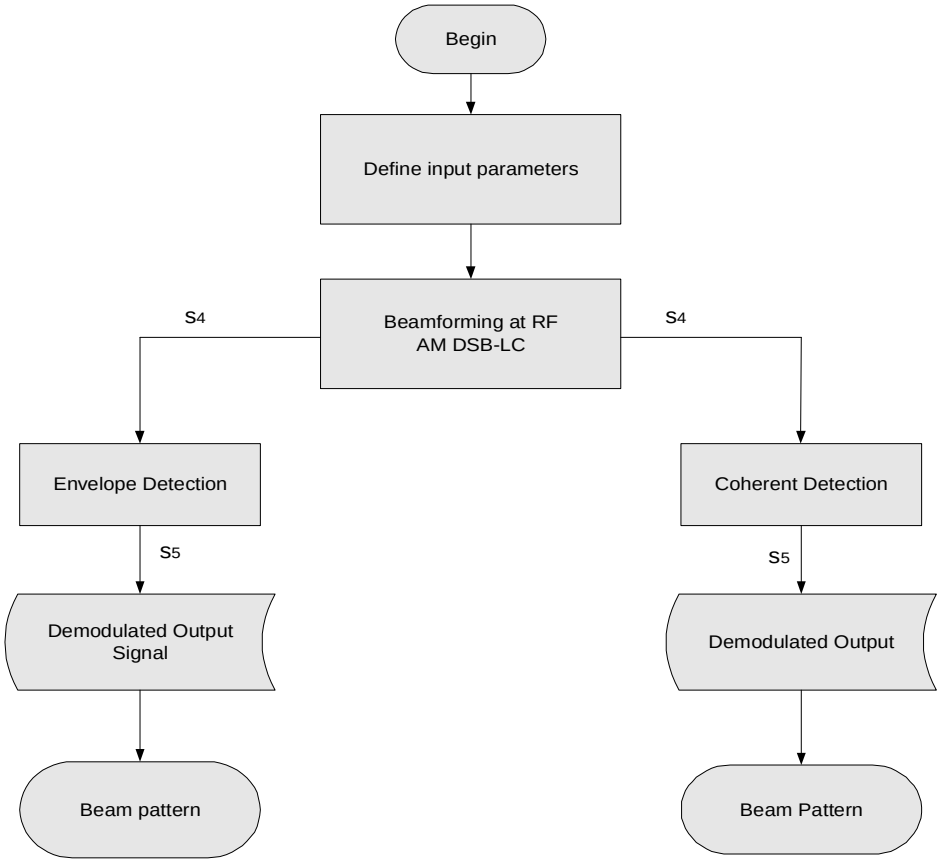

Figure 3.7: *AM DSB-LC beamforming at RF analysis structure flow diagram. The same analysis applies for the QBB case though for the QBB case, only the coherent case was looked at to avoid repetition in the analysis.*

3.6.2.1 Coherent detection

The detection process under this method is done by multiplying the summed signal with a local oscillator whose frequency is synchronized to the carrier frequency. i.e $s_5=s_4(LO)$. The demodulated output is give below as

$$s_5=[s_5]_{LPF.} \tag{3.8}$$

The amplitude of s_5 is the taken and a polar plot of the amplitude against theta is done to give the beam pattern.

3.6.2.2 Envelope detection

Under this detection method, the summed signal is rectified using a half-wave rectifier (HWR) and then the rectifier output is lowpass filtered to give the demodulated output signal [33]. The envelope detector circuit is given earlier in Chapter 2. The expression below illustrates the process.

$$s_{4r}=[s_4]_{\mathrm{HWR}} \tag{3.9}$$

The demodulated output is the lowpass filtered version of s_{4r} .

$$s_5=[s_{4r}]_{\mathrm{LPF}} \tag{3.10}$$

This gives us the demodulated output from which our beam pattern will be formed by taking the maximum value of the output and making a polar plot.

3.6.3 Simulation results:- AMDSB-LC Beamforming at RF

The simulation results for beamforming at RF for the coherent and non-coherent method are given in the following sections. For this simulation the number of samples was increased to 2048 and the sampling frequency used was 32000Hz.

3.6.3.1 Coherent detection

This method as already explained earlier does employ a local oscillator whose frequency is equal to the carrier frequency. The block diagram shown below is an illustration of the MatLab code which is used in this analysis.

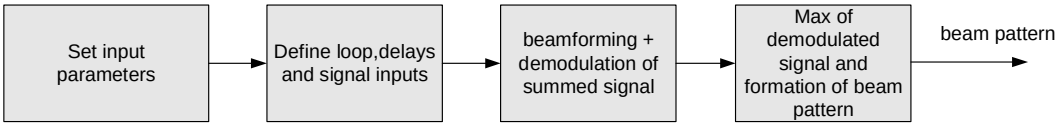

Figure 3.8: *MatLab code structure:-Coherent detection.*

Figures 3.9(a), (b), (c) and (d) below illustrate the graphical results of our MatLab analysis. The beamformed / summed signal in Figure 3.9(a) is multiplied with the local oscillator frequency and this translates the low frequency summed up signal to $\pm 2\omega_c$ on the frequency spectrum. The resulting signal is shown in Figure 3.9(b). The higher (double) frequency components are then effectively filtered out by a low pass filter resulting in the spectrum shown in Figure 3.9(c). The resulting demodulated signal is shown in Figure 3.9(d).

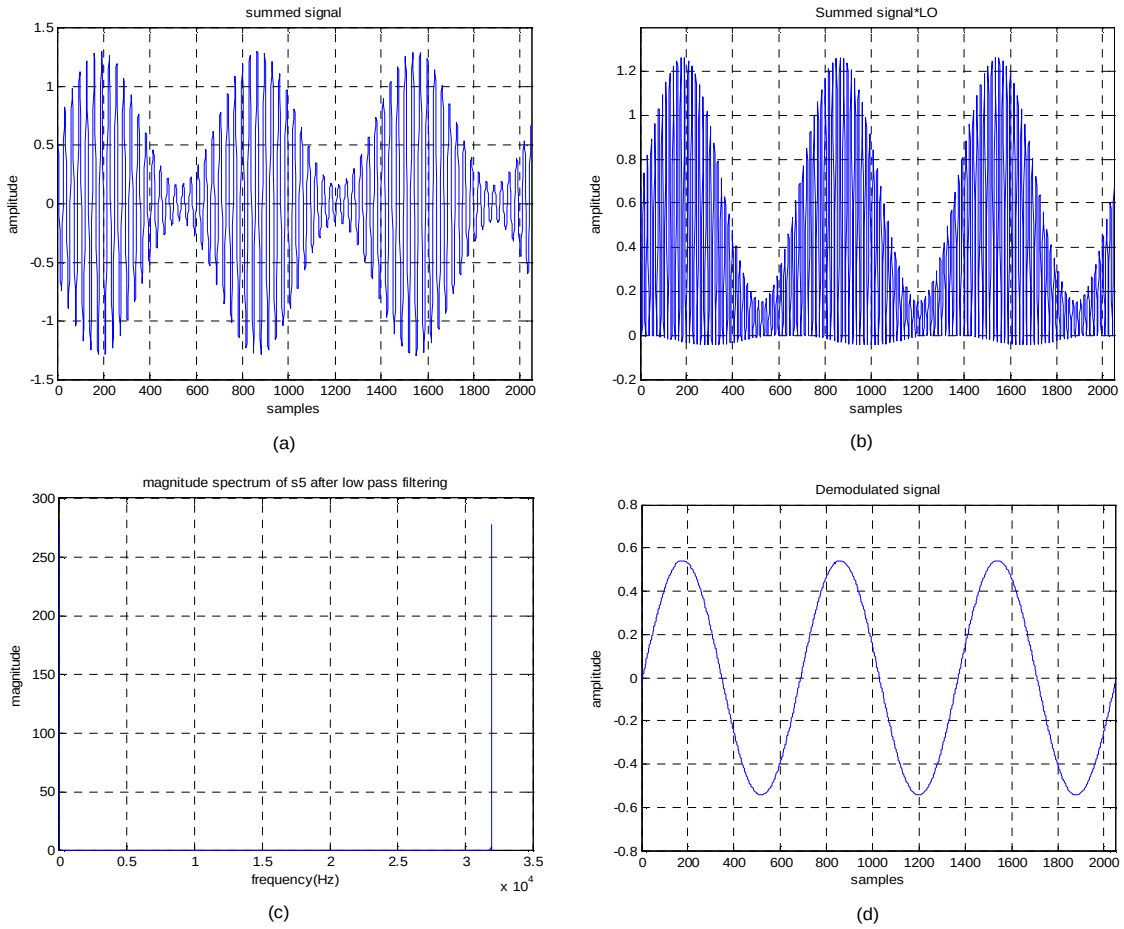

Figure 3.9: *Simulation plots.***(a)** *Summed signal* **(*b*)** *Summed signal*Local oscillator* **(*c*)** *Magnitude Spectrum after LPF.* **(*d*)** *Demodulated output signal.*

A polar plot of the maximum value of the demodulated output gives the required beam pattern entailing the successful beamforming process using the coherent method. The resulting beam pattern is given in the figure on the next page.

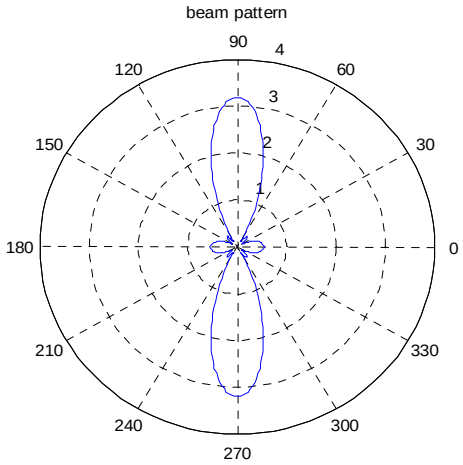

Figure 3.10: *Beam pattern.*

3.6.3.2 Envelope Detection

The beamforming was now carried out for the non-coherent method which is also referred to as the envelope detector. It will be interesting to see the changes that take place in the resulting beam pattern from this type of demodulation. The block diagram shown below illustrates the MatLab code used for the analysis.

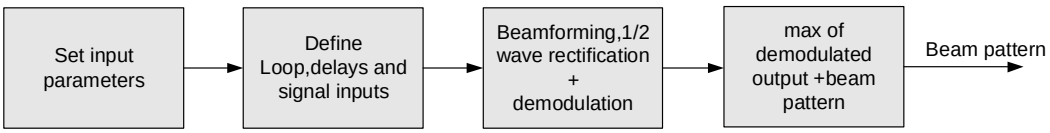

Figure 3.11: *Matlab code structure*:*-Envelope detector simulation.*

The simulation results are given in the figures on the next page. The beamformed signal remains the same as in the coherent case. The summed signal was passed through a simulated half-wave rectifier where it was seen that the diode in the rectifier clips out the negative cycles of the signal leaving the positive cycles from which our envelope will be extracted.

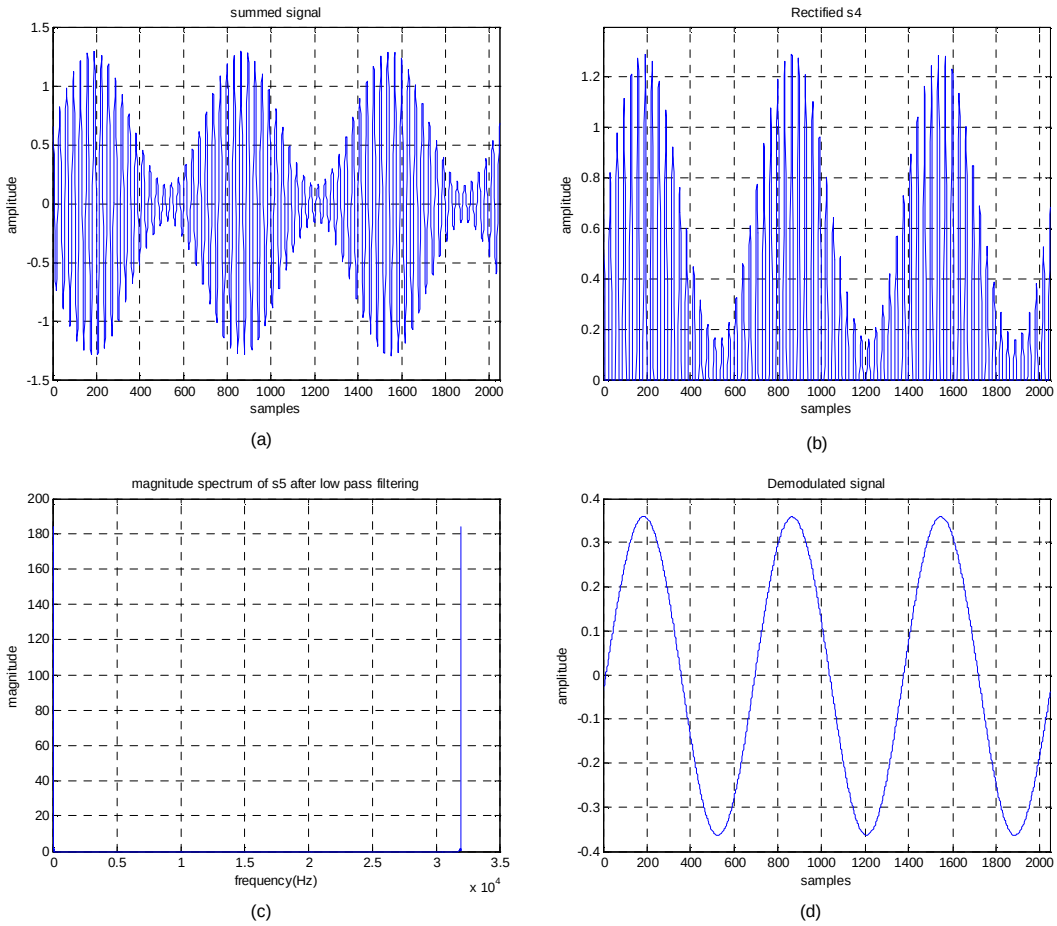

Figure 3.12: *Simulation results.* **(a)** *Summed signal* **(b)** *Rectified summed signal* **(c)** *Magnitude spectrum of LPF signal* **(d)** *Demodulated output signal.*

The magnitude spectrum in Figure 3.12(c) shows a reduction in the magnitude as compared to its coherent counterpart and this is also reflected in the reduced amplitude of the demodulated signal output. Thus the beam pattern is equally expected to have a reduced maximum value and this is shown in the figure on the next page. Basically, the results from the envelope detection simulation showed that the beam pattern obtained was different for the coherent and non-coherent modes of demodulation. The focus of the study remains that of investigating the possibility carrying out selected demodulation algorithms at QBB coupled with the expected benefits and therefore, going into details about analysing the coherent and non-coherent difference in beam patterns obtained diverts our focus from the core of the study. Having said this, only the coherent detection QBB results were discussed and considered for the comparison purposes in terms of processing load and simulation runtime given later in the chapter.

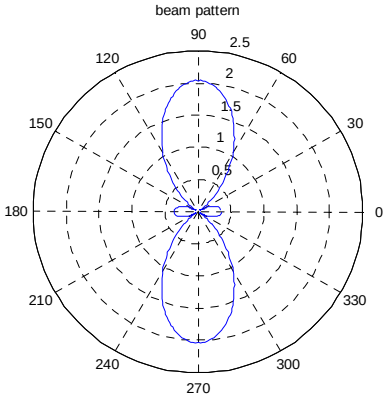

Figure 3.13: *Beam pattern*

3.6.4 Simulation results:- AMDSB-LC Beam forming at QBB

The simulation for the QBB analysis was done for the coherent and non-coherent methods though only the coherent method was discussed below due to the fact that the results obtained for the two methods are similar and as required by focus of the study, we basically aim to show that processing carried out at RF can equally be carried out at QBB with the processing load expected to be less at QBB which will be verified later in the chapter. The block diagram below illustrates the MatLab code structure.

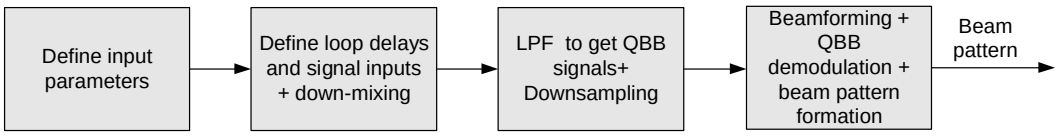

Figure 3.14: *MatLab code structure.*

Figures 3.15(a), (b), (c) and (d) on the next page are the simulation results obtained for the beamforming process at QBB. The input parameters used in the simulation were the same as those used for the two RF methods and hence this will facilitate for the correct comparison of the beam pattern outputs for the two procedures (RF and QBB). The procedure for the beamforming remains the same as explained earlier for the AMDSB-SC process and hence the earlier explanation given does suffice in explaining the current situation. Figure 3.15(a) represents the complex QBB beamformed signal and its magnitude spectrum in Figure 3.15(b). The magnitude spectrum is plotted in terms of

samples so as to show the reduction in samples resulting from the downsampling process. The downsampling factor was 4 and hence the 4-fold reduction in the number of samples from 2048 to 512. The beamformed signal undergoes QBB demodulation which was illustrated earlier in Chapter 2 and this results in the demodulated signal from which the beam pattern in Figure 3.15(d) was plotted. A first glance at the resulting beam pattern does show that it is similar to the coherent RF pattern but this has to be proved numerically and in terms of the beam pattern properties which are given in the following section of the chapter.

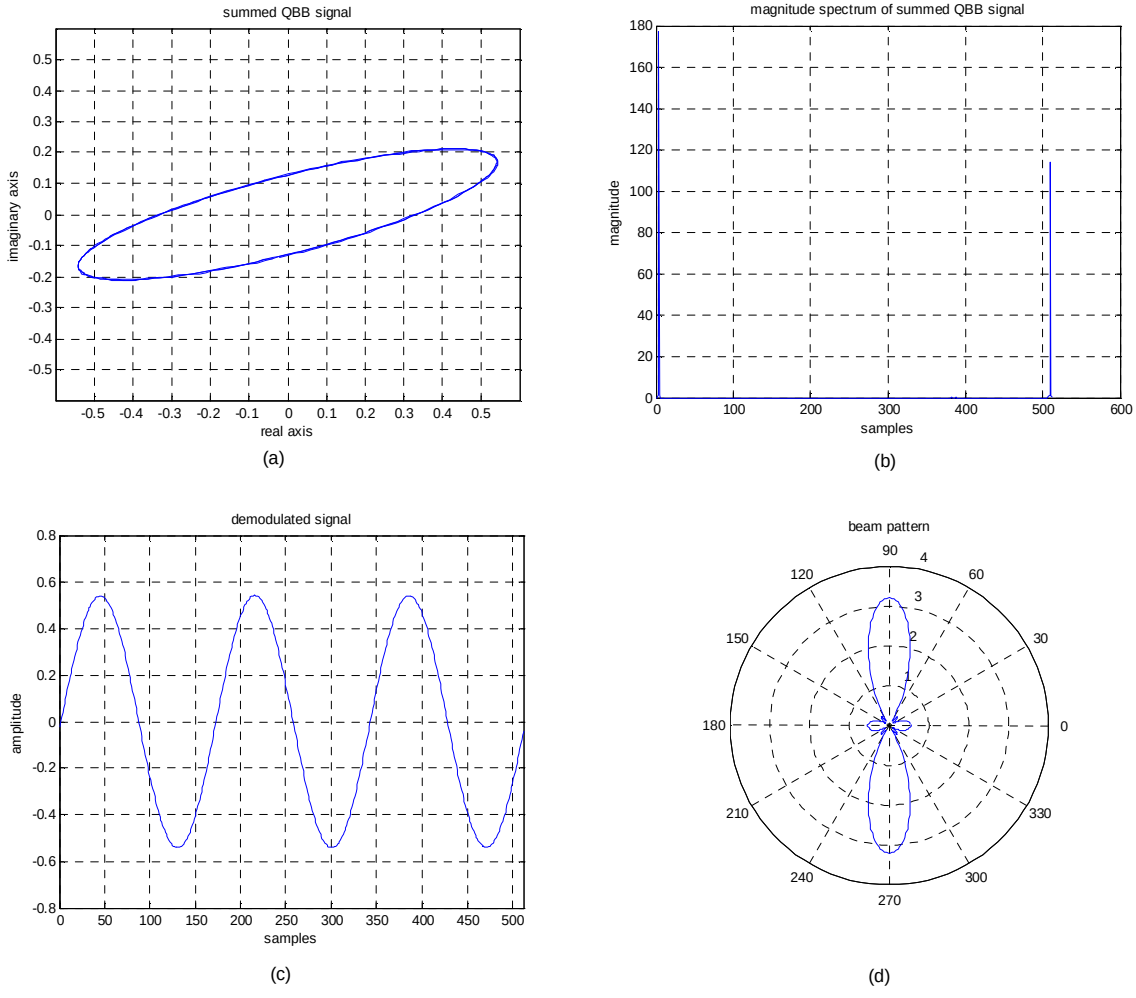

Figure 3.15: *Simulation results.***(a)** *Summed QBB signal* **(b)** *Summed QBB magnitude spectrum* **(c)** *Demodulated signal* **(d)** *Beam pattern.*

3.6.5 Beam pattern comparisons

As with the previous analysis, the beam patterns resulting from the analysis done are compared so as numerically verify the similarity of the beam patterns. The figure below shows the comparison structure and resulting error plot.

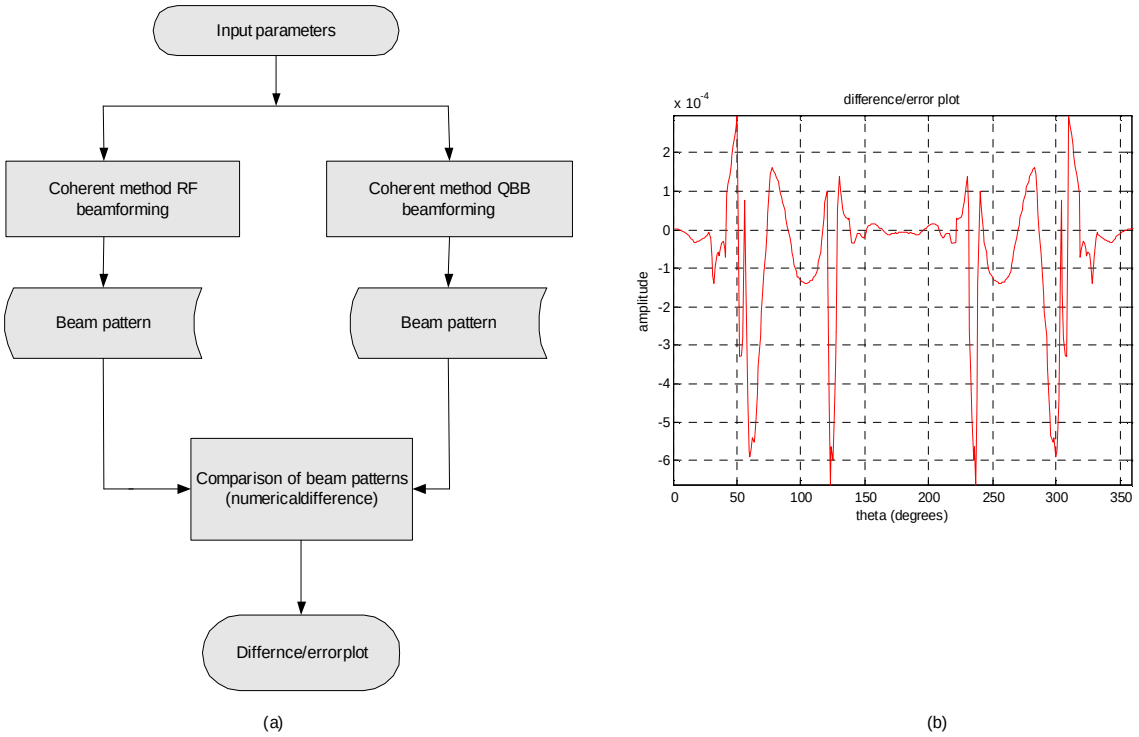

Figure 3.16: (a) *MatLab simulation structure for beam pattern comparison* **(b)** *Difference/error plot: the error is very minimal and thus the beam patterns are similar.*

3.7 MatLab Analysis Simulation Results:– Frequency Modulation

The results of the FM beamforming simulations are outlined in this section and a numerical comparison is made between the resulting beam patterns and draws up a conclusion over the possibility of beamforming at QBB

3.7.1 Simulation results:– Beamforming for FM at RF

The analysis results for RF beam forming for FM are given and discussed below. For this analysis, the sampling frequency used was 3000Hz, the deviation was 100Hz, and

the number of samples used to represent a signal was 512. The Matlab code structure is the same as that given earlier in the chapter. The figures that follow are the simulation results obtained at RF. The summed signal in Figure 3.17(a) resulted in the magnitude spectrum in Figure 3.17(b). From the spectrum it is seen that the signal sits at 'f_c' and has harmonics spreading out on the spectrum. The in-built 'fmdemod' Matlab function effectively demodulates the beamformed signal and which is shown in Figure 3.17(c). The resulting beam pattern is given in 3.17(d).

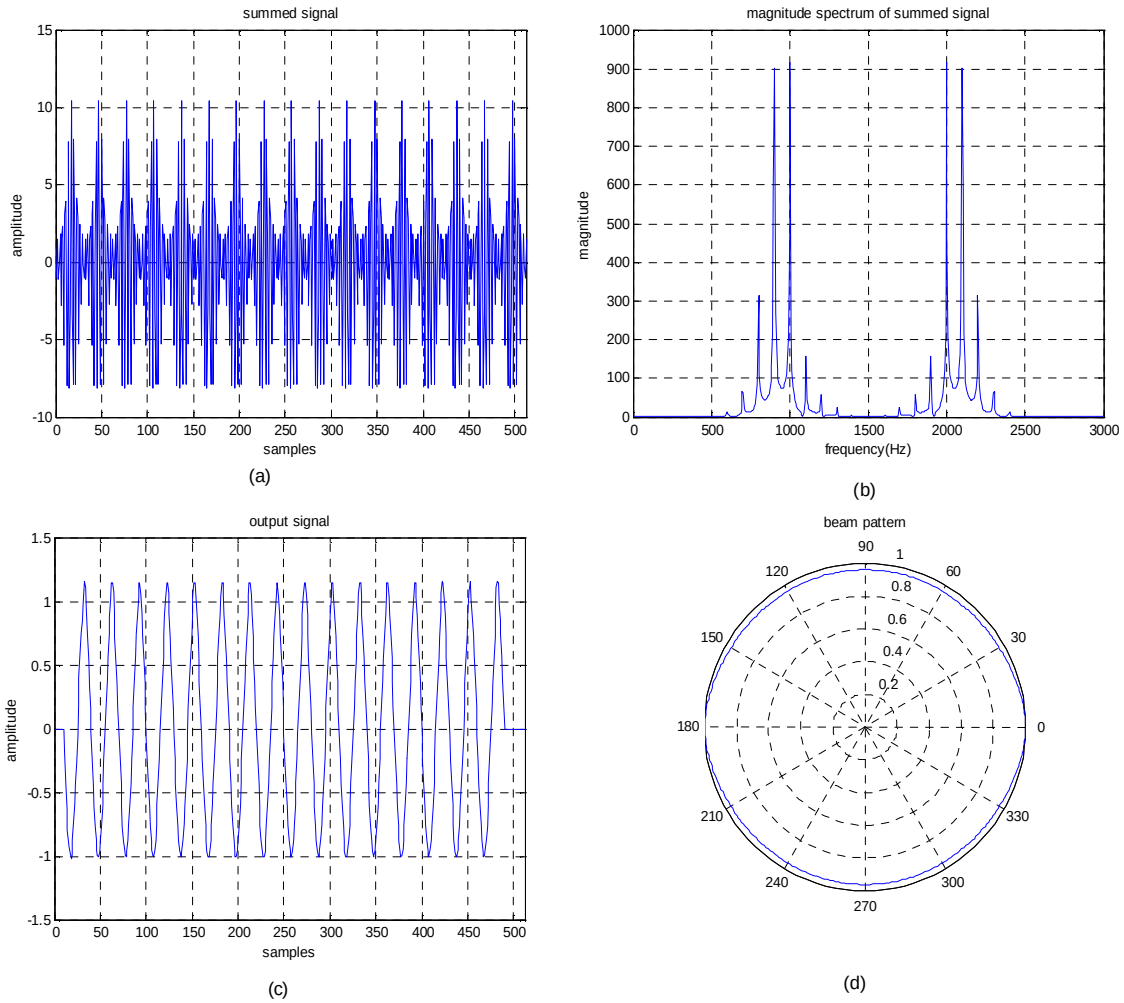

Figure 3.17: *Simulation results* **(a)** *Summed signal* **(b)** *Magnitude spectrum of summed signal* **(c)** *Demodulated output signal* **(d)** *Normalised beam pattern.*

3.7.2 Simulation results:-Beamforming for FM at QBB

The graphical results below show quadrature baseband beam forming for FM signals. The demodulation of FM signals at QBB was outlined earlier in Chapter 2. The conditions and parameters used are the same as at for the RF simulation. The sampling frequency being 3000Hz and the number of samples 512. The summed QBB signal and its downsampled spectrum are shown in Figures 3.18 (a) and (b) respectively. The downsampling factor was 2 and hence the 2-fold reduction in the number of samples. The demodulated signal and the resulting beam pattern are shown in Figure 3.18(c) and (d) respectively on the next page.

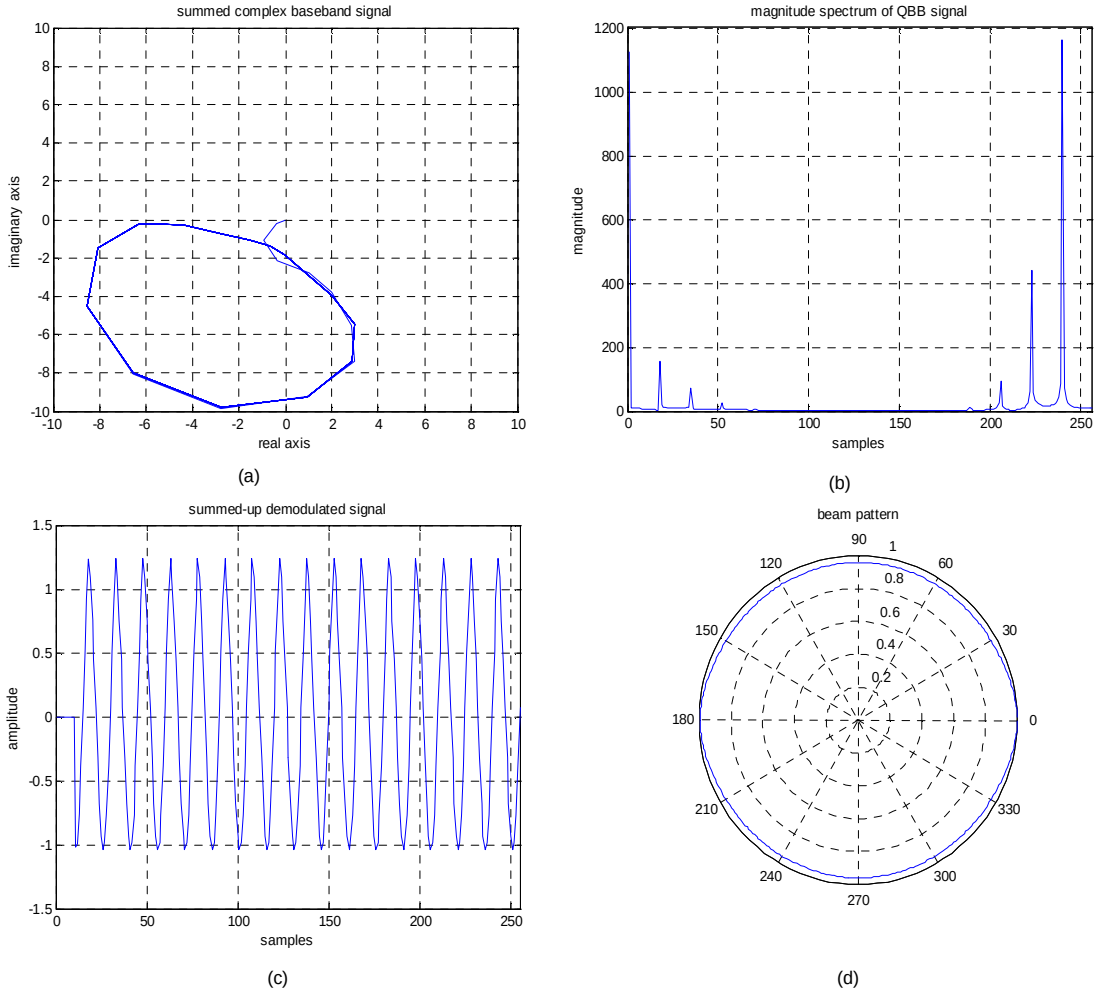

Figure 3.18: *Simulation results* **(a)** *Summed QBB signal* **(b)** *Magnitude spectrum of summed QBB signal* **(c)** *Demodulated signal output* **(d)** *Normalised beam pattern.*

The RF and QBB beam patterns look similar and it will be validated by the numerical proof in the following section where a difference plot will show the actual numerical difference between the two beam patterns.

3.7.3 Numerical Comparison of beam Patterns

The normalised beam patterns for the RF and QBB beamforming were compared numerically using a MatLab program. The figure below shows the difference plot flow between the two beam patterns produced and the error/difference plot against theta (degrees).

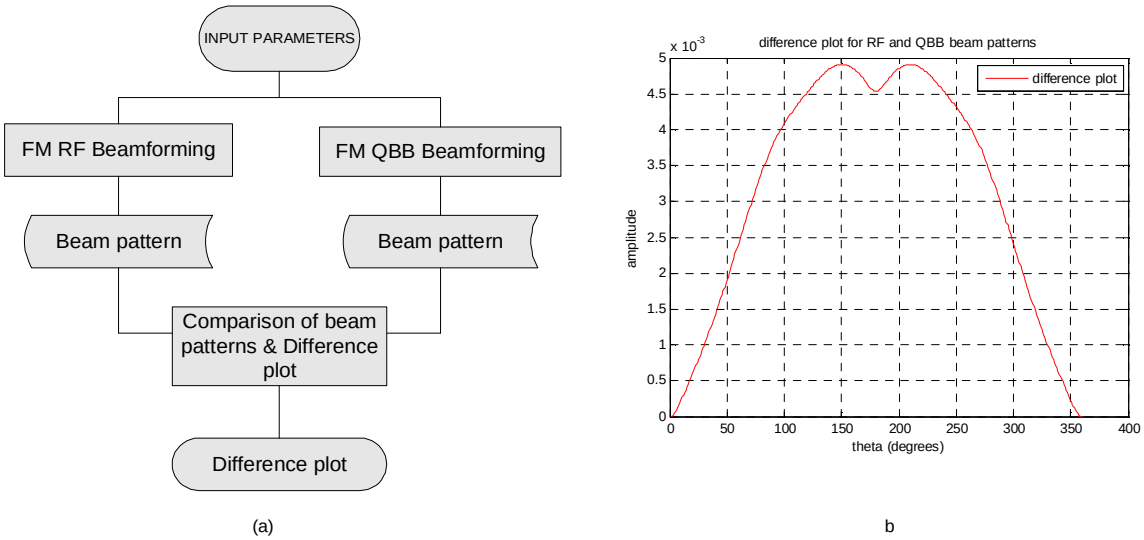

Figure 3.19: (a) *Difference plot Matlab structure flowchart.* **(b)** *Difference plot.*

From the difference plot between the two beam patterns, it is seen that the two beam patterns match perfectly/precisely and so, it suffices to say that the two beam patterns are similar and that it has been verified that beamforming in QBB gives a similar beam pattern to its RF counterpart. This justification also entails that beamforming can be done at quadrature baseband which for reasons already mentioned; does have more advantages than the traditional RF method. The Table 3.3 on the next page further illustrates the beam pattern properties for the beam patterns plotted under the FM simulations. It is seen that the two patterns match in terms of the pattern properties and

hence substantiating the purpose of this part the study which aims to beamform at QBB and achieve the same results as at RF. The benefits in terms of processing load and time of QBB versus RF beamforming will be seen in the next section of the chapter.

3.8 Benefits of beamforming at quadrature baseband

The benefits of beamforming at quadrature baseband can be expressed in terms of the sampling frequency. The fast growing telecommunications industry does strive to make efficient and effective use of the available resources of which bandwidth is very significant. The benefits of processing at QBB were investigated and a conclusion was drawn from the results obtained from the simulation runtimes and theoretical calculations based on the simulation code.

3.8.1 Sampling frequency and bandwidth

According to nyquist's criterion [4], the sampling frequency must be at least twice the bandwidth.

$$f_s \geq 2(f_c + \frac{B}{2}) \tag{3.11}$$

where *B* represents the signal bandwidth. Consider the figure shown below.

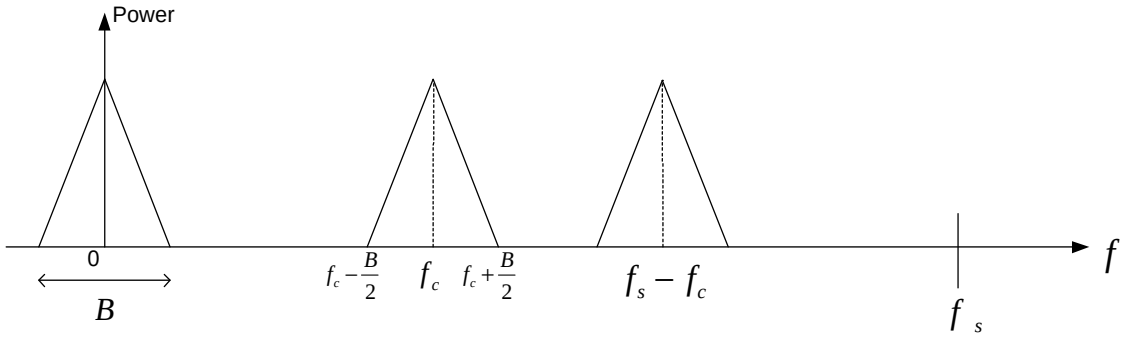

Figure 3.20: *RF/QBB sampling frequency comparison.*

Referring to the figure above, the sampling frequency for the signal at RF is twice the sum of the carrier frequency and signal bandwidth. And hence this entails that the beamforming at RF is done at a higher frequency too. However, looking at the

QBB case, the required bandwidth is equal to the signal bandwidth itself and this is because the carrier frequency is eliminated by the shifting down process. The percentage saving in terms of sampling frequency is significant in ensuring more efficient usage of available resources like bandwidth. The mathematical derivation of the saving is given below. Let f_{sqbb} denote the QBB sampling frequency and f_{srf} the RF sampling frequency. The ratio of f_{sqbb} to f_{srf} is found as follows:

$$\begin{aligned} f_{sqbb} &\geq | \, 2(f_c + \frac{B}{2}) \, |_{f_c=0} \\ f_{sqbb} &\geq 2(\frac{B}{2}) = B \end{aligned} \tag{3.12}$$

Similarly

$$\begin{aligned} f_{srf} &\geq 2(f_c + \frac{B}{2}) \\ f_{srf} &= 2fc + B \end{aligned} \tag{3.13}$$

The required ratio is given below.

$$\therefore \frac{f_{sqbb}}{f_{srf}} = \frac{B}{2f_c + B} = \frac{B}{2f_c + B} \tag{3.14}$$

Assuming f_c =1000Hz and B=40Hz, then the percentage saving by working at QBB in terms of bandwidth is calculated below:

$$\therefore \frac{f_{sqbb}}{f_{srf}} = \frac{40}{2040} = \frac{1}{51} \tag{3.15}$$

The percentage saving is thus equal to

$$\frac{(2040-40)}{2040} \times 100 \approx 98\%$$

Therefore, the above ratio shows a very significant saving being achieved by operating at QBB in terms of the sampling frequency [2].

When f_c=0.5B

This worst case scenario assumes that f_c=0.5B. Therefore, considering Equation 3.14, B is neglected and the ratio reduces to ½. This implies that the minimum saving in terms of sampling frequency reduction that can be achieved is 50%.

When $f_c >> B$

This scenario presents another extreme case. From Equation 3.14, it is seen that for this particular case, the ratio f_{sqbb}: f_{srf} approaches $1/2f_c$.

3.8.2 Sample processing and simulation time

This aspect of showing the savings achieved from working at QBB looks at the *number of calculations in the simulation code* carried out RF and QBB in terms of 'N' which represents the number of samples. Therefore, the MatLab code for the RF and QBB simulations was redefined in terms of N. The filtering process involves taking the FFT and then killing off the unwanted part of the spectrum by multiplication with the filter response and then taking the IFFT to get back to the time domain. It is already known that carrying out an FFT involves $N\text{Log}_2N$ multiplications when N is a power of 2 [7]. The same is assumed for the IFFT. As mentioned earlier the processing load was measured using a relative method. The simulation runtime was measured using the inbuilt Matlab [5] commands 'tic' and 'toc'. Therefore, timers were introduced into the simulations so as to measure the elapsed time for each simulation. It should be noted that the time and numerical calculation measurements start from the received signal models down to the demodulation as this is forms the focus of the analysis with other defined parameters not shown. The sample processing measurements for the simulations that were run, is given in the CD in Appendix C illustrates how the simulation time and number of processing calculations was measured. The table on the next page summarises the sample processing for AMDSB-SC beamforming at RF and QBB.

Simulation Stages	**Radio Frequency**	**Quadrature baseband (simulated)**
Mixing down + QBB	____	$4N + 4N\text{Log}_2N + 8kN + 4kN\text{Log}_2kN$
Beamforming	3N	3kN
Demodulation	$N+2N\text{Log}_2N+N$	____
Total 'N' operations	$5N + 2N\text{Log}_2N$	$4N+ 11kN+ 4kN\text{Log}_2kN+4N\text{Log}_2N$
Total : N=512 and k=1/4	11776	25472

Table 3.1: *Number of calculations at RF and QBB*

For the simulation carried out for AMDSB-SC beamforming, N had a value of 512 and the downsampling factor was 4 (i.e. k=1/4). Substituting into the expressions given in the table above facilitates the evaluation of the amount of numerical processing calculations for the simulations run at RF and QBB.

Let N_{rf} and N_{qbb} represent the sample processing at RF and QBB respectively, then the ratio of the RF to QBB sample processing is given as:

$$\frac{N_{rf}}{N_{qbb}} = \frac{11776}{25472} = 0.463 \tag{3.16}$$

Therefore, it was seen that the amount of processing taking place at QBB was more than that taking place at RF. Therefore, it suffices to say that for the simulated case, the beamforming at RF was more efficient than at QBB in terms of the amount of sample processing required. What is meant by this statement is that the sample reduction due to the downsampling process does not directly translate to a reduction in the amount of processing and hence the simulation time will verify this as it is expected that beam forming at RF should take less time than beam forming at QBB. The ratio of the number of calculations at RF to those at QBB in the simulation code was verified by correlating against the simulation processing time ratio. For the real life case, as was mentioned in chapter 2, the processing commences from the QBB signal components and thus the QBB generation stage in the Table 3.1 is skipped. This reduces the number of calculations reduces to '3kN' which has a numerical value equal to 384. Thus we notice a big reduction in the number of calculations at QBB.

The ratio of the number of calculations for the real life QBB processing to the number of calculations at RF is given below as

$$\frac{N_{rf}}{N_{qbb}} = \frac{11776}{384} = 30.67 \tag{3.19}$$

The result above should translate into a much reduced simulation runtime too. Therefore, it is seen that despite the simulation of beamforming at QBB falling short of being advantageous as compared to the RF case, it does significantly become more advantageous for the real life case which processes the QBB signals. Therefore, we see that working at QBB did indeed maintain its superiority in terms of processing and runtime over working at RF. The table on the next page summarises the results obtained for the simulations at RF and simulated QBB in terms of simulation runtime and number of calculations for the simulation codes. It should be noted that the number of calculations for the coherent AMDSB-LC simulation is the same as at for the AMDSB-SC simulation. However, the FM theoretical prediction did have limitations in that the representation for some of the commands used in the demodulation process could not be theoretically quantified or rather is too complicated to come up with. Therefore, in such cases, the simulation runtime had to be solely relied upon.

	RF (t_{rf})	QBB(t_{qbb})	t_{rf}/t_{qbb}	N_{rf}	N_{qbb}	N_{rf}/N_{qbb}
BEAMFORMING	Time in seconds		Ratio	Number of calculations		Ratio
1. AM DSB-SC	0.36318	0.74992	0.48	11776	25472	0.46
2. AM DSB-LC	0.35836	0.77418	0.46	11776	25472	0.46

Table 3.2: *Simulation time and sample processing comparison table:- the results show a close match between the theoretical prediction from the sample processing ratio and the actual simulation time ratio with a maximum discrepancy of 4.2% attributed to the variation in the computer processing time variance.*

3.9 Conclusion

The chapter discussed the simulation results for the beamforming process for AMDSB-SC, AMDSB-LC and FM at RF and QBB. The results showed that Beamforming could take place at QBB with the key advantage being the lower frequency of operation. The beam pattern comparisons did justify the similarity between the RF and QBB beam patterns obtained. The latter part of the chapter looked at the benefits and outcomes of the simulation analysis carried out where it was seen that despite the saving in terms of sampling frequency due to the sub-sampling that took place at QBB, the beamforming process for the simulated RF case was less tedious when compared to the simulated QBB case for the simulations carried out. This was seen from the theoretical prediction and simulation results obtained which showed less processing being done at RF and the simulation time equally followed suit. The ideal QBB case which represents the processing in an actual DSP does however become superior over RF in terms of processing load and simulation runtime.

Chapter 4

Multipath compensation-simulation results

This chapter looks at multipath compensation at RF and QBB. Simulations were run and the results are given and discussed. Difference plots will be given by comparing the compensated output to the original input and this will act as the proof of compensation entailing a successful compensation process. As was done under beamforming, the results obtained at RF and QBB will be compared in terms of the simulation runtime and number of calculations in the simulations. Later in the chapter it will be seen that compensating at QBB does prove more advantageous than at RF in terms of simulation runtime and processing load.

4.1 Multipath Compensation

In Chapter 2 a brief background of multipath and its compensation process was given. In this part of the study, the simulated multipath signal will be modelled and the compensation process is analyzed graphically and theoretically. The figure below illustrates a simple multipath signal reception scenario.

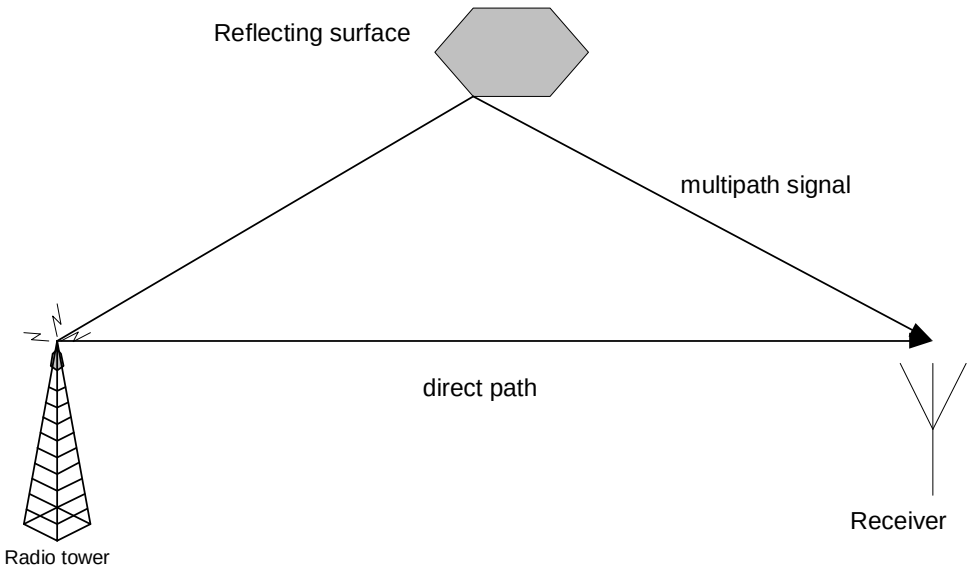

Figure 4.1: *Multipath signal reception model*

In Figure 4.1 on the previous page, it is seen that the antenna at the destination receives two signals namely the direct-path and delayed signal. For analysis purposes, we will restrict the number of multipath signals to one. Before carrying out the analysis, there is need to model the multipath signal and correct compensator which will eliminate the multipath effects and resulting in the required direct-path signal output.

Multipath signal modelling

The multipath channel *H* comprises a component of the direct path signal and the delayed multipath signal. The multipath signal is undesired and hence the need for us to compensate for its presence and thus eliminate its effects. The goal of the compensation is to recreate the characteristics of the original signal just as it was before the delayed signal was introduced. This requires us to have knowledge of the characteristics of the channel (i.e. frequency or impulse response) in order to determine the correct compensator denoted as H_c. It is well known that convolving in the time domain is equivalent to multiplication in the frequency domain and vice-versa [3]. This means that we can equally have a model for the multipath signal by convolving in the time domain. However, using the time domain method, there are some important limitations in that we are restricted to discrete sample delays 'nTs' and thus the compensation process is limited by the fact that we cannot carry out downsampling beyond a point where the echo does not lie on a sample instant anymore and this has much to do with the echo positioning. The multipath channel modelling was done in the frequency domain and hence the signal compensation equally took place in the frequency domain. The famous time delay Fourier transform [3, 5] does facilitate for operating in the frequency domain. This is given below.

$$f(t-\tau) \leftrightarrow F(\omega)e^{-j\omega\tau} \tag{4.1}$$

Therefore, the received signal as already mentioned in Chapter 2 has the direct and multipath components in it and so the multipath channel 'H' will be given as

$$H = 1 + e^{-j\omega\tau} \tag{4.2}$$

It should be noted that in this case, τ is not restricted to nTs. The modelling of the multipath signal is thus done in the frequency domain and hence it is required that an equivalent domain is used in the compensation process. The QAM/FM modulated signal direct path signal is '*zero padded* 'and its FFT [5] is taken. This facilitates the circular convolution in the frequency domain whose equivalent is linear convolution in the time domain [24].

Similarly, the channel response is zero padded and followed by the FFT so as to have its frequency domain equivalent in readiness for the circular convolution. After carrying out the circular convolution, the resulting signal is transformed back to the time domain by taking its IFFT. The signal at hand is now a real multipath signal in readiness for analysis. The analysis then moves to the receiving end where the compensation takes place. Here, the received signal was transformed back to the frequency domain by taking the FFT and this was done so as to compensate in the frequency domain.

4.2 Multipath Compensation:–Radio Frequency

RF multipath compensation represents a traditional method of compensating for unwanted multipath signal effects. In this study, we assumed noiseless channels since, we are basically showing the possibility of compensating for multipath at RF and QBB with the latter being the new method and showing the expected benefits of compensating at quadrature baseband.

Theoretical Analysis

The theoretical analysis for the multipath compensation at RF is given below. In this part of the study, QAM and FM modulation were analyzed.

The direct path signal is represented as x_d . The received multipath signal being the sum of the direct path and its delayed echo is thus given as

$$x_{mp} = x_d + kx_d(t-\tau) \tag{4.3}$$

The compensator should thus eliminate the delayed signal component in the received multipath signal. The block diagram below is a representation of the Matlab analysis simulation structure showing the expected outputs at various points of the simulation.

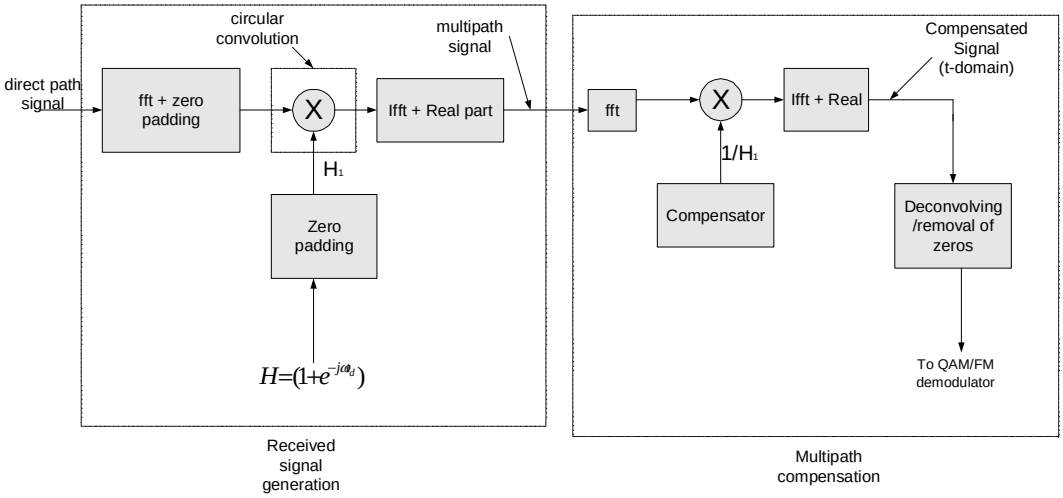

Figure 4.2: *RF multipath compensation theoretical analysis structure flow diagram.*

In order to test the accuracy of the compensation process, a parallel path was created in the simulation where the direct path alone was under analysis giving us a basis for comparing the compensated demodulated outputs with the direct path demodulated outputs. The results will be shown in a latter stage of the chapter.

The mathematical expressions below are a summary of the step-by-step processing carried out by the simulation. Firstly, the FFT of the direct path is given as

$$X_d = fft(x_d) \tag{4.4}$$

The signal is zero padded to facilitate for circular convolution to take place. It should be noted that the zero padding length is pre-determined by the conditions necessary for a successful circular convolution [7] to occur. Thus, the padding length L is given below as

$$L \geq P + N - 1 \tag{4.5}$$

where P is the length of the direct path signal and N the length of the channel impulse response [24]. Therefore, the frequency domain multipath signal X_{mp} which now has a length twice that of x_d is given as

$$X_{mp} = X_d H \tag{4.6}$$

Taking the real part of the IFFT of X_{mp} gets rid of the small imaginary part due to limited numerical accuracy resulting in the received multipath signal expressed below as

$$x_{rmp} = \mathrm{Re}[ifft(X_{mp})] \tag{4.7}$$

where x_{rmp} represents the received multipath signal. As mentioned earlier, the compensation will take place in the frequency domain and hence the need to convert the received signal x_{rmp} to the frequency domain before compensation can take place. Now $H_c=H^{-1}$ and *H being* a frequency domain vector means the compensator is thus in the frequency domain and thus the compensation can now proceed, having achieved the same domain of operation for the received signal and compensator.

$$X_{rc} = X_{rmp} H_c \tag{4.8}$$

where X_{rc} represents the compensated received signal in the frequency domain. The time domain equivalent of the compensated signal is given below as

$$x_{rc} = \mathrm{Re}[ifft(X_{rc})] \tag{4.9}$$

The original size of the compensated signal is achieved by removing the padded zeros. The original modulated signal is thus retrieved and the demodulated outputs achieved by carrying out QAM/FM demodulation resulting in the compensated demodulated output x_{rcd} .

4.3 Multipath compensation:- Quadrature baseband

The analysis moves down to quadrature baseband where the compensation will now take place. This in itself presents a major advantage of operating at lower sampling frequencies added on to the fact that operating at baseband also facilitates for downsampling which further reduces the operating frequency of the compensation process.

Theoretical analysis:-QBB

The input parameters used for this analysis are the same as those of their RF counterparts. This implies that we have the same signal parameters like amplitude, angular velocity etc. Similarly we have the same initial sampling rate (f_s) and the local oscillator frequency used in the complex down-mixing process is coherent with the carrier frequency.

Upon analysis of the results, a decisive conclusion was to be reached about the possibility of compensating at QBB accompanied by the various benefits that come with working at QBB frequencies. Some of the advantages of working at baseband frequencies are attributed to the ease of handling of baseband digital signals by software defined radios and hence resulting in the immense benefits of SDR technology being utilized [16]. The expressions for the direct path and multipath signals have already modelled under the RF theoretical analysis. And thus the analysis moves on to the receiver where it is required that we compensate at QBB. The received signal 'x_{rmp}' is down-mixed and lowpass filtered so as to generate its QBB equivalent.

$$x_{rmpqbb} = [x_{rmp} e^{-jw_c t}]_{LPF} \tag{4.10}$$

where x_{rmpqbb} represents the QBB version of the received multipath signal. The block diagram on the next page is a representation of the Matlab analysis simulation structure showing the expected outputs at various points of the simulation. The figure on the next page summarises the theoretical analysis.

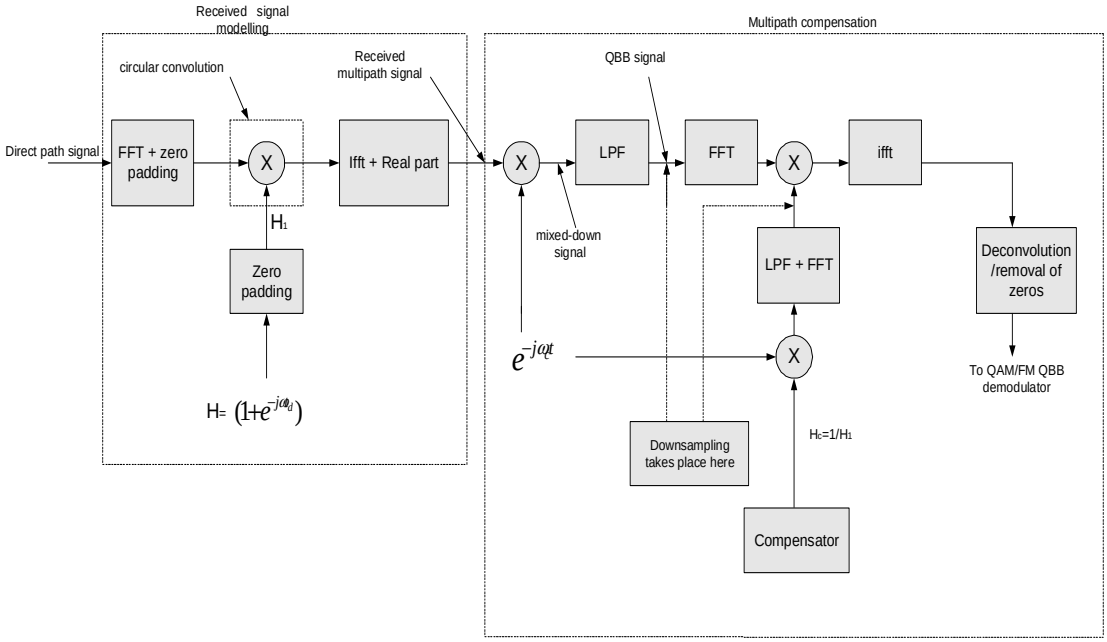

Figure 4.3: *QBB multipath compensation theoretical analysis flow structure.*

The compensation is thus done at QBB as required by the study. The simulation results will verify the compensation process illustrated theoretically by the figure above. Upon generating the QBB equivalent of the multipath signal, down sampling is also carried out. The quadrature baseband signal is downsampled by a factor 'n' whose value is restricted to the point where there is no aliasing in the spectrum. What this statement implies is that one can only downsample up to a certain point and that point is where aliasing begins to take place. It is a well known factor that aliasing is an undesirable situation and thus it has to be avoided at all costs. The downsampled signal is given in Matlab as

$$x_{rqbbds} = xrqbb(1:n:end) \tag{4.11}$$

where x_{qrbbds} represents the downsampled QBB signal. At this stage, the analysis focuses on the compensation process where it was required to compensate for the multipath effects. Now, in order to compensate for multipath at this stage, it is required to shift the compensation down to baseband because the signal now sits at baseband. This in itself is an added advantage of compensating at QBB because this takes place at much lower frequencies unlike for the RF situation. The compensator should equally be

downsampled before the compensation can take place. The QBB downsampled compensator is denoted as H_{cds}. The compensation can now take place and this is done by multiplying H_{cds} with the FFT of x_{rbbds} denoted as X_{rqbbds}. This is shown below as

$$X_{rc} = X_{rqbbds} H_{cds} \tag{4.12}$$

where X_{rc} denotes the compensated signal in the frequency domain whose time domain equivalent is given in Equation 4.13 below. The padded zeros should be eliminated at this stage. There is need to take into consideration the fact that the signal length has reduced by a factor 'n' and hence this should not be overlooked when removing the padded zeros. The IFFT of X_{rc} is given below as

$$x_{rc} = ifft(X_{rc}) \tag{4.13}$$

The signal x_{rc} is then demodulated and is denoted as x_{rcd}. In the simulations that follow, a parallel analysis is run for the direct path signal which is demodulated and compared with the compensated output so as to test the accuracy of the compensation process. The demodulated output from the parallel analysis is denoted as x_{rd}. The next section of the chapter gives the RF simulation results.

4.4 Simulation Results:–QAM RF compensation

The figures below are the results obtained from the multipath compensation simulation at RF. The sampling frequency f_s used was 4000Hz and x_1 and x_2 shown in Figure 4.4(a) are the unmodulated inputs of the QAM direct path signal shown in Figure 4.4(b). As mentioned under the RF theoretical analysis, the zero padding during the multipath signal generation doubles the signal length and this is evidenced in Figure 4.4(c). Compensating for multipath as outlined in the theoretical analysis results in the output shown in Figure 4.4(d). It can be seen here that the QAM signal has been retrieved and the multipath effects compensated for. The demodulated outputs and difference plot should further consolidate the accuracy of the compensation.

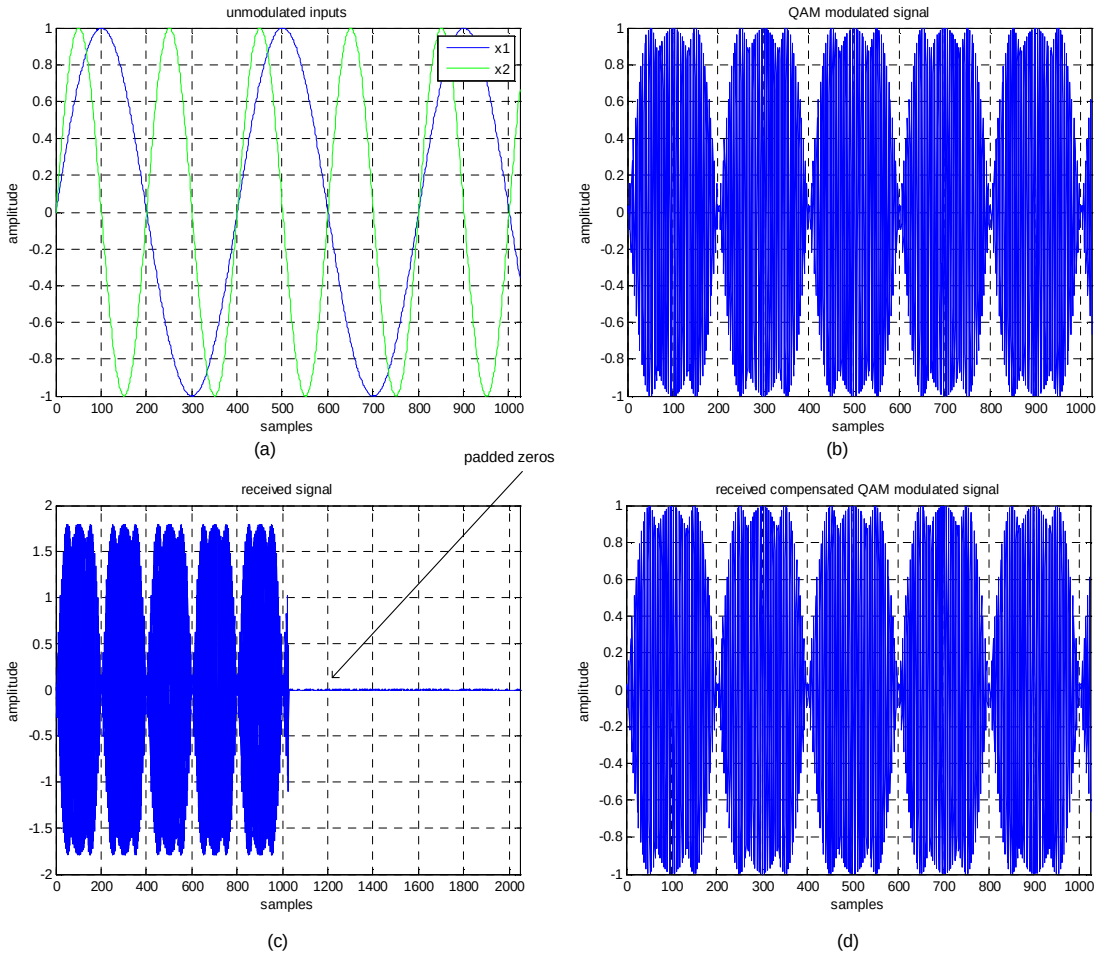

Figure 4.4: *Simulation results* **(a)** *Unmodulated inputs:- these represent the inphase and quadrature phase inputs of the QAM signal* **(b)** *QAM modulated signal* **(c)** *Received signal:-the last 1020 samples consist of padded zeros* **(d)** *Compensated signal.*

The figures below show the demodulated outputs and difference plot.

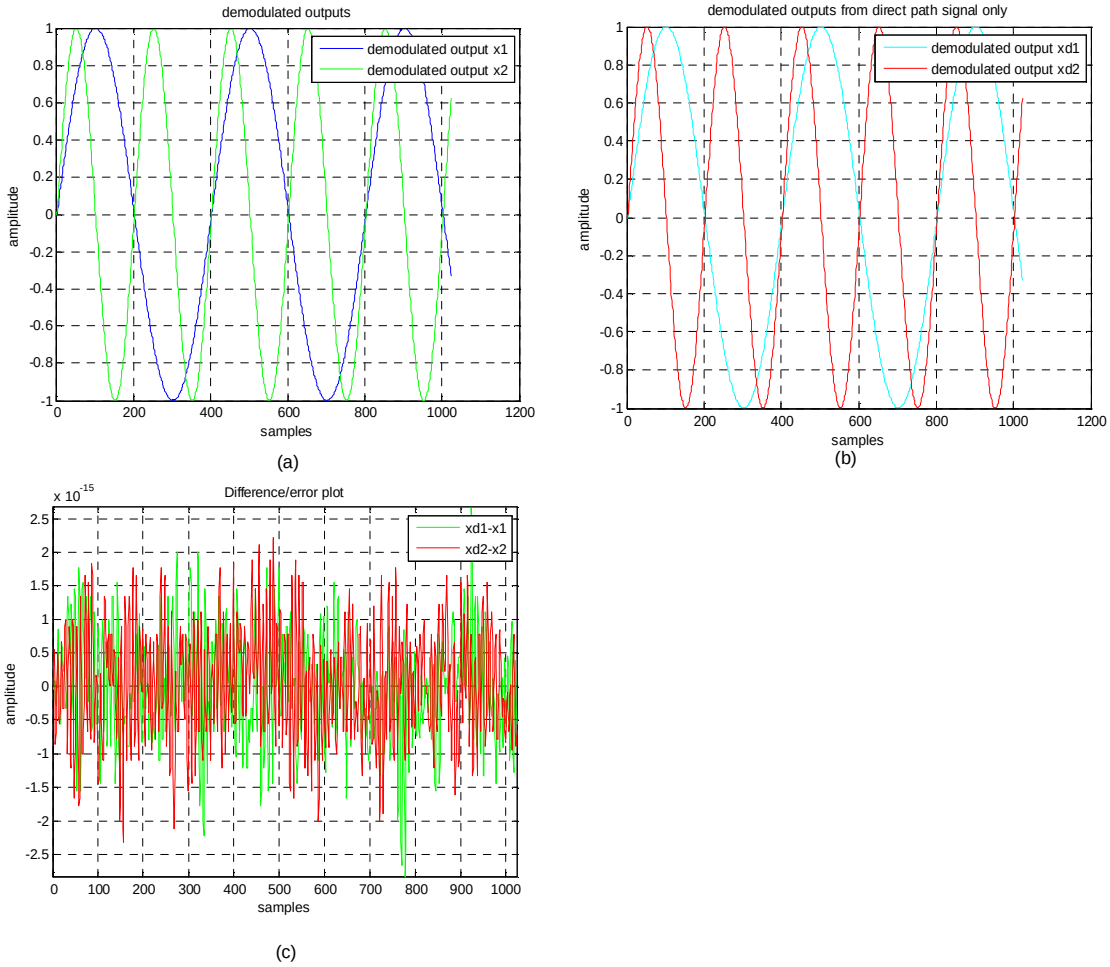

Figure 4.5: *Simulation results.* **(a)** *Demodulated output after compensation* **(b)** *Demodulated output from direct path* **(c)** *Difference plot between direct path and multipath compensated demodulated outputs.*

The difference plot clearly shows a very small and insignificant error. This proves that the compensation was accurate and successful. A look at the spectral changes in the following section of the chapter further consolidates the proof of a successful compensation.

Spectral Analysis of results

The figures below represent the magnitude spectra of the signals resulting from the RF multipath compensation simulation. The spectral changes that took place are analyzed in order to have proof of the compensation from the spectral point of view.

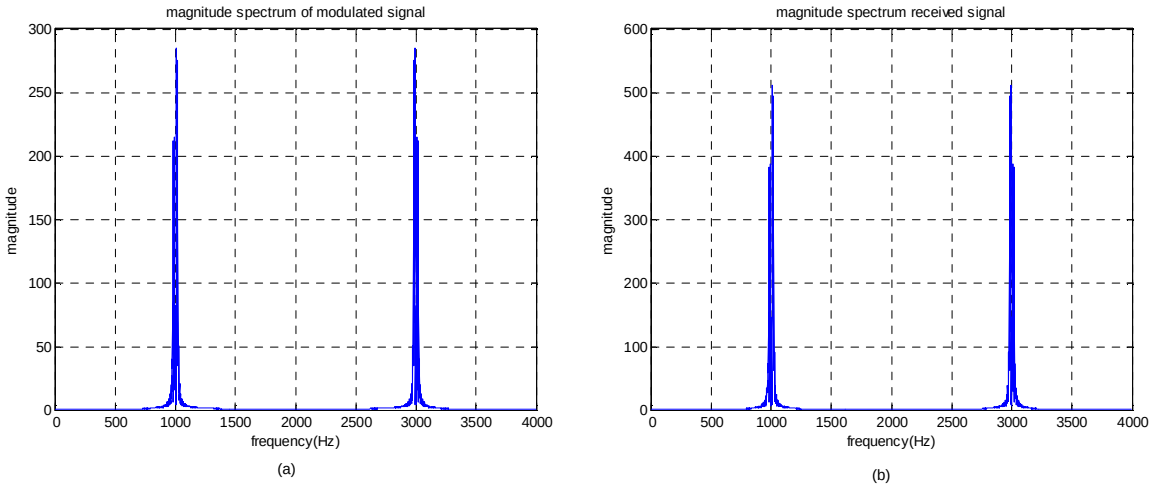

Figure 4.6: *Magnitude spectrum of* **(a)** *Modulated input signal* **(b)** *Received signal*

The Figure 4.6 (a) above illustrates the magnitude spectrum of the QAM modulated signal before multipath and Figure 4.6(b) represents the magnitude spectrum of the received signal. The multipath component increased the magnitude of the spectral content of the signal as can be seen. Figure 4.7 below shows that the compensation process restored the original spectrum of the signal.

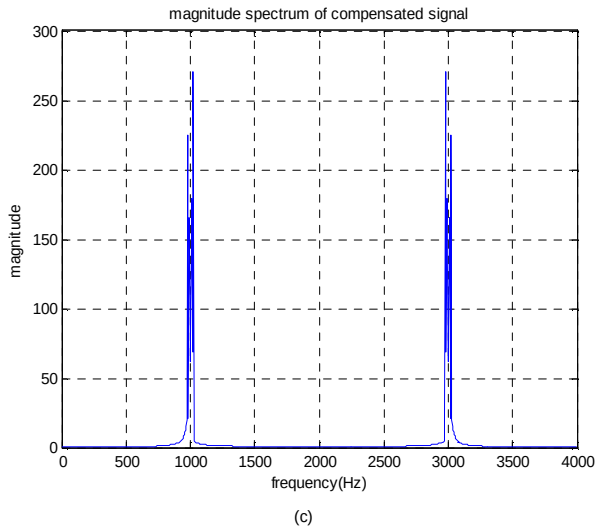

Figure 4.7: *Magnitude spectrum of compensated signal.*

The plots below illustrate the multipath channel response and it was seen from the graphical plots that the impulse response of the multipath channel was perfect and a 'zoomed in' plot shows and reveals the 4 sample delay in the multipath signal as well as an echo factor of 0.8.

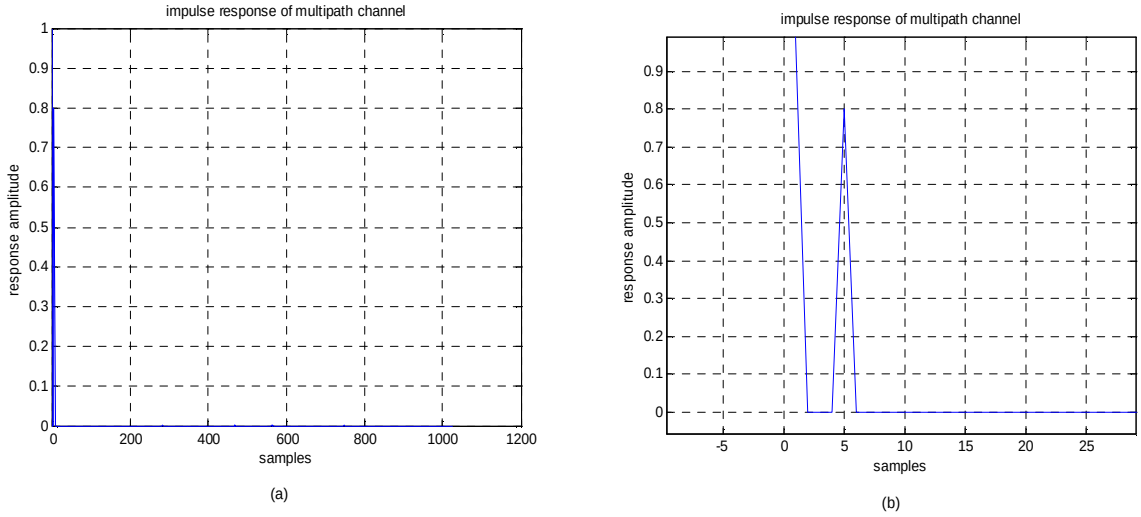

Figure 4.8: **(a)** *Channel impulse response* **(b)** *Channel impulse response enlarged*:- *the 4 sample delay is now visible from the zoomed in plot .*

4.5 Simulation Results:–QAM QBB compensation

The results of the MatLab simulations are now given and analyzed in this section of the chapter. It should be noted that the generation of the received signal remains the same as was done under RF and so the graphical results to be analyzed will be from the receiving end down to the compensation and demodulation. The figures on the next page show the plots resulting from the simulation of the QBB multipath compensation.

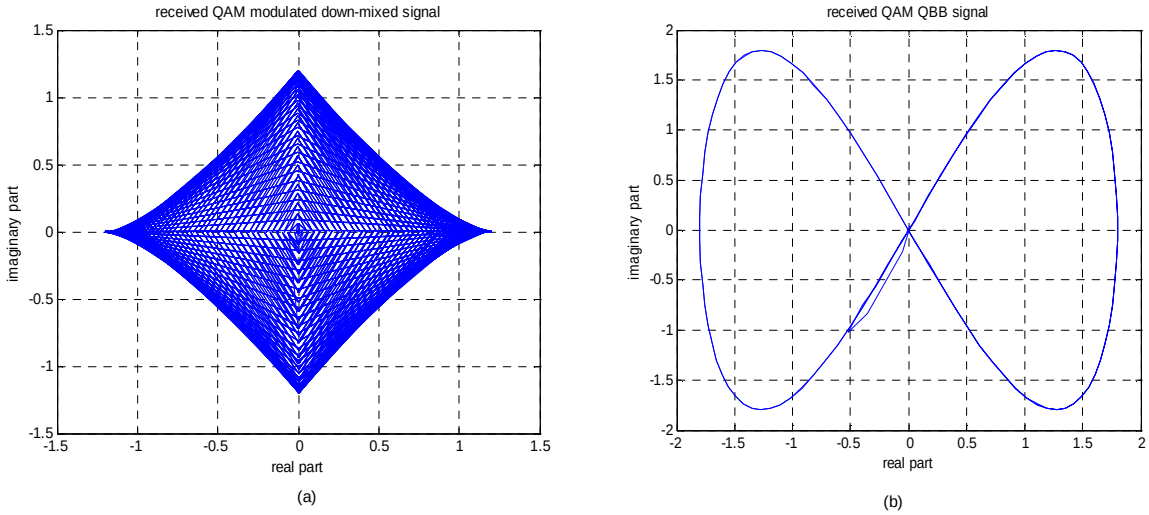

Figure 4.9: *Simulation results* **(a)** *Down-mixed received signal* **(b)** *QBB received signal before compensation..*

The figures below show the QBB signal after compensation and the demodulated output. It is seen that the original inputs were successfully retrieved from the multipath signal.

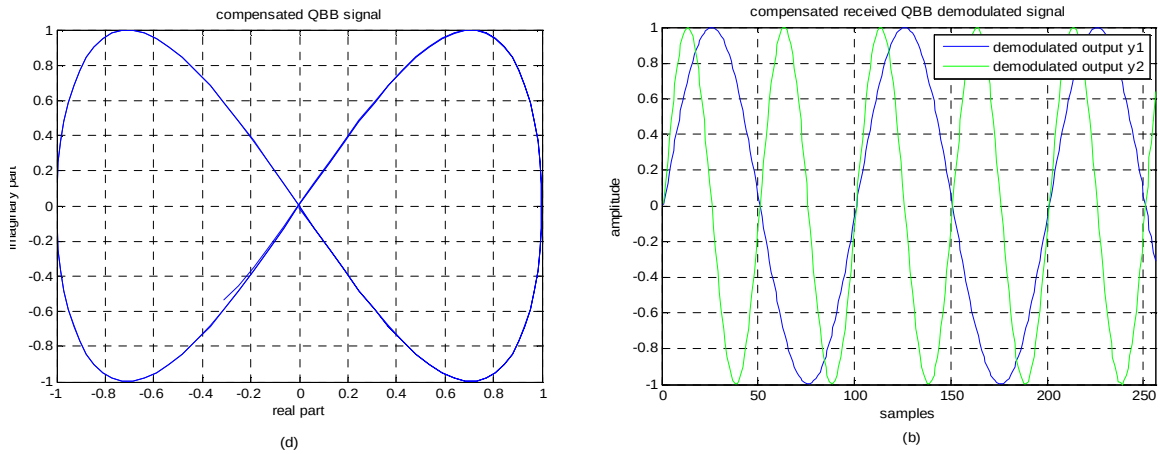

Figure 4.10: (a) *QBB signal after compensation* **(b)** *Demodulated compensated output.*

The compensated signal had the padded zeros, that were introduced in the generation stage, removed, and the original signal length was thus restored. The signal length was reduced by the downsampling factor 'n' and in this particular case, the demodulated signal outputs have a length of 256 samples the due to the downsampling factor being equal to 4. The figures on the next page show the demodulated outputs from the direct path signal demodulation for comparison purposes.

A difference plot is also given to further verify the compensation accuracy.

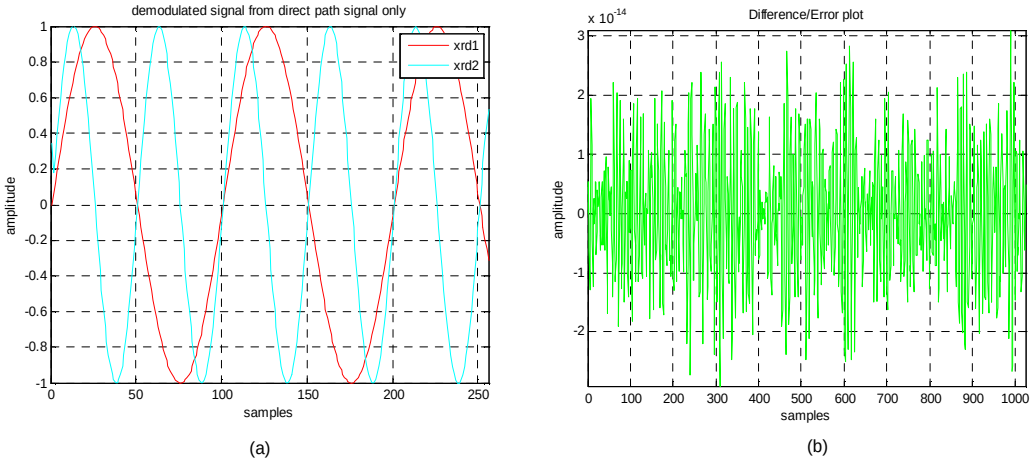

Figure 4.11: (a) *Direct path demodulated output:-forms the basis for comparison so as to determine the preciseness of the compensation process.* **(b)** *Difference/error plot:-indicates that the compensation was successful despite the error being slightly higher than for the previous analyses.*

4.5.1 Spectral Analysis

The spectral changes and results of the QBB compensation process are shown in the figures on the next page. The spectral changes do elaborate more on the compensation process and also show that the compensation process took place at quadrature baseband.

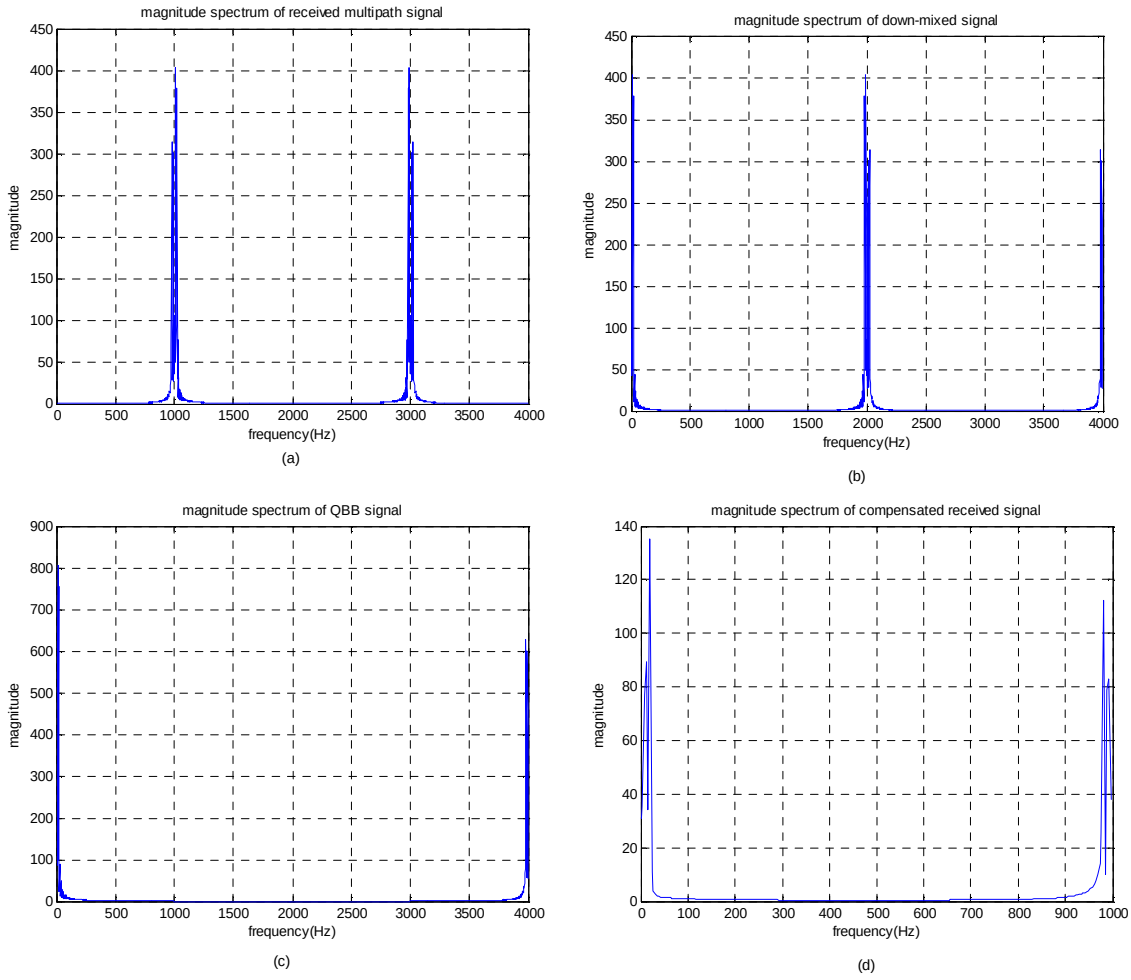

Figure 4.12: *Magnitude spectra plots.***(a)** *Received signal* **(b)** *Down-mixed signal* **(c)** *QBB downsampled signal* **(d)** *QBB downsampled compensated signal.*

The conversion process from RF to QBB has been outlined in earlier chapters. The down conversion of the sample rate is an important part of digital signal processing. The compensated signal spectrum is shown at quadrature baseband in Figure 4.12(d).

4.6 Simulation results:– FM RF compensation

This section continues the multipath compensation analysis but looks at FM modulated signals. The simulation results are given and discussed. It should be noted that the spectral analysis done in the previous QAM study does suffice in explaining the changes that will take place in under the FM analysis and hence referring back does suffice in explaining the current analysis so as to avoid repetition. The principles of the

compensation process carried out under QAM compensation remain the same under FM and therefore, it suffices to go straight to the actual simulation results. The figures below illustrate the simulation results obtained for compensation at RF. The sampling frequency used was 4000Hz and the number of samples was 1024. As done in the previous simulations, the parameter conditions used for the RF simulations are the same as those used for the QBB simulations so as to have a fair comparison between the two.

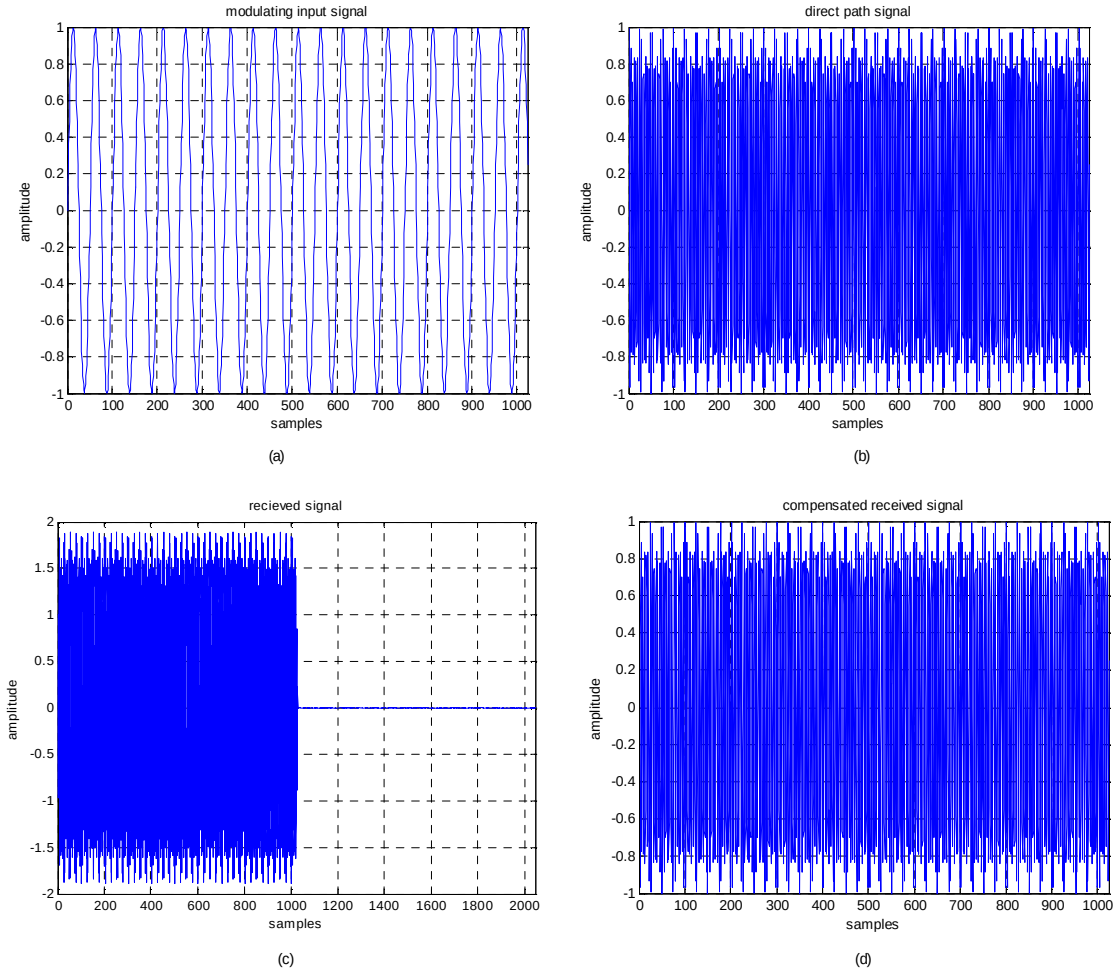

Figure 4.13: *Simulation results.* **(a)** *modulating signal* **(b)** *FM modulated input signal* **(c)** *Received signal:-comprises the actual signal with padded zeros* **(d)** *Compensated signal: the original signal is restored.*

From Figure 4.13(c) it is seen that the signal has 2048 samples of which the last 1020 are zeros and this is due to the zero padding that was done when carrying out the circular convolution. The delay in the FM analysis was 4 samples too and so the received signal had non-zero values up to 1028 samples. The compensation process effectively compensated for the multipath effects and therefore, the compensated signal

had non-zero values up to 1024 and the remaining zeros were eliminated to retain the original input signal length. The figures on the next page show the demodulated output resulting from the compensated signal and the direct path signal only and the difference plot between the demodulated compensated output and the direct path demodulated output**.**

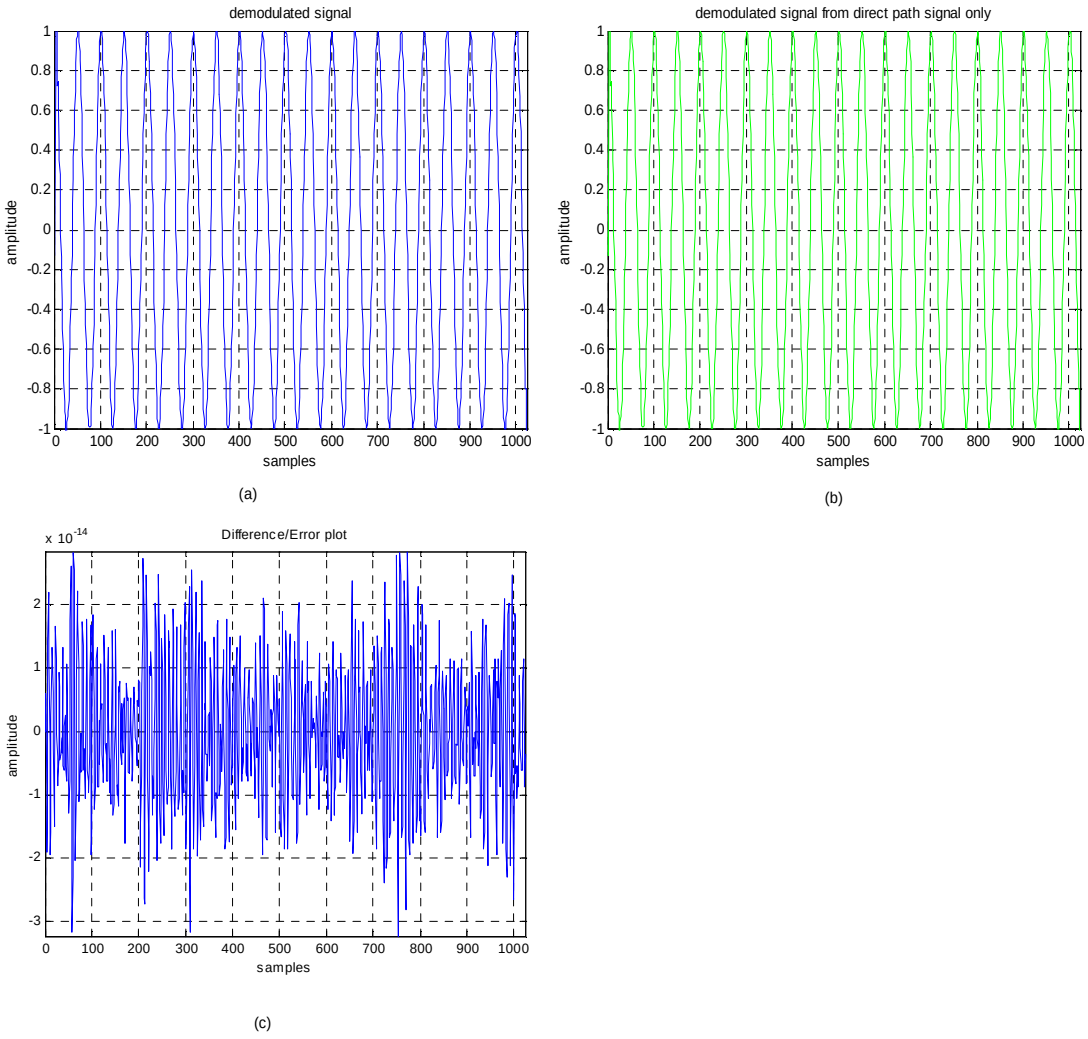

Figure 4.14: (a) *Compensated signal demodulated output*: *the compensated modulated output was demodulated and gives this signal output. The effectiveness or accuracy of the compensation process remains to be tested by demodulating the direct path signal with the same filter characteristics and compare the results.* **(b)** *Direct path signal demodulated output: this signal output facilitates for measuring of the accuracy of the compensation process by plotting its difference from the compensated demodulated out put.* **(c)** *Difference/error plot: shows a successful compensation was done.*

4.7 Simulation results:– FM QBB compensation

Here, we are again carrying out multipath compensation process but at QBB frequencies. The multipath compensation is also done at much lower sampling rates after carrying downsampling of the QBB received signal at baseband. The first four figures below represent the received signal, down-mixed signal QBB signal before compensation and after compensation. The FM modulated signal remains as given in Figure 4.13(b) and is therefore not shown. Referring back to the QAM QBB description of the above mentioned signals does suffice in describing the signals below taking note however, that the modulation being considered is FM.

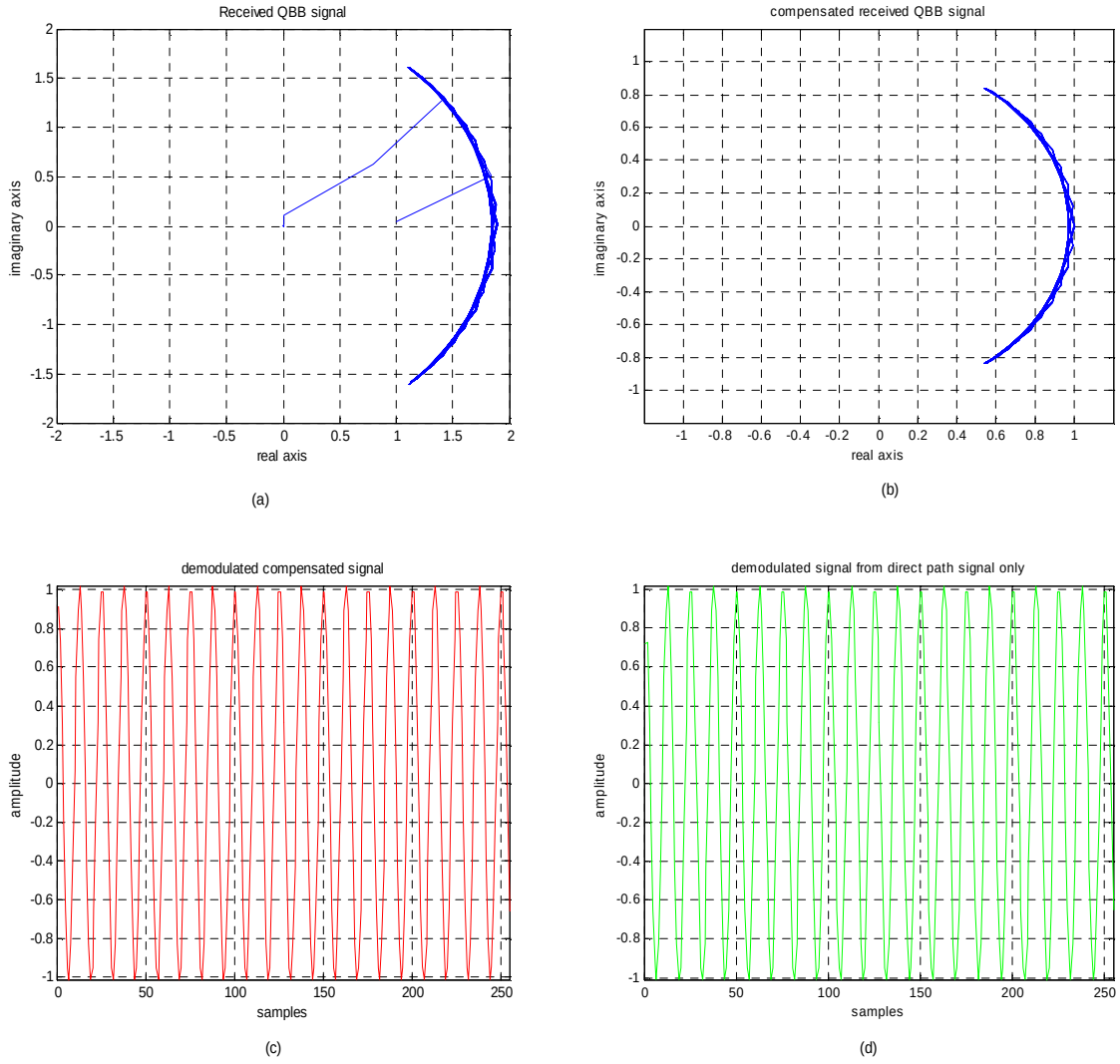

Figure 4.15: *Simulation results* **(a)** *QBB signal before compensation.***(b)** *Compensated QBB signal.* **(c)** *Compensated demodulated output* **(d)** *Direct path demodulated output.*

It is seen from Figure 4.15(c) and (d) that the direct path demodulated signal is similar to the demodulated output from the compensated signal.

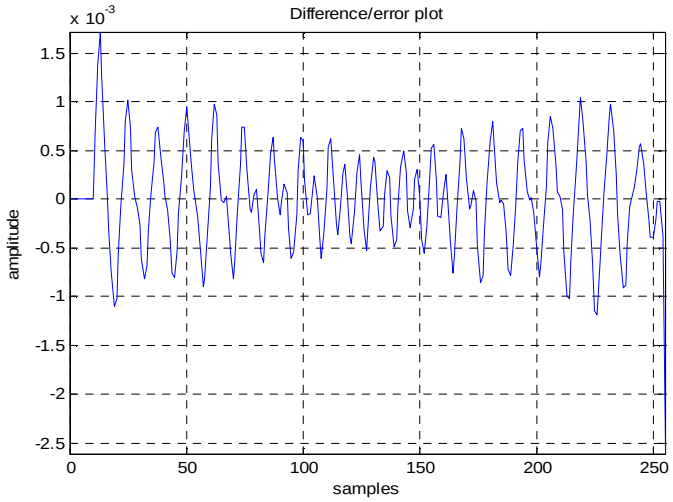

Figure 4.16: *Difference/error plot: shows that the compensation process was successful with insignificant mismatches expected at some points of the plot.*

The difference plot above does justify the accuracy and efficiency of the compensation. The spectral changes are as seen under the QAM case and therefore the explanation given earlier does suffice in explaining the expected spectral changes throughout the FM QBB multipath compensation process. Therefore, it suffices to fairly conclude that the multipath compensation has been successful and the error plot in itself serves as the *proof of compensation.*

4.8 Benefits of compensating for multipath at QBB

Having run the simulations and analyzed the results, it is necessary to consolidate the results by comparing the sample processing and sampling times as was done under beamforming. The table on the next page summarises the sample processing at RF and QBB for the multipath compensation simulation carried out for QAM modulation. The sample processing was derived from the simulation code in the same way as was done in the previous Chapter 3 for the AMDSB-SC RF/QBB simulations under beamforming and is given in Appendix C which contains the simulation M-Files too.

For the simulated QBB case, the number of samples reduces after the downsampling stage determined by the factor k.

Simulation Stages	**Radio Frequency**	**Quadrature baseband(simulated)**
Mixing down + QBB + Down sampling	____	$2N+2NLog_2 2N$ $2N+2kN$
Compensation process	$2N+ 2NLog_2 2N$ $2N+ 2Nlog_2 2N$ $2N+ N+ N$	$2kN+2kNLog_2 2kN$ $2kN+2kNLog_2 2kN$ kN
Demodulation	$2N + 2NLog_2 N+ N$ $2NLog_2 N + N$	_____
Total sample processing	$10N+4NLog_2 2N+$ $4NLog_2 N$	$2N+6kN+2NLog_2 2N+$ $4kNLog_2 2kN$
Total sample processing for N=1024 and k=1/4	98304	37632

Table 4.1: *Number of calculations at RF and QBB*

The value of N was 1024 representing the number of samples with the downsampling factor used for the simulation QBB case being equal to 4 (i.e. k=1/4). The sample processing result shows that more processing was done at RF than QBB. The sub-sampling done at QBB is the main reason for the reduction for the reduction in sample processing at QBB. The runtime time for each simulation was measured as illustrated earlier under beamforming. The simulation runtime comparisons given in the Table below show that the processing at RF equally took longer than the processing at QBB and this is due to the obvious reason that less samples were being processed for the QBB simulation. Therefore, the sample processing results serve as the theoretical verification of the actual simulation results. The table on the next page summarises the simulation runtime and sample processing for the RF and QBB simulations carried out.

	RF (t_{rf})	QBB(t_{qbb})	t_{rf}/t_{qbb}	N_{rf}	N_{qbb}	N_{rf}/N_{qbb}
Multipath compensation	Time in seconds		Ratio	Number of calculations		Ratio
QAM	0.02715	0.01025	2.65	98304	37632	2.61

Table 4.2: *Simulation runtime and number of calculations: RF/QBB ratio comparison.*

It is seen from the table that the discrepancy between the simulation and theoretical results is small (about 1.5%) and hence it suffices to say that the analysis carried out by the simulations was correctly done. The analogue real life QBB method should result in even further reduced calculations due to the fact that the real life situation assumes the processing of the signals at QBB already. Thus from Table 4.1, the number of calculations for the case at hand reduces to 10496 resulting in the ratio of the number of calculations at RF to those at QBB being equal to

$$\frac{N_{rf}}{N_{qbb}} = \frac{98304}{10496} = 9.37 \tag{4.14}$$

Thus we see a bigger reduction in the number of calculations for the analogue QBB case with the simulation processing time expected to follow suit. The limitation faced for the FM case is also encountered here for reasons explained earlier under the beamforming simulation result analysis. From the results obtained it is seen that compensating for multipath at QBB reduced the amount of processing carried out as compared to the RF case and consequently the simulation runtime was less for the latter which entails that processing at QBB was thus faster.

4.9 Conclusion

The chapter illustrated that multipath compensation is possible at baseband frequencies and there are benefits that come with operating at baseband which have been stressed already. The study analysis did bring to light another added advantage: the downsampling possibilities when operating at baseband. Therefore, latest baseband technologies will be *gaining* on costs and reduced operation complexity by implementing quadrature baseband multipath compensation. It was observed that the analysis started with a much higher sampling rate and at baseband, the sampling rate was reduced by a quarter and it should be noted that further reduction is possible and the furthest point the downsampling can go is at the point where aliasing begins to occur. However, it does suffice to say that QBB compensation surpasses RF compensation in terms of operational advantages. Multipath does have *remedies* and the traditional means of compensating for its effects have worked well over the years. However, increasing *technological awareness* has given room for further research of which Software defined radio technology stands out as the most prominent driving factor. The study was able to carry out simulation analysis and it has been verified that compensation at quadrature baseband can take place and indeed it comes with significant processing advantages which would make it more preferable to radio frequency compensation. Therefore, the study was worthwhile and relevant so as to verify the possibility and effectiveness of quadrature baseband multipath compensation for which we saw that we are able to downsample our signal during the analysis facilitating for much lower sampling frequencies and hence reducing the complexity [35] of the overall compensation process. The benefits are expected to pour down to SDR technologies which currently make use of baseband processing.

Chapter 5

Doppler Shift compensation-Simulation results

This chapter briefly outlines the Doppler shift theorem. The Doppler shift compensation process is also analyzed in general and simulation results from the compensation process for the QAM and FM modulation schemes are given and discussed. The proof of compensation is illustrated by the difference plot and this was done for each simulation. The simulation runtimes and number of calculations show how much more advantageous compensating for Doppler shift at QBB than at RF is. A much bigger gain in terms of simulation runtime and number of calculations is expected for the real life QBB scenario as will be shown from the benefits of working at QBB.

5.1 Doppler Shift

The Doppler effect refers to the change in frequency and wavelength of a signal as seen by a receiver moving relative to the transmission source [25]. The overall Doppler effect may therefore result from either motion of the source or motion of the receiver. Each of these effects is analyzed separately. For signals requiring a medium, such as light or gravity in specific relativity, only the relative difference in velocity between the observer and the source is worth considering. The figure below illustrates the Doppler effect.

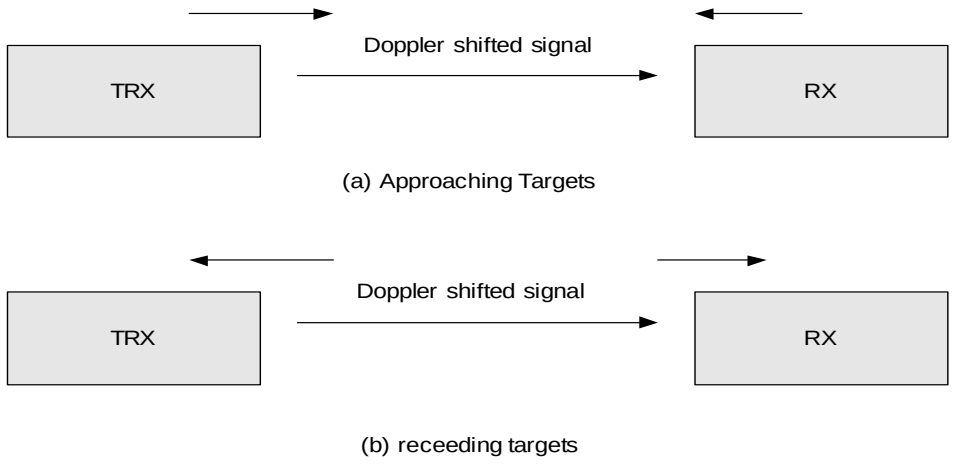

Figure 5.1: *Doppler Shift Model* **(a)** *Approaching Targets*: *result in a positive Doppler shift frequency.* **(b)** *Receding targets*: *results in a negative Doppler shift.*

In Figure 5.1(a) on the previous page the transmitter and the receiver approach each other resulting in a positive Doppler shift due to compression of the signal waveforms resulting in a higher received frequency. This is also referred to as a positive Doppler shift. In part Figure 5.1(b), the targets are receding from each other resulting in expansion of the received signal waveforms which results in a lower received frequency. This is referred to as a negative Doppler shift. Appendix B derives the Doppler shift frequency for a slowly fluctuating target. For analysis purposes, the Doppler shift used in the simulations was large enough so as to be able to see and analyze the spectral changes taking place. This assumption is an exaggeration of the real life situation in terms of the Doppler shift frequency size merely for analytical purposes. The assumption entails frequency shifting and not frequency scaling for the modeling of the Doppler signal.

5.2 Doppler shift model signal modeling

A Doppler signal can be modeled using frequency translation analysis in the time domain. Therefore, in order to successfully model a Doppler signal in MatLab, we need to fully understand the frequency translation or frequency shifting theorem [3]. Therefore, the next part of this section illustrates the frequency translation theorem in detail. The Doppler signal in our case is assumed to have a higher frequency than the original direct path signal and hence the transmitter and receiver are assumed to be approaching each other. This part of the study aims to compensate for Doppler shift at RF and compare and at QBB so as to show that it is equally possible to compensate for Doppler shift at quadrature baseband as it is done at RF. The RF and QBB theoretical analysis are given in the following sections of the chapter.

5.3 Theoretical analysis:- Doppler shift compensation at RF

Let x_d represent the direct path signal. The Doppler shifted version of the signal thus is given as

$$x_{dp} = x_d e^{j\omega_d t} \tag{5.1}$$

It must be noted that the received signal must be real and hence, the resulting complex signal from the multiplication above is transformed to a real signal. The Doppler

shifted signal is given below as

$$x_{dpr} = \mathrm{Re}\{[x_{dp}]_{FILTER}\} \tag{5.2}$$

At the receiving end, it is required that the frequency shift caused by the Doppler effect is compensated for by restoring the frequency spectrum to its original form. The Doppler shift compensation analysis structure was illustrated by means of a flow diagram in Chapter 2. Having modeled the Doppler shifted signal, it is thus required to compensate for the Doppler shift using an appropriate compensator. Considering the generation of the doppler signal model, it is seen that multiplication with $e^{j\omega_d t}$ shifts the direct path signal spectrum up by ω_d and so the compensator must be able to shift back the frequency spectrum of the received signal by the same amount so as to return the original frequency characteristics of the transmitted signal before the doppler effect occurred.

Let $h = e^{j\omega_d t}$ represent the Doppler shift channel and h_c the compensator transfer function both being in the time domain. It will be seen that in order to compensate for the Doppler shift, the compensator has to undo the effects of the Doppler shift channel on the direct path signal and therefore, the compensator turns out to be the inverse of the Doppler shift channel. Thus we have:

$$x_{dpr} = \mathrm{Re}[x_d h] \tag{5.3}$$

Let x_{dprc} represent the Doppler shift compensated received signal and h is related to h_c by the following expression;

$$h = h_c^{-1} = 1/h_c \tag{5.4}$$

Or

$$h_c = e^{-j\omega_d t} \tag{5.5}$$

Having formulated the compensator, we have our Doppler shift compensated signal given as

$$x_{dprc} = x_{dpr} h_c \tag{5.6}$$

Therefore, the compensated signal is the output of the multiplication between the received Doppler shifted signal and the compensator h_c and it is seen that the compensation takes place in the time domain. At this stage the resulting signal is still complex and hence the need to convert it to a real signal by filtering the higher frequency component and taking the real part as was done in the generation of the doppler shift signal. This is given below as

$$x_{rc} = \mathrm{Re}\{[x_{dprc}]_{FILTER}\} \tag{5.7}$$

At this stage, the compensated signal is ready for demodulation so as to retrieve the message signal. QAM/FM demodulation is then carried out resulting in the compensated demodulated output. The figure below summarizes the theoretical analysis discussed above.

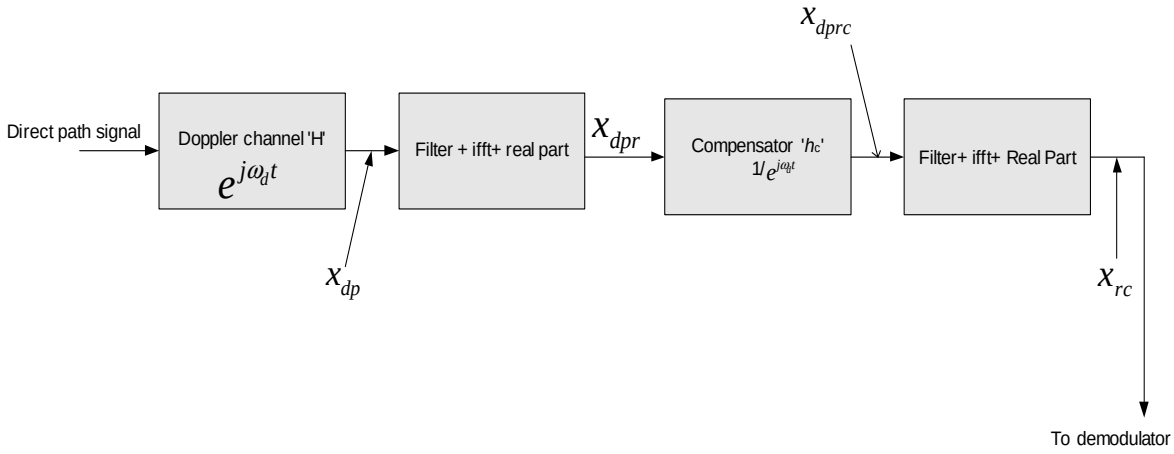

Figure 5.2: *Theoretical analysis general structure.*

The generation of the Doppler shift signal model remains the same as in the previous chapter with the difference being the compensation process. The aim of the study entails compensating at quadrature baseband and hence we will justify its possibility and compare the results with those from the RF process so as to show the accuracy of the compensation process.

5.4 Theoretical analysis:- Doppler shift compensation at QBB

The received signal x_{dpr} is mixed down at the receiver giving us the received down-mixed signal given as

$$x_{dprdm} = x_{dpr} e^{-j\omega_c t} \tag{5.8}$$

where x_{dprdm} denotes the Doppler received down-mixed signal. The down-mixed signal is then lowpass filtered resulting in the QBB signal x_{dprqbb}.

$$x_{dprqbb} = [x_{dprdm}]_{LPF} \tag{5.9}$$

The Doppler QBB Doppler compensation process does allow for downsampling to be incorporated and in this case it is implemented at this stage. The downsampling is implemented as done in previous analysis. This should equally be done for the compensator.

$$x_{dprqbbds} = x_{dprqbb}(1:n:end) \quad \text{and} \quad h_{cds} = h_c(1:n:end) \tag{5.10}$$

where $x_{dprqbbds}$ represents the quadrature baseband Doppler shifted down sampled signal and h_{cds} the downsampled compensator. The compensation then proceeds as shown in below:

$$x_{rc} = x_{dprqbbds} h_{cds} \tag{5.11}$$

It will be interesting to note that the same compensator used at RF is used at QBB. However, QBB provides even further advantages in that there is no need to carry out any further filtering unlike in the RF process so as to have our real demodulated output signals. This will be seen from the simulation results. This is in itself a big advantage of the QBB Doppler shift compensation process because the number of processing stages will reduce which in turn reflects in reduced costs and complexity of equipment. Demodulation then follows resulting in the demodulated outputs.

The figure below summarizes the theoretical analysis showing the expected signals at different points of the analysis.

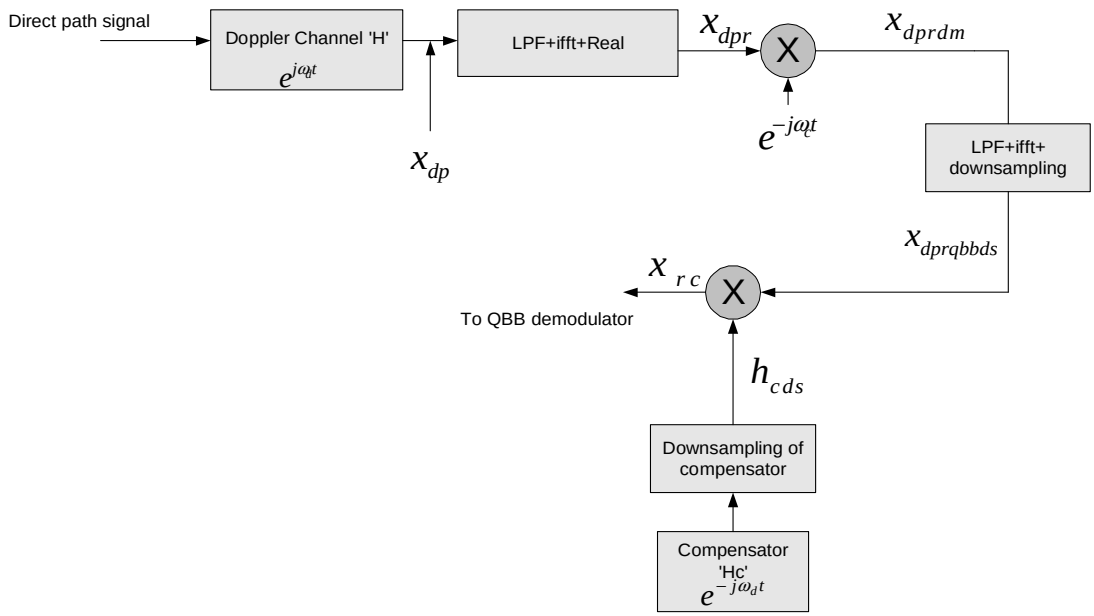

Figure 5.3: *Theoretical analysis block diagram for compensation at QBB. The signal outputs at various points of the analysis are given.*

5.5 Simulation Results:- QAM RF compensation

The figures below show the simulation results obtained for the RF Doppler shift compensation. The sampling frequency used was 4000Hz and the number of samples was 1024.

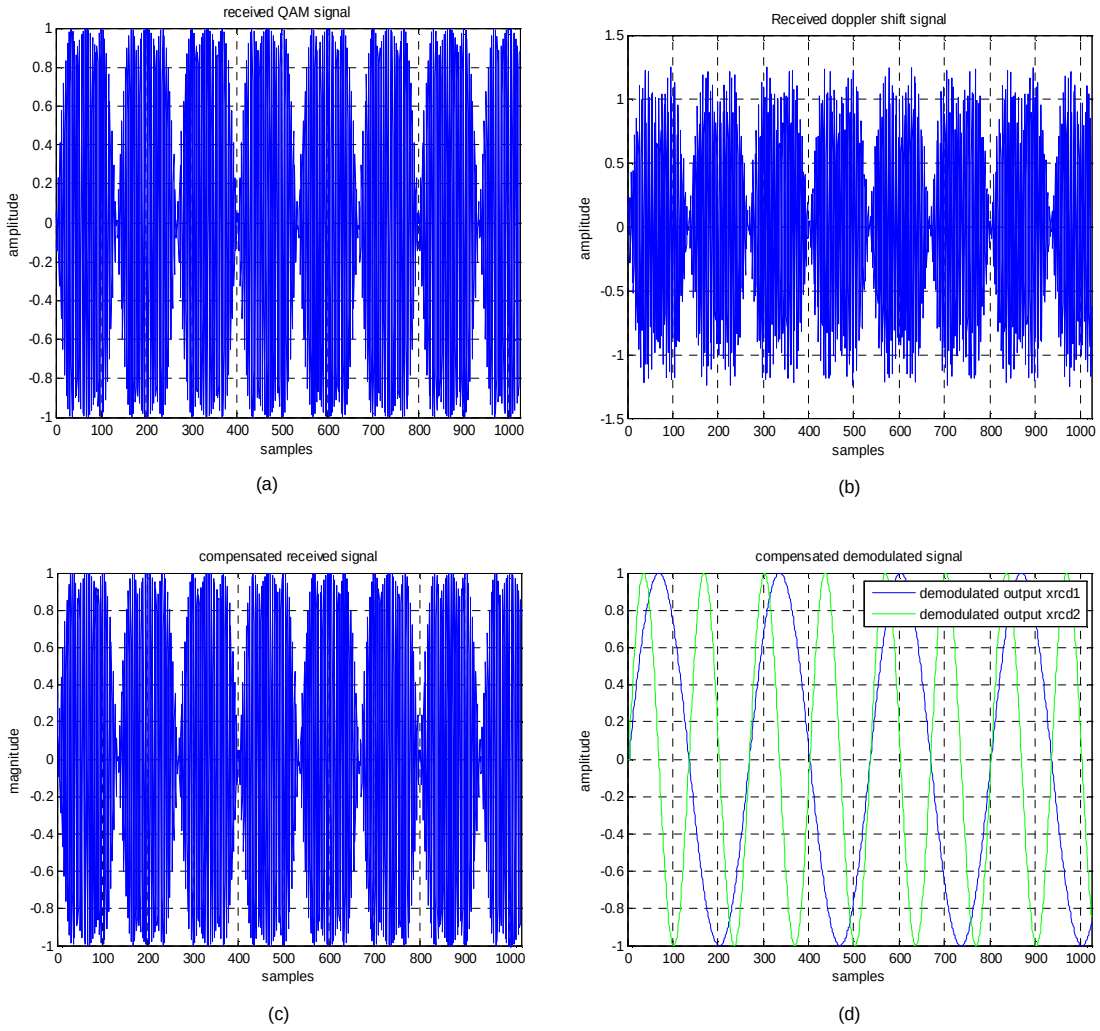

Figure 5.4: (a) *QAM direct path signal* **(b)** *QAM doppler shifted signal* **(c)** *Compensated output signal* **(d)** *Demodulated compensated output signal.*

From the plots given above, it is seen in figure 5.4(b) that the Doppler shift caused a change in the received signal amplitude. The compensation process retrieved the original direct path signal from the Doppler shifted signal as shown in figure 5.4(c). The demodulation then followed resulting in the demodulated outputs denoted as x_{rcd1} and x_{rcd2} in Figure 5.4(d). The proof of an accurate compensation process was given by the difference plot which according to Figure 5.5 (b) on the next page shows a

successful and accurate compensation process.

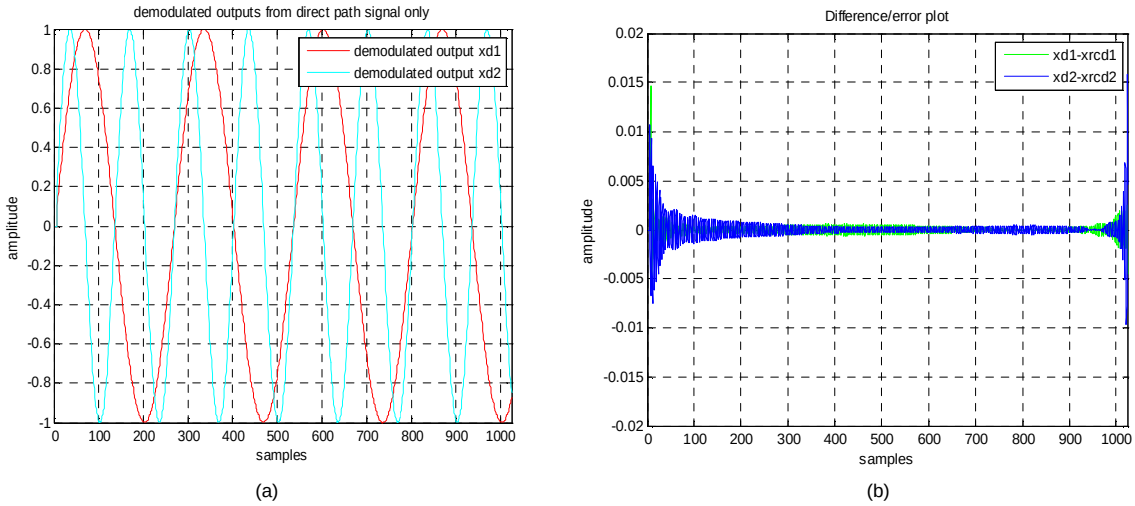

Figure 5.5: (a) *Direct path demodulated output:- the inphase and quadrature phase demodulated outputs are denoted as xd1 and xd2 respectively.* **(b)** *Difference plot:- shows that the compensation was with minimal error.*

Spectral analysis:- RF

The spectral analysis of the frequency spectral changes taking place in the whole compensation process is given and discussed in this part of the chapter. Figures 5.6 (a), and (b) below represent the spectral changes from the QAM signal down to the Doppler shifted signal model.

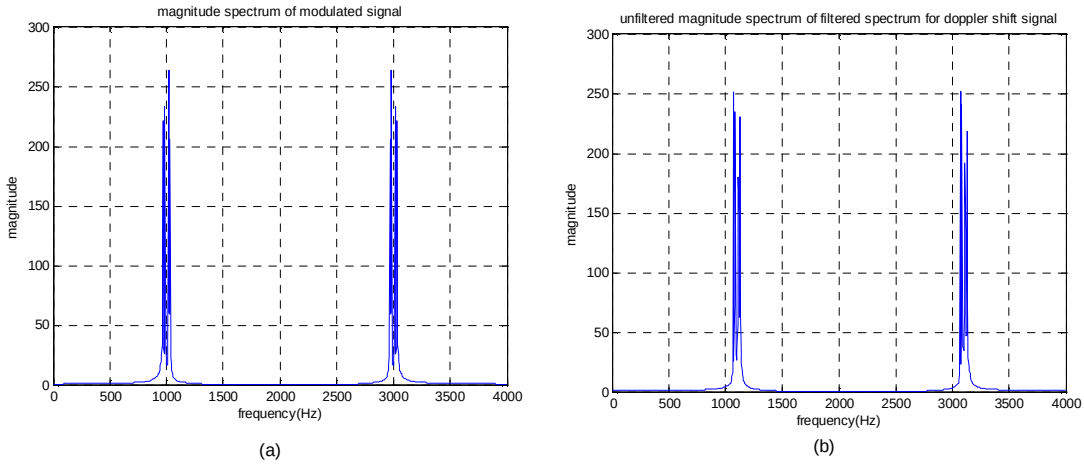

Figure 5.6: (a) *QAM direct path signal spectrum* **(b)** *Frequency shifted QAM signal.*

The direct path signal was multiplied with $e^{j\omega_d t}$ which shifted the spectrum up by ω_d which represents the Doppler shift. However, it is seen that this is not a true model of a typical Doppler spectrum because the spectrum is reflective of a complex signal and therefore, we have to transform this spectrum into a real Doppler shift signal spectrum. This is done by filtering out the spectral component that sits at 3100Hz and then taking the real part of the remaining component so that they eventually sit at 1100Hz and 2900Hz so as to have a real Doppler shifted signal spectrum. The Doppler shift frequency has been exaggerated for analytical purposes so as to be able to see the spectral changes clearly. In reality, this shift is much smaller but significant enough to cause reasonable signal distortions. Figure 5.7(a) below illustrates the filtered part of our signal spectrum which leaves the component at 1100Hz and taking the real part results in the symmetrical spectrum shown in Figure 5.7(b) which is reflective of a true Doppler shifted signal model.

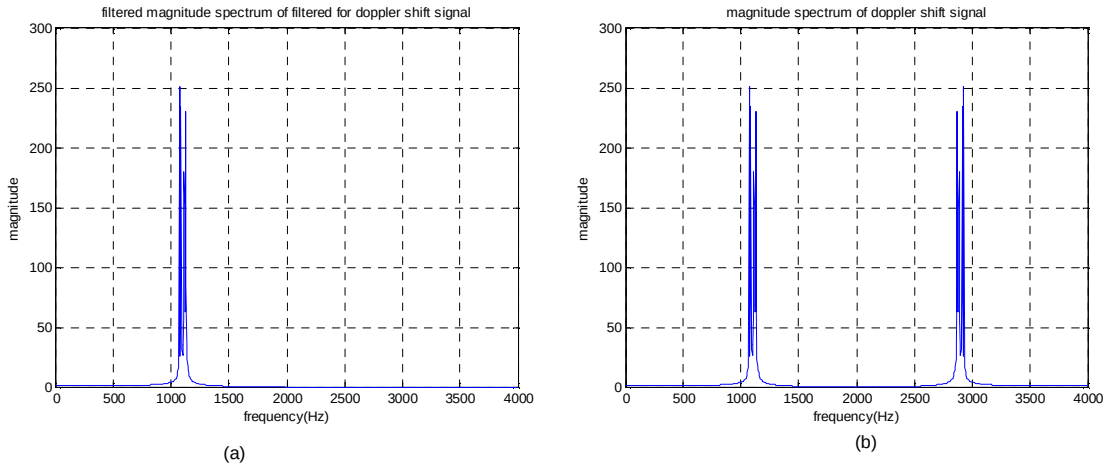

Figure 5.7: *Spectral plots.***(a)** *Filtered signal spectrum:- this is done to create a spectral representation of a real doppler shifted signal.* **(b)** *Doppler shift signal spectrum:- the Doppler shifted signal spectrum is even and hence it is now representative of a real Doppler shifted signal.*

Having seen the Doppler shifted signal spectrum the analysis focuses on the compensation and aims to verify whether the original signal spectrum is retained by the compensation process. The theoretical analysis did explain the compensation process and the graphical simulation results do verify the theoretical expectations. In Figure

5.8(a) below, it is seen that that the compensator managed to successfully shift down the lower frequency component of the Doppler shifted signal spectrum to 1000Hz with the higher frequency component moving down to 2800Hz. At this stage, we have a complex signal output. Therefore, the filtering process that occurred earlier is repeated as this stage so as to have a real compensated signal output in readiness for the demodulation process. Thus the 2800Hz component was filtered out as shown in Figure 5.8(b) and taking the real part results in the Doppler shift compensated signal spectrum in Figure 5.8(c). This is a real signal spectrum due to its symmetrical properties. A comparison between the compensated signal spectrum and original signal spectrum shows that the original spectrum was restored. This further verifies the accuracy of the compensation process carried out and the analysis in the next section looks at the quadrature baseband way of compensating for Doppler shift in a signal.

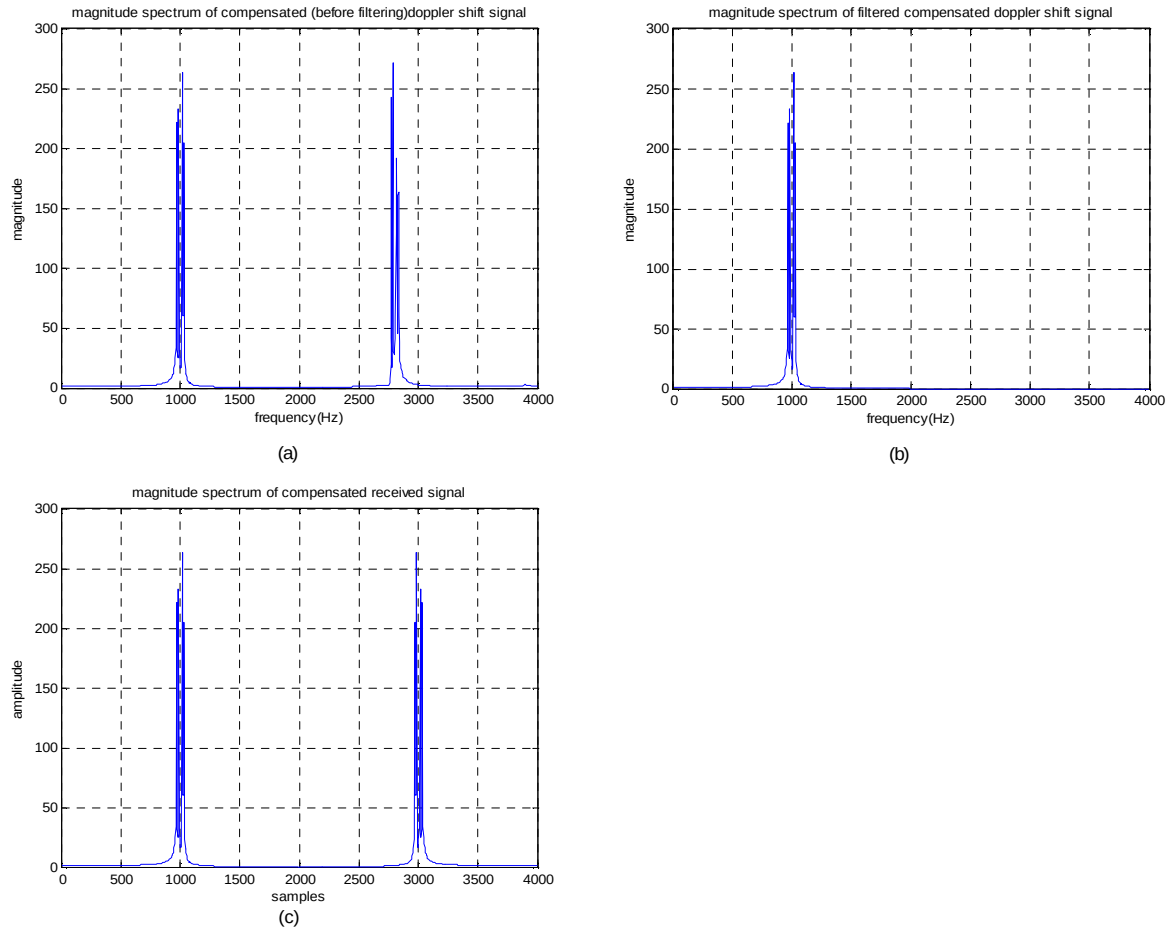

Figure 5.8 *Magnitude spectra plots* **(a)** C*ompensated complex signal spectrum* **(b)** *Filtered compensated signal spectrum* **(c)** *Real compensated signal spectrum*: *it is seen that the original spectrum has been restored.*

5.6 Simulation Results:- QAM QBB compensation

The simulation analysis results are given and discussed below. The same parameters used for the RF simulation were used for the QBB simulation too.

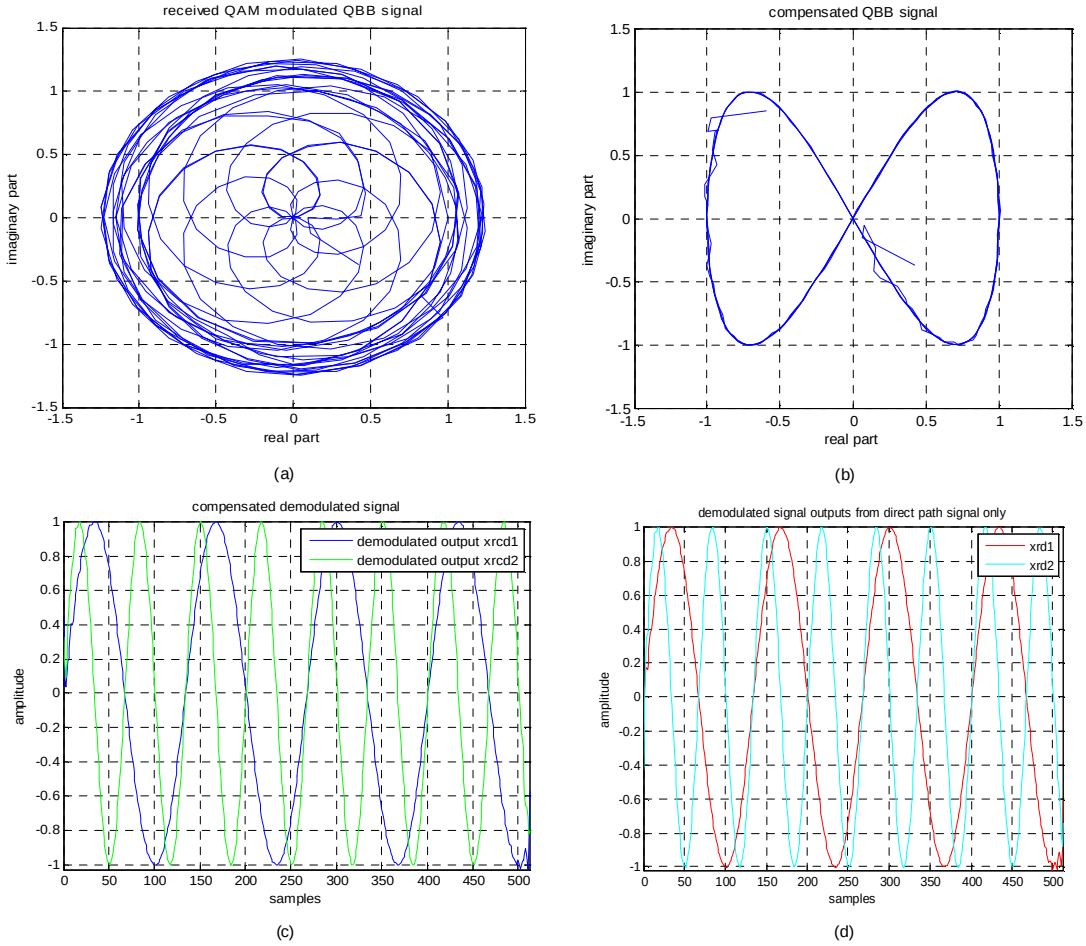

Figure 5.9: *Simulation plots.* **(a)** *QBB received signal* **(b)** *Compensated QBB signal* **(c)** *compensated* d*emodulated output*. **(d)** *Direct path demodulated output*.

Figure 5.9(a) represents the quadrature baseband version of the received signal. The signal was then downsampled by a factor of '2' resulting in a 2-fold sample reduction from 1024 to 512. The compensator is downsampled to so as to adequately compensate for the Doppler shift in the downsampled QBB received signal. Thus, sample processing is reduced for the QBB case and this could translate to a much faster operating speed or less operating time as will be shown in the concluding part of the chapter. The compensation then followed resulting in the compensated QBB signal in

Figure 5.9(b) on the previous page. At this stage, it is interesting to note that there is no need for any filtering so as to come up with a real doppler shift compensated signal spectrum as was done under the RF Doppler compensation analysis because the signal sits at QBB and QBB demodulation is able to retrieve the original input from the complex QBB signal spectrum. This further entails reduced processing under this the QBB and hence presents a significant advantage of this method of Doppler compensation. Below is shown the difference plot resulting from a numerical comparison between the compensated demodulated output in Figure 5.9 (c) and the direct path demodulated output. It is seen that again, the compensation was a success.

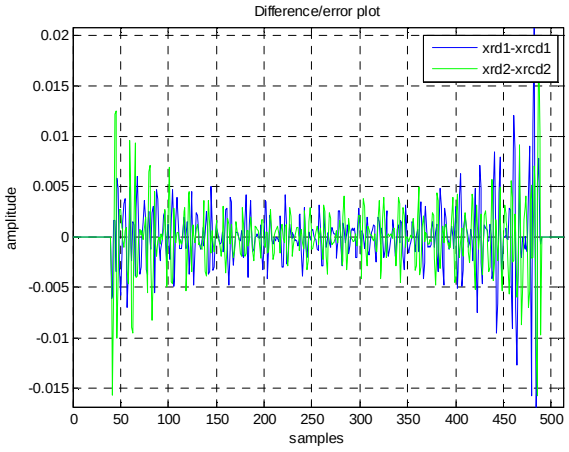

Figure 5.10: *Difference plot: shows the numerical difference between the direct- path demodulated signal and the compensated demodulated output.*

Spectral analysis:- QBB

Figure 5.11 on the next page illustrates the spectral changes taking place for under the QBB analysis process. Figure 5.11(a) represents the Doppler shifted signal spectrum. Figure 5.11(b) shows the spectral components shifted down after the down-mixing process and converted to QBB by lowpass filtering resulting in the spectrum shown in Figure 5.11(c). It is seen that the number of samples has reduced by a factor of 2 due to the reduction in the sampling rate by a similar factor. Figure 5.11(d) shows the compensated signal spectrum plotted in terms of the samples so as to show the sample reduction that took place. It is also seen from the figure that the Doppler shift has been eliminated hence restoring the original spectrum which is now at quadrature baseband which provides evidence of a successful compensation process.

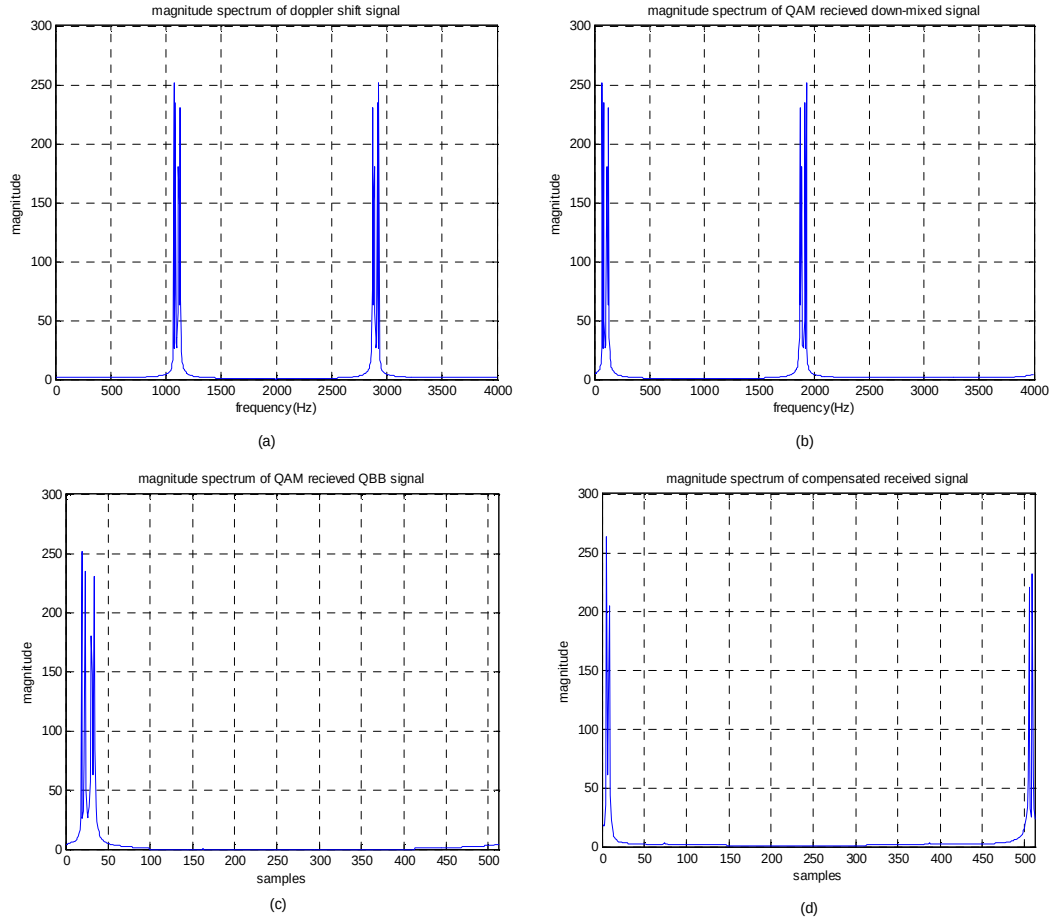

Figure 5.11: *Magnitude spectrum of* **(a)** *Doppler shifted signal* **(b)** *Down-mixed signal* **(c)** *QBB downsampled signal: the downsampled signal results in an equal reduction in the number of samples to 512* **(d)** *Compensated signal at QBB.*

The Doppler shift compensation analysis continues in the following section but in this case, the modulation scheme being analyzed is Frequency modulation. The Doppler shift compensation will be analyzed for the RF and QBB cases.

5.7 Simulation results:-FM Doppler shift compensation at RF

The simulation results are given and discussed below. The sampling frequency was 4000Hz and the number of samples was 1024.

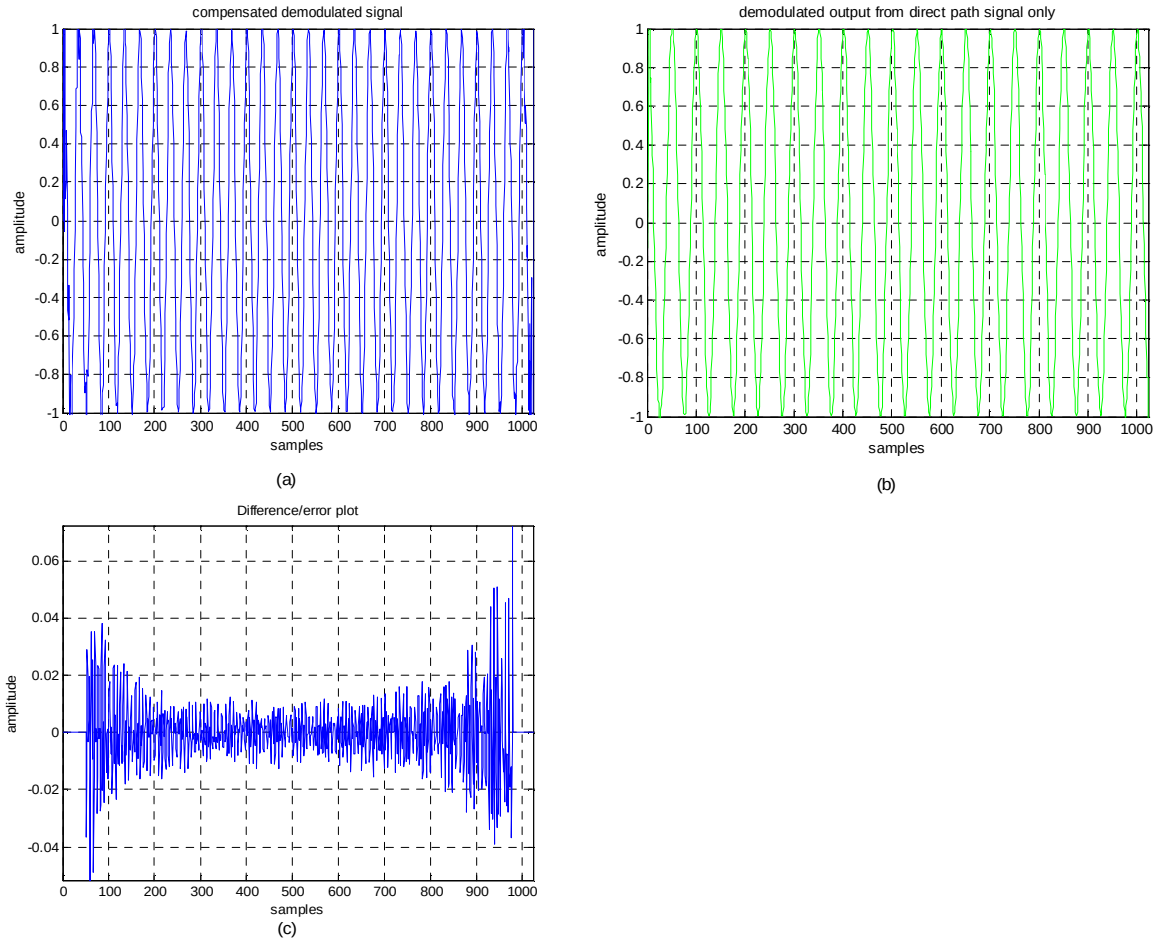

Figure 5.12: (a) *Direct path demodulated FM signal* **(b)** *Compensated output signal*:- *the successful compensation process does manage to eliminate the Doppler shift effects and restores the original modulated signal.* **(c)** *Difference/error plot.*

The simulation results given above show that the compensation was successful since the original direct path signal was retrieved. The figures on the next page show the direct-path demodulated output and difference plot to further prove the accuracy of the compensation process.

Therefore, it can be concluded from the difference plot that the compensation was successful with the error being minimal.

5.8 Simulation results:-FM Doppler shift compensation at QBB

The figure below illustrates the graphical simulation results of the Doppler shift compensation analysis. The simulation input parameters remain the same as those used in the RF simulation. The compensation process at QBB was already outlined under the QAM QBB case and therefore, referring back does suffice in explaining the compensation process under the current FM QBB analysis.

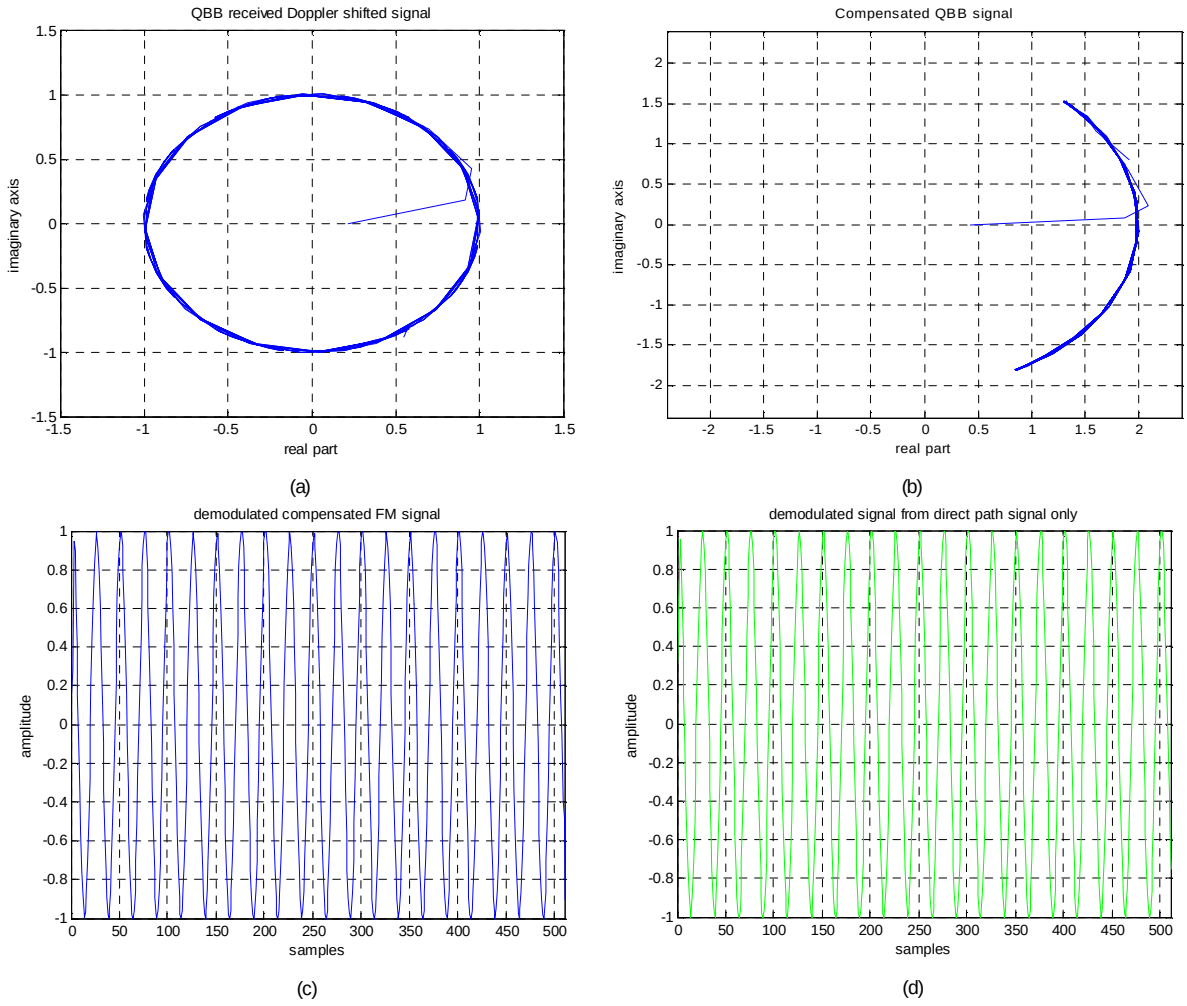

Figure 5.14: *Simulation plots* **(a)** QBB r*eceived doppler shifted signal* **(b)** *Compensated QBB signal* **(c)** *Compensated demodulated output* **(d)** *Direct-path demodulated output.*

It can be seen that there is a clear contrast between the QBB Doppler shifted received signal in Figure 5.14(a) and the compensated QBB signal in Figure 5.14(b) and this shows the severe effects of the Doppler shift. As done under the QAM analysis, downsampling was carried out and the compensated demodulated and direct path demodulated outputs both show a 2-fold reduction in the number of samples (i.e from 1024 to 512). The figure below shows the difference plot between the two outputs given in Figure 5.14(c) and (d) on the previous page. It is seen that the compensation process at quadrature baseband has been a success and thus motivates the purpose of the study in that it has been seen that compensation at QBB is carried out successfully with less sample processing and this will be shown in the conclusion of the chapter.

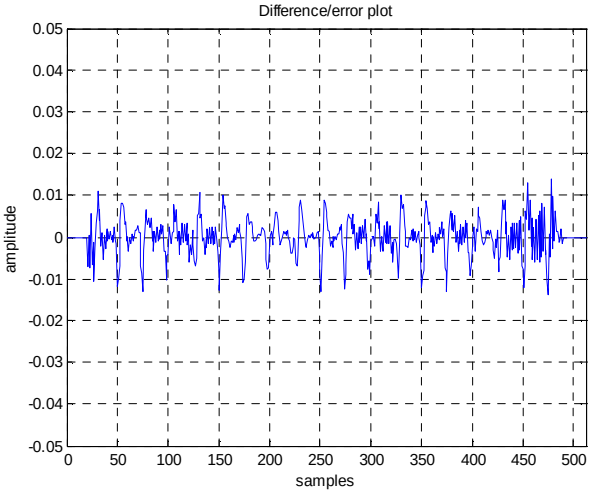

Figure 5.15: *Difference/error plot.*

The following section of the chapter summarises the benefits observed from the simulations carried out at RF and QBB.

5.9 Benefits of compensating for Doppler shift at QBB

The core advantage of compensating at QBB remains as discussed earlier and therefore as was done under multipath and beamforming, the simulation processing time and amount of processing, ratio at RF and QBB are compared so as to see the discrepancy between the theoretical prediction and actual simulation results. The table on the next page summarize amount of sample processing at RF and QBB for the QAM simulation.

It should be noted that the FM simulation sample processing evaluation did face the same constraints faced under the beamforming and multipath analysis.

Simulation Stages	**Radio Frequency**	**Quadrature baseband**
Mixing down + QBB + Down sampling	____	$N+N\text{Log}_2N$ $N+ N\text{Log}_2N+kN$
Compensation process	N $N+ 2N\text{Log}_2N$	kN kN
Demodulation	$2N+N\text{Log}_2N+N$ $N\text{Log}_2N+N$	_____
Total sample processing	$6N+4N\text{Log}_2N$	$2N+3kN+2N\text{Log}_2N$
Total sample processing for N=1024 and k=1/2	47104	24064

Table 5.1: *Sample processing for QAM at RF and QBB. This was derived from a step-by-step representation of the processing done at RF and QBB by the MatLab simulations in terms of* N *and* k.

From the table above it is seen that there was less processing at QBB than at RF which is expected to verify the simulation runtime measured in MatLab by appropriate commands. The real life QBB method in this particular case reduces the number of calculations to 3kN which has a numerical value of 1536. The ratio of the number of calculations at RF to those at QBB is thus given as:

$$\frac{N_{rf}}{N_{qbb}} = \frac{47104}{1536} = 30.7 \tag{5.12}$$

Here we see a much bigger increase in the ratio which concludes that operating at QBB does indeed result in a reduction in the number of operations which implies reduced amount of processing and reduced processing time. It should be emphasised again that this is just but a small picture of the real world situation where millions of samples are processed in much bigger and complex systems but like every other study, we aim to show that indeed, the model simulations do give an insight into

the actual real life situation. The table below summarises the results obtained in terms of simulation time and sample processing. As was encountered in the previous analysis, the simulation runtime ratio and number of calculations was done for the QAM case only whose results are given in the table below. For the FM case, despite the limitation faced, it was still seen from the simulation runtime that the QBB processing was faster.

	RF (t_{rf})	QBB(t_{qbb})	t_{rf}/t_{qbb}	N_{rf}	N_{qbb}	N_{rf}/N_{qbb}
Doppler shift compensation	Time in seconds		Ratio	Number of calculations		Ratio
1. QAM	0.00119	0.00062	1.92	47104	24064	1.96
2. FM	0.005664	0.005056	1.12	-	-	-

Table 5.2: *Simulation processing time and sample processing ratio summary*

The results show that there was a small discrepancy (about 2.1%) between the simulation runtime ratio and the sample processing ratio caused by the computer processing time which had a small variance each time the simulations were run. The programs are almost instant in terms of the simulation runtime and hence the significantly small value of the runtime values given in the table.

5.10 Conclusion

The chapter introduced the compensation process and a theoretical analysis of the compensation process was given. It was seen that the filtering process was needed both during the generation stage of the doppler shift signal as well as at the compensation stage so as to compensate for the errors introduced during the generation and compensation stages. It thus suffices to say that the compensation was successful as can be seen from the difference plots. The simulation processing time and sample processing also showed that it is more beneficial to compensate for Doppler shift at QBB as compared to the traditional RF method. The reduction in the amount of processing is much more for the real life quadrature baseband case and this translates to reduced processing time too. Therefore, it can be safely concluded that the QBB way of compensating results in less processor load and hence less processing time elapses.

Chapter 6

Multiple compensation- simulation results

This chapter now considers a scenario where the received signal comprises multiple input signals. This is a case where we have a single antenna with multiple inputs but with a single output. The compensation is expected to be carried out at the simultaneously for both multipath and Doppler shift and the obtained results will be discussed and analyzed. Is it possible to compensate for multipath and Doppler shift at the same time? The chapter should answer this question. It will be interesting to see how the simulation runtimes and amount of processing differ for the RF and QBB cases.

6.1 Signal modelling

The received signal for the case at hand comprises the following signals:

(i) Direct path
(ii) Multipath
(iii) Doppler shift
(iv) Multipath + Doppler shifted signal

The received signal is thus the sum of these 4 signals. The figure below shows a model for the analysis under discussion in this chapter.

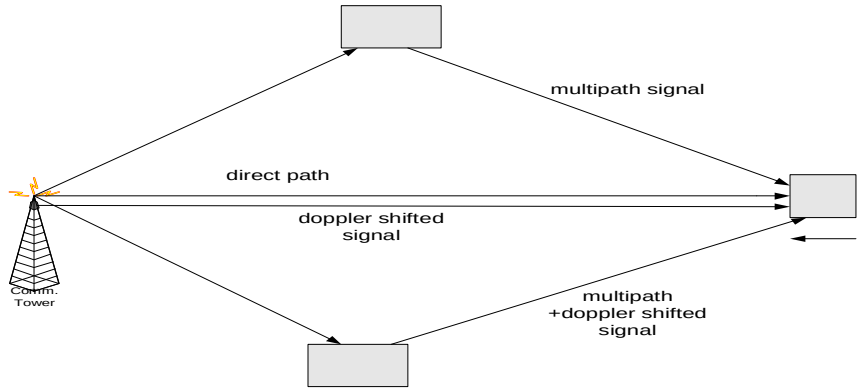

Figure 6.1: *Multiple Signal reception model*

In this part of the study, it is required to compensate for the multipath and Doppler shift at the same time. This presents a very interesting and complex scenario. However, simulating the received signal does not present any difficulty. The compensation process is required to undo the changes brought about by the multipath and Doppler shifts. Taking the direct path received signal x_d as the reference, the multipath and Doppler shift signals should be easily simulated as was done in the previous analysis. In order to generate a signal that has both multipath and Doppler shift effect, we can generate the delayed signal first and then introduce a Doppler shift to the signal or vice-versa. The question arises as to what is the correct way of simulating the combined multipath and Doppler shifted signal. The correct procedure of simulating the required multipath and Doppler shifted signal is to generate the delayed signal first followed by subjecting it to a Doppler shift [26]. Coming to the case at hand, a theoretical analysis of the problem is given which will form the basis for simulating the compensation process in MatLab. Whereas in the multipath and Doppler shift analysis, we had the compensator being the inverse of the channel transfer function, we will find out whether reciprocity exists between the channel and the compensator for this case. It is required that the whole analysis be theoretically and mathematically verified so as to see the processing taking place in terms of theoretical and mathematical models. Therefore, the theory will derive expressions for the four input signals before going into the actual analysis process. The multipath and Doppler shifted signals are generated as outlined in the previous chapters. The received signal in the time domain is given as

$$x_r = x_d + x_{mp} + x_{dp} + x_{mpdp}. \tag{6.1}$$

The equation above written in the frequency domain is given below as

$$X_r = X_d + X_{mp} + X_{dp} + X_{mpdp} \tag{6.2}$$

We intend to compensate for the multipath and Doppler effects so as to retrieve the direct path signal from the received signal. The direct path is related to the received signal by the following expression:

$$X_d = X_r.H_c = X_c \tag{6.3}$$

where X_c denotes the compensated signal which is the direct path signal itself.

The figure below illustrates the received signal generation structure model.

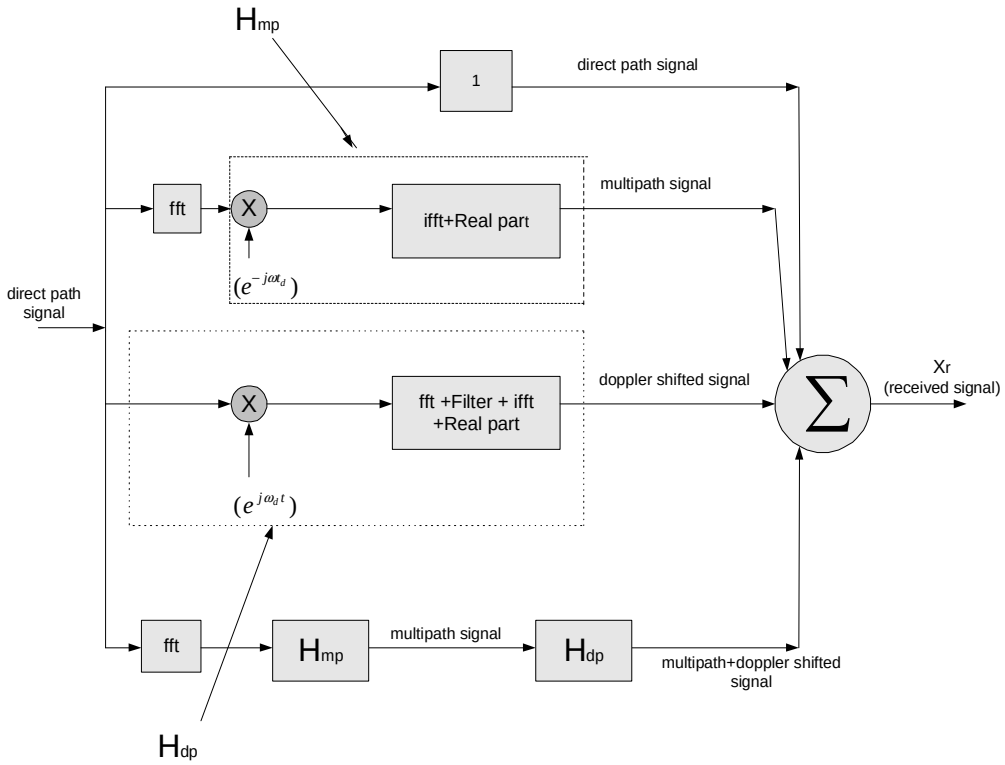

Figure 6.2: *Received signal generation structure.*

For the analysis, it was seen that the received signal did turn out to be complicated and not linear because and the direct path signal could not be extracted from the final equation hence providing the main hindrance to compensating for multipath and Doppler shift at the same time. The reason for this is that the received signal spectrum does not allow for isolation of the multipath and Doppler components from the spectrum due to the Doppler shift frequency being less than the signal bandwidth. It is seen that the received signal does show properties of non linear time-invariancy [18, 28] as illustrated mathematically below.

Neither

$$x_d = x_r * h_{eff}$$
$$nor \qquad (6.4)$$
$$X_d = X_r . H_{eff}$$

Thus a mathematical analysis did fail to isolate X_d through the use of an effective compensator transfer function denoted as 'H_{eff}'. It is however possible to compensate

using simulation provided the bandwidth is less than the doppler shift which is considered in the following section under what will be termed the 'special case'.

6.2 Special Case

A special case that will be discussed is that of compensating when the Doppler shift is much larger than the signal bandwidth. This means that there is a clear frequency separation between the direct path, multipath and combined multipath and Doppler shifted signal. Consider the figure below showing one half of the spectra for the special case being discussed.

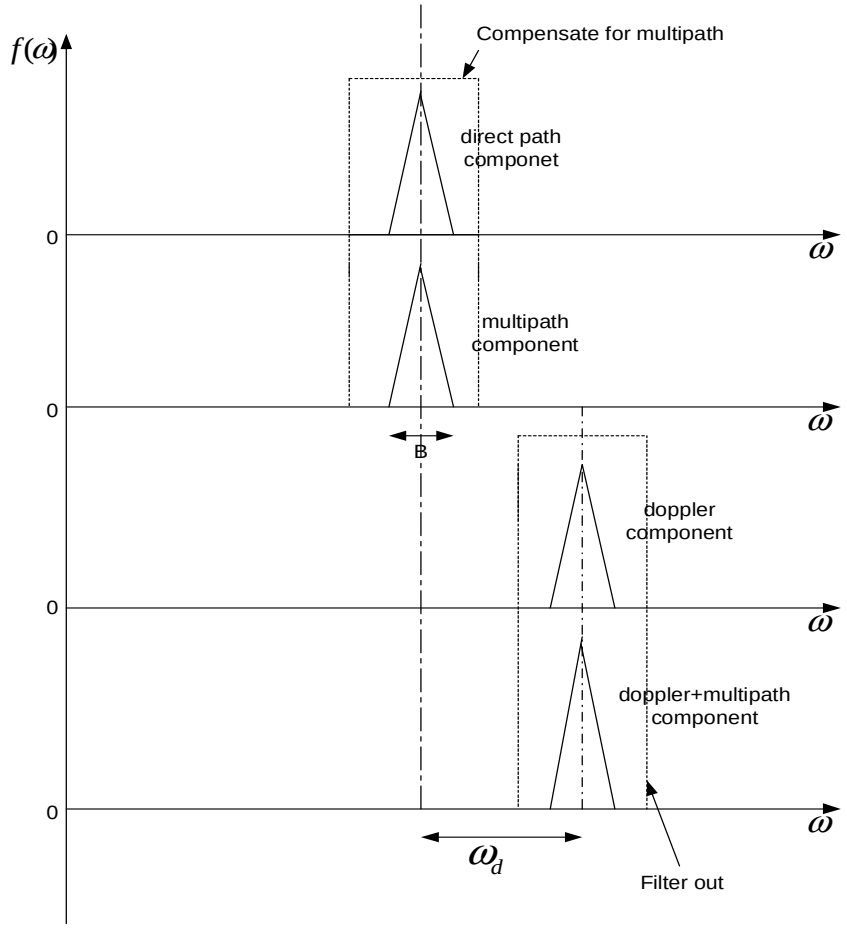

Figure 6.3: *Spectra of input signals for special case*.

From the figure above, it is seen that in a case where the Doppler shift is large enough, it is possible to carry out compensation for the multiple input signal case through the use of filtering. This entails that the filter eliminates the Doppler signals and the

combined multipath and Doppler shifted signals leaving the multipath and direct path signal from which the direct path signal can be retrieved because the simulation now reduces to a multipath compensation case which was handled already under multipath compensation. The main condition applied to the case above is that the signal band width ought to be less than the Doppler shift (i.e $\omega_d > B$). The filter leaves us with the direct and multipath signal and therefore, the required direct path signal can eventually be extracted using multipath compensation. The same special case scenario would apply when the Doppler shift is much lower than the bandwidth of the signal. Therefore, it suffices to say that philosophical ways of carrying out compensation can be deduced but with specific conditions applied in each case.

6.3 Simulation Results

Figure 6.4 below shows the combined multipath and Doppler signal with its spectrum. This signal is a time and Doppler shifted version of the direct path signal. The signal was delayed in time first and then Doppler shifted. This signal brought about the complexity of the compensation process and thus it was not possible to come up with a combined transfer function from which X_d would be extracted from the received signal. The signal and its magnitude spectrum are shown in the figure below.

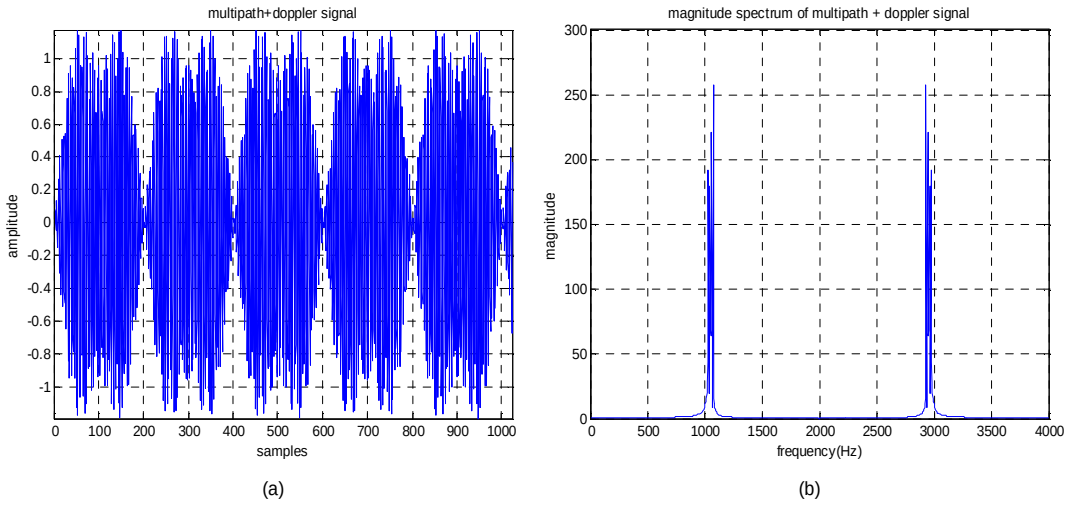

Figure 6.4: (a) *Multipath and Doppler shifted signal.* **(b)** *Magnitude spectrum of signal. For the above results, the sampling frequency was* 4000Hz *and the carrier frequency of* 1000Hz. *The Doppler shift used was* 50Hz (*large merely for analysis purposes*).

The magnitude spectrum of the signal shows that there exists a Doppler shift and multipath component in the signal. One of the challenges at the compensation stage was in getting the correct domain in which the compensation must take place. Under multipath, the compensation took place in the frequency domain whilst for Doppler shift, we compensated in the time domain. Now this case presents a situation where we had both present and hence this in itself presented a major problem in trying to carry out the compensation process. The received signal and its spectrum are shown in the figure below. As was mentioned earlier, if the Doppler shift were much larger than the bandwidth, a possibility for compensation would exist and this is considered under the 'special case' later in the chapter.

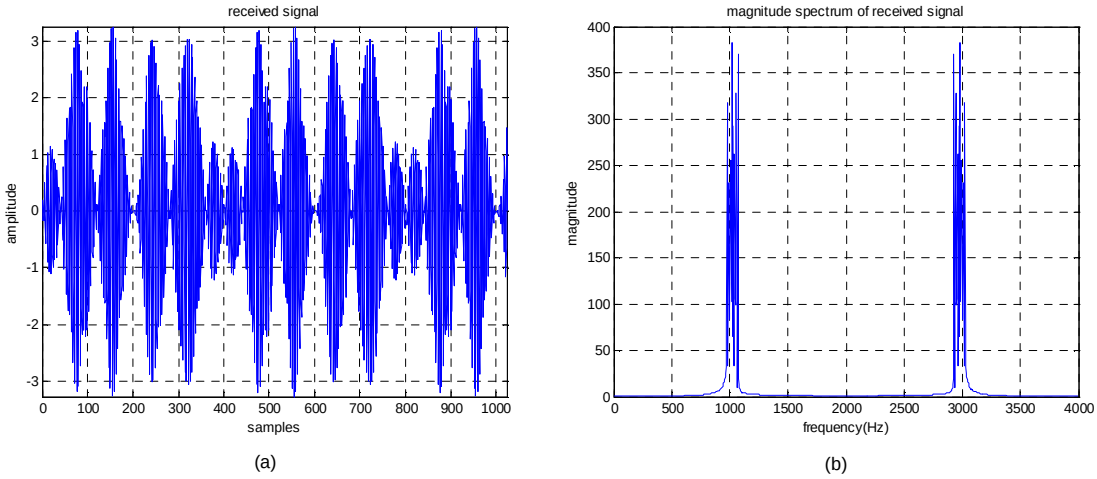

Figure 6.5: (a) *Received signal* **(b)** *Magnitude spectrum of received signal.*

At this point, the limitation facing the compensation process comes in. From the simulation results, it was seen that the Doppler components aliased with the multipath components and hence a successful compensation was not possible. The mathematical analysis stalemate faced does halt the compensation process at this stage. However, as was discussed under the special case, the compensation is possible for the simulation despite the barrier faced from the theoretical analysis and this is on condition that the bandwidth-doppler shift ratio is small or less than 1.

6.4 Special Case:– Simulation results for Radio frequency

Figure 6.6(a) below shows the received signal having all the four input signals added together and the resulting spectrum shown in (b). Here it is clear to see the separation between the multipath, direct path, Doppler and multipath and Doppler spectral components. The Doppler shift used was exaggerated to 500Hz which was large enough for analytical purposes so as to clearly see the separation in the spectral components. Therefore, it is intended to eliminate the Doppler and multipath components of the spectrum and hence the need to filter out the unwanted part.

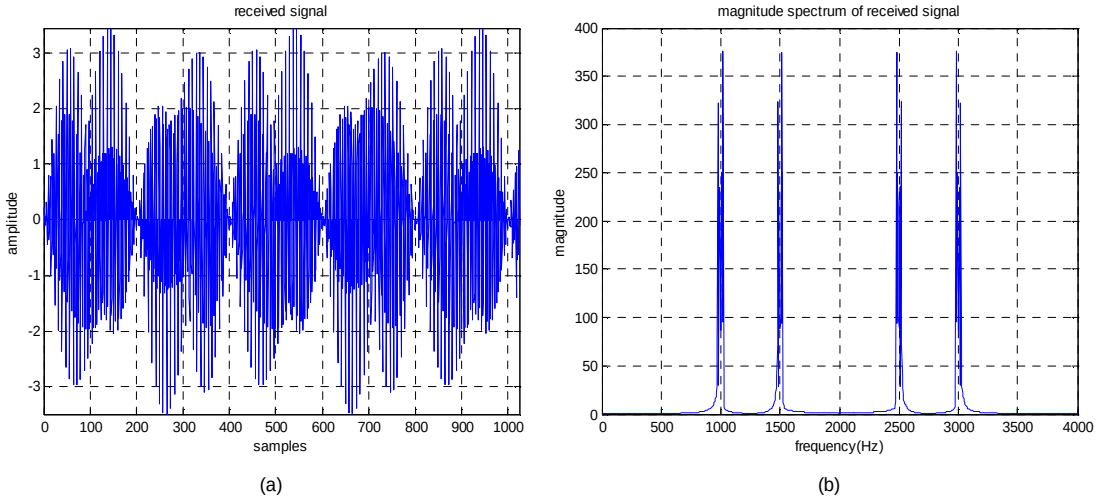

Figure 6.6: (a) *Received signal* **(b)** *Magnitude spectrum of received signal.*

The figures on the next page show the filtered spectrum and the compensated spectrum resulting from the compensation process. Figure 6.7(a) shows the filtered spectrum of the received signal. It is seen that the Doppler content of the spectrum has been filtered out together with the combined multipath and Doppler shifted signal components. This leaves the multipath and direct path components from which the multipath component was eliminated by the carrying out multipath compensation as was done in Chapter 4.

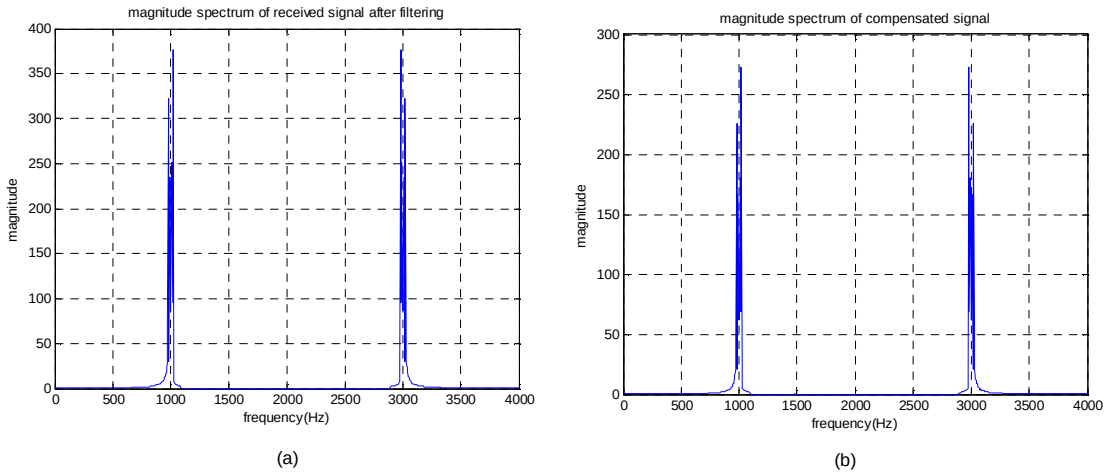

Figure 6.7: *Spectral plots of :***(a)** *Filtered received signal* **(b)** *Compensated signal*.

The figures on the next page show the resulting compensated demodulated outputs x_{rcd1} and x_{rcd2} and the difference plot which is a plot of the numerical difference between the compensated demodulated output and the direct-path demodulated outputs x_{d1} and x_{d2}.

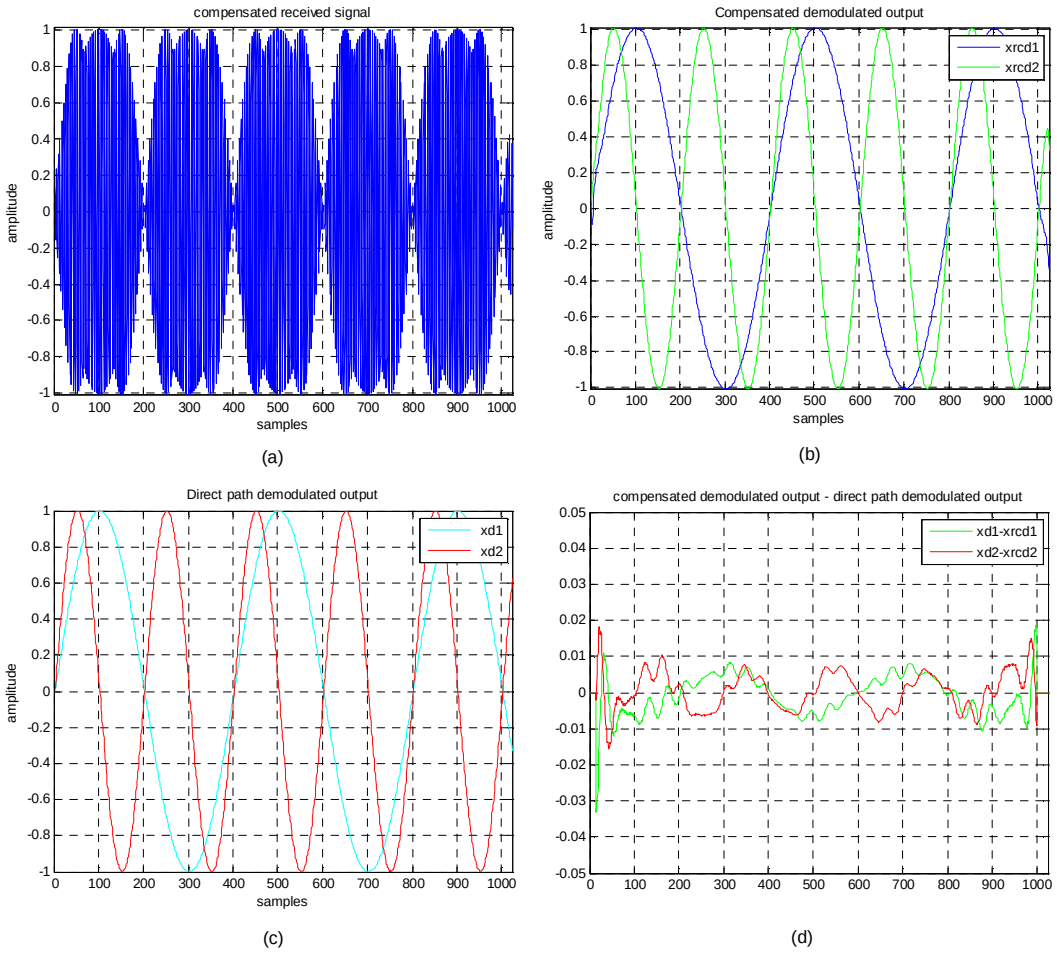

Figure 6.8: (a) *Compensated received signal* **(b)** *Compensated demodulated outputs signal.* (c) *Direct-path demodulated outputs* (d) *Difference plot.*

The error/difference plot show shows a small error and is evident of a successful compensation process carried out under the special case. It therefore suffices to conclude that it is possible to compensate simultaneously for multipath and Doppler shift provided the Doppler shift is greater than the signal bandwidth. The analysis now moves to quadrature baseband so as to see whether the special case is applicable at QBB too.

6.5 Special Case – Simulation results for Quadrature baseband

The figures on the next page show the plots resulting from the simulation carried out at QBB.

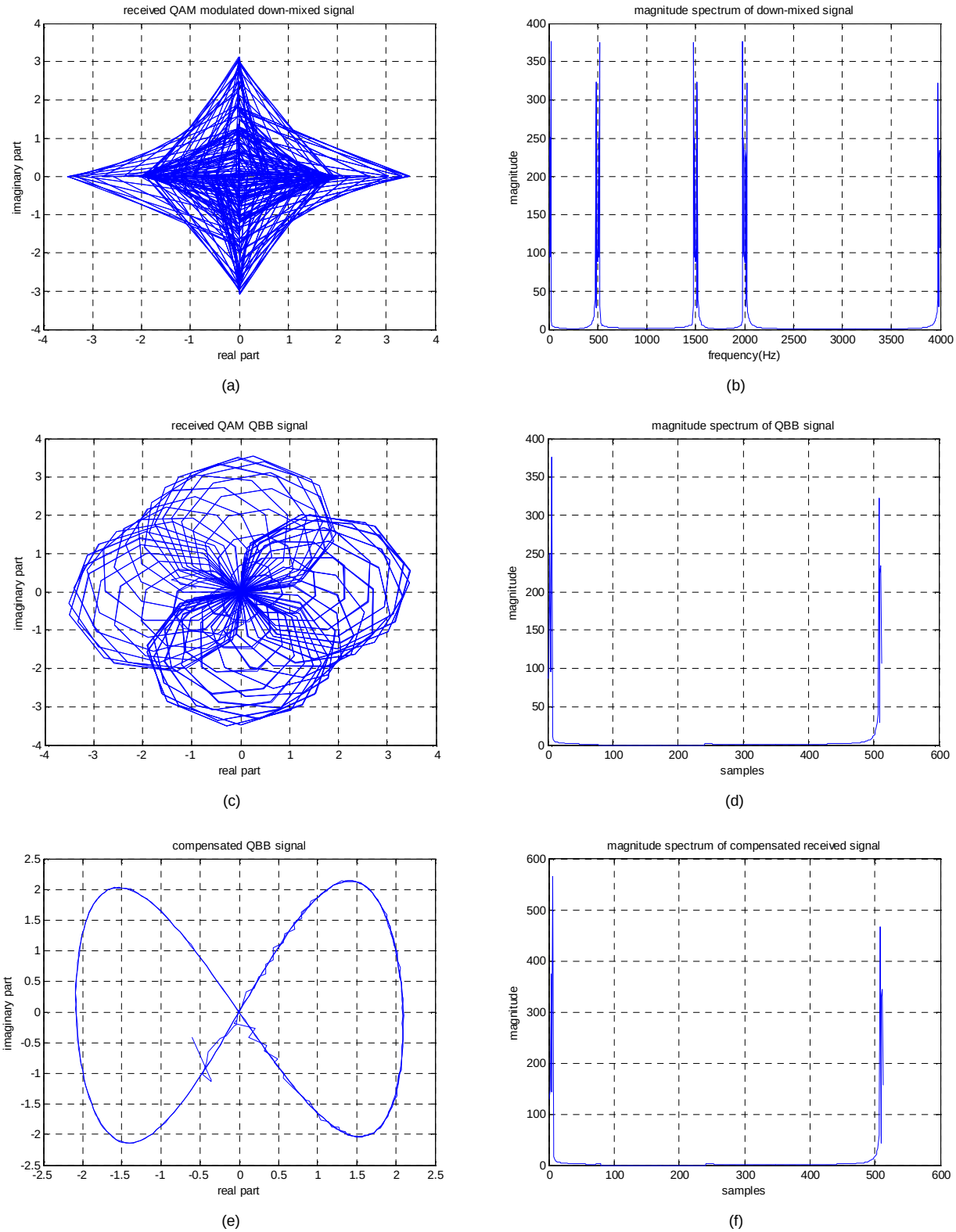

Figure 6.9: *Simulation results.* **(a)** *Down-mixed received signal* **(b)** *Down-mixed signal spectrum* **(c)** *QBB received signal*.**(d)** *QBB received signal spectrum* **(e)** *Compensated QBB signal* **(f)** *Compensated downsampled QBB signal spectrum. The sub-sampling factor used was 2.*

The plots in the figures on the previous page show the simulation results for the QBB compensation analysis. As mentioned earlier, downsampling was carried out and hence the sample reduction from 1024 to 512 due to the downsampling factor of '2'.

The spectral changes are also shown and it is seen that the uncompensated QBB spectrum has the Doppler components filtered out and it was seen that the same filter used in achieving QBB was used to filter out the Doppler components of the spectrum. The signal now sits at QBB and compensation was carried out at this stage. The real and imaginary parts were then taken to give the demodulated output signals y_1 and y_2 shown below.

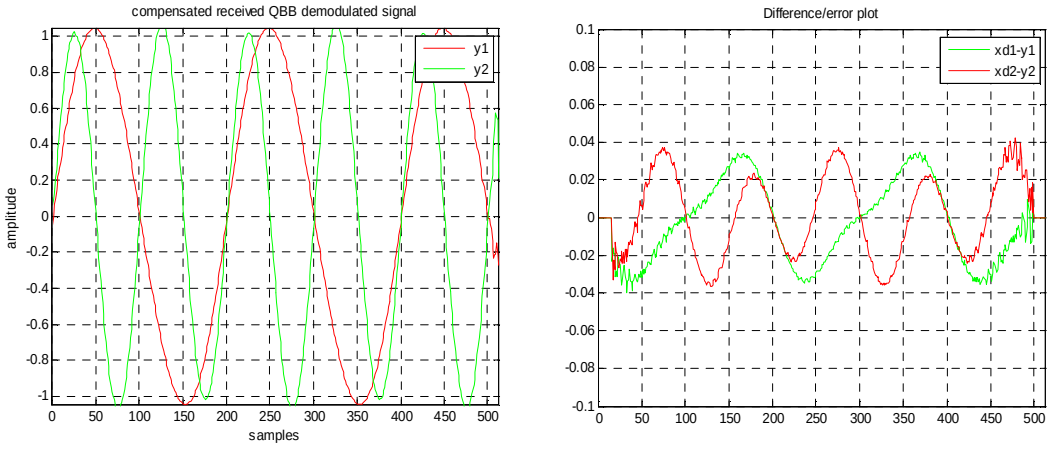

Figure 6.10: (a) *Compensated demodulated output.* (b) *Difference plot.*

The difference plot above where xd_1 and xd_2 are the direct-path demodulated outputs shows that the compensation was successful with the error having a maximum value of approximately 3%.

6.6 Benefits of Multiple compensation at QBB

The sample processing and simulation runtime results are now compared for the RF and QBB QAM simulation for the multiple input signal case. As mentioned earlier, the comparison starts from the received signal stage through the compensation and down to the demodulation. The tables on the next page summarize the sample processing and simulation runtime at RF and QBB.

Simulation Stages	**Radio Frequency**	**Quadrature baseband**
Mixing down + QBB + Down sampling	____	$N + NLog_2N$ $2kN + kNLog_2kN$
Compensation process	$NLog_2N$ $N+ NLog_2N$ N	$kN + 2kNLog_2kN+2kN$ $kN + 2kNLog_2kN$ $kN + 2kNLog_2kN +$ $kN +2 kNLog_2kN$
Demodulation	$2NLog_2N+2N$ $2NLog_2N$	_____
Total sample processing	$4N+ 6NLog_2N$	$N+8kN+NLog_2N+$ $9kNLog_2kN$
Total sample processing for N=1024 and k=1/2	67584	56832

Table 6.1: *Sample processing at RF and QBB.*

	RF (t_{rf})	**QBB(t_{qbb})**	**t_{rf}/t_{qbb}**	**N_{rf}**	**N_{qbb}**	**N_{rf}/N_{qbb}**
MIMO compensation	Time in seconds		Ratio	Number of Calculations		Ratio
QAM	0.00122	0.00099	1.23	67584	56832	1.19

Table 6.2: *Simulation runtime and sample processing ratio summary. The discrepancy between the sample processing ratio and simulation runtime is 3.25% which is reasonable enough given the variance in the computer processing time.*

The results interms of the simulation runtime and number of calculations, we see a significant reduction in the ratios for the multiple compensation case. From the Table 6.1 it can be seen that despite the downsampling process, the number of calculation/operation taking place at QBB is a lot and as such the expected advantage interms of reduced number of calculations and reduced simulation runtime is not as large as in the previous analysis. The analogue QBB case too has a ratio output equal to:

$$\frac{N_{rf}}{N_{qbb}} = \frac{67584}{45568} = 1.48 \tag{6.5}$$

It was seen that the analogue QBB case still proved slightly more advantageous than the digital QBB case. However, we still saw a reduction in terms of the ratio for the analogue case as compared to the values obtained in the previous analysis. The simulation runtime should follow a similar trend.

6.7 Conclusion

The study carried out showed that compensating for multipath and Doppler shift simultaneously a complicated and tedious task for cases where the Doppler shift is less than the signal bandwidth. The compensation was however, possible for a smaller bandwidth- doppler shift ratio and its is true to say that the smaller the ratio, the better the compensation due to the easier filtering out of the Doppler components. This presents a case where the simulation results had to be relied upon despite the stalled mathematical analysis. The study considered QAM only because the same limitations faced under QAM would be encountered under FM. It therefore, suffices to say that compensating for multipath, Doppler shift simultaneously being reflective of a MIMO system where we have multiple signals inputs and a single output is possible but under certain conditions. An area of application is in multi-rate digital signal processing techniques which improves the flexibility of software defined radio [23]. The benefits for working at QBB here were seen to be less pronounced for this case as compared to the previous analysis carried out but still, QBB does have the upper hand. Thus it is seen that indeed the processing load at QBB was less and this equally translated to a reduction in the processing time.

Chapter 7

Matched Filter Detection

This part of the overall study ventures into the digital signal arena by analyzing a simple chirp signal where a positive chirp represents a digital '1' and its absence represents a digital '0'. The analysis carried out involved carrying out matched filter detection of the chirp signal at RF and QBB for different cases which include multipath, Doppler shift and a combination of the two as was done in the previous study which involved compensating for these effects. The study firstly assumes noiseless channels and considers one case involving matched filter detection in a noisy channel. The core purpose of the study remains investigating carrying various signal processing techniques at QBB with the main advantage of working at QBB being the low operating frequencies involved.

7.1 Matched Filter Detection

Before going down to the analysis results, it is necessary to get a brief background of matched filter detection so as to understand the resulting outputs from the simulations carried out. Matched filtering is a process known to be the optimum linear filter for detecting a known signal in random noise [29]. The DSP responsible for the processing of signals has a copy of the signal it should detect. It then time reverses the signal for detection and cross-correlates it with the received signal [38]. A detailed derivation of the matched detector is given in Appendix B.

The study looked at matched filter detection for noiseless transmissions before looking at the real life situation where noise is a factor that affects the detection process. The study looked at the direct path signal with no multipath or Doppler shift effects and then subsequent simulations were carried out where multipath and Doppler shift were introduced. As mentioned earlier the signal used in the simulations was a chirp signal whose generation is discussed in the next section.

7.2 Matched filter detection:- noiseless channels

The analysis was firstly carried out at RF and this involved analyzing the direct path, multipath, Doppler shift and the combined multipath and Doppler shift cases. The results will then be compared with there corresponding results achieved at QBB so as to come up with a conclusion about investigating the results obtained at QBB coupled with the already mentioned benefits of working at QBB.

7.2.1 Theoretical analysis:- RF

Consider the block diagram below which illustrates the analysis process carried out at RF.

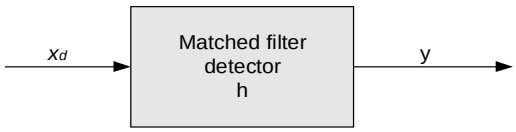

Figure 7.1: RF chirp signal matched filter detection

The input chirp signal is fed into a matched filter whose output is a convolution between the received signal and its time reversed version. Let the chirp input be x_d . Matlab uses an inbuilt command to execute the time reversal of the chirp input 'x_d'.

$$h = flipr(x_d) \tag{7.1}$$

The matched filter then convolves the chirp input '*x*' with h given as

$$y = conv(x_d, h) \tag{7.2}$$

The matched filter output has its peak value at $t=T$. The theoretical analysis for the QBB simulations is given in the next section and the simulation results which follow in subsequent sections of the chapter will compare the results obtained at RF and QBB for the multipath, Doppler shift and the combined multipath and Doppler shift cases.

7.2.2 Theoretical analysis QBB

The sole purpose of the study is to investigate the possibility of carrying out certain signal processing techniques at quadrature baseband and hence, it is required to outline the theory used to carryout the simulations at QBB.
Consider the figure below

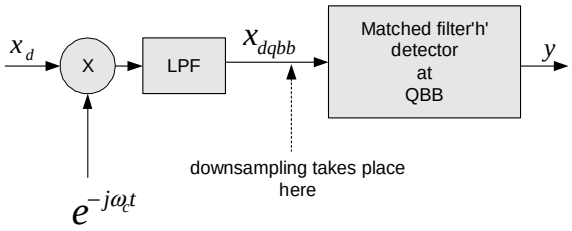

Figure 7.2: *QBB chirp signal matched filter detection.*

From the figure above, it is seen that the chirp is mixed down and lowpass filtered to quadrature baseband before being fed into the matched filter which has a time-reversed copy of the QBB input chirp. The output does have its peak at t=T as in the previous RF analysis. The simulation results will give a more detailed comparison of the graphical results obtained from the RF and QBB simulations.

$$\therefore x_{qbb} = | x. * e^{-j\omega_c t} |_{LPF} \tag{7.3}$$

The matched filter output should show a perfect match occurs when the QBB chirp input and its time-reversed copy make a complete overlap at $t=T$ resulting in the large spike at that point. A piece of Matlab code used to implement the matched filter detection at QBB is given below:

```
h=conj(fliplr((xqbb)));          % matched filter at QBB
y=real(conv(xqbb,h));            % takes place at QBB
```

7.3 MatLab Simulation Results RF and QBB

This paragraph gives the simulation results for the analysis carried out at RF and QBB for the direct path, multipath, Doppler shift and combined multipath and Doppler shift cases. The results at RF and QBB are then compared and discussed.

7.3.1 RF:–Direct path

The figure below shows the simulation results obtained for the direct path analysis at RF.

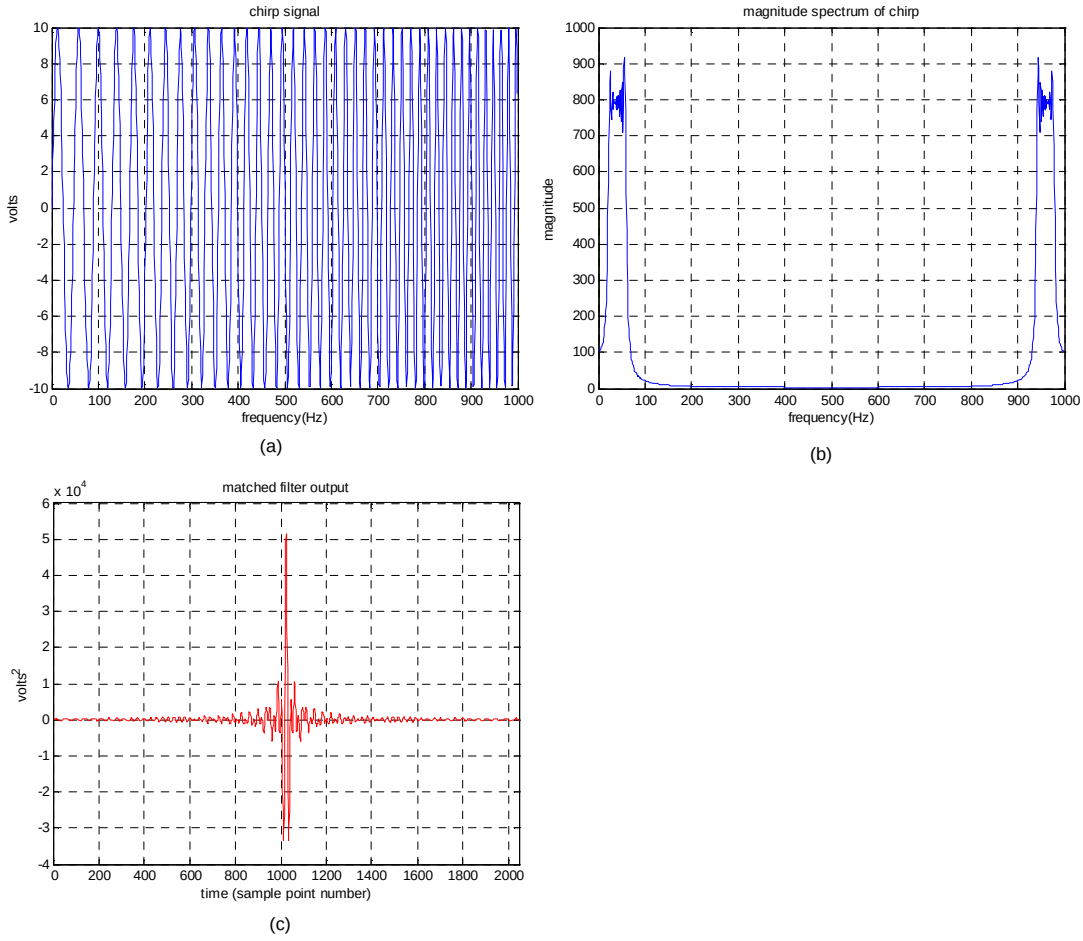

Figure 7.3: (a) *Input chirp* **(b)** *Chirp signal magnitude spectrum* **(c)** *Matched filter output.*

From the figure as explained under the theoretical analysis, it is seen that the peak of the matched filter output appears at $t=T$ which in the current case due to the discrete

domain being used, the point *T* corresponds to the sample point number n= 1024. The matched filter output has a peak value of 5.12e4 at this point and this value was verified mathematically. Let $y(n)$ represent the matched filter output in the discrete domain. As mentioned earlier the convolution is a point-wise multiplication and integration which in the discrete domain is represented by the following operation.

$$y(n) = \sum_{n=1}^{N} x(n)h(n) \tag{7.4}$$

Now for the current simulation, the input chirp *x* was sinusoidal having a peak value of 10 and the sampling frequency f_s being 1000Hz. Replacing the expressions for $x(n)$ and $h(n)$ with the discrete domain versions of $x(t)$ and $h(t)$ and ignoring other parameters of the chirp expect for the amplitude and signal form(i.e. sine or cosine)
We have;

$$y(n) = \sum_{n=1}^{N=1024} x(n)h(n) \tag{7.5}$$

or

$$y(n) = \sum_{n=1}^{N=1024} (10\sin[...])(10\sin[...])* \tag{7.6}$$

Note that the '*' denotes the conjugate of the *time-reversed* version of the chirp. It is seen that a product of the two inputs of Equation 7.7 summed from n= 1 to N results in a trigonometric expression given below which upon applying a trigonometric identity reduces to the Equation 7.8 below.

$$y(n) = \sum_{n=1}^{1024} 100\sin^2[....] \tag{7.7}$$

or

$$y(n) = \sum_{n=1}^{1024} 100(\frac{1}{2} - \frac{1}{2}\cos 2[....]) \tag{7.8}$$

The absolute value of the matched filter output thus reduces to:

$$|\, y(n) \,| = \frac{1}{2}(1024 \times 100) = 5.12 \times 10^4 \qquad (7.9)$$

Therefore, the output of the matched filter was correct as has been verified numerically.

7.3.2 QBB:- Direct path

The analysis then moves down to quadrature baseband where the matched filter detection is now being implemented at QBB. The figures shown below are the simulation results obtained from the QBB simulation. The parameters of the input chirp are the same as those used for the RF simulation.

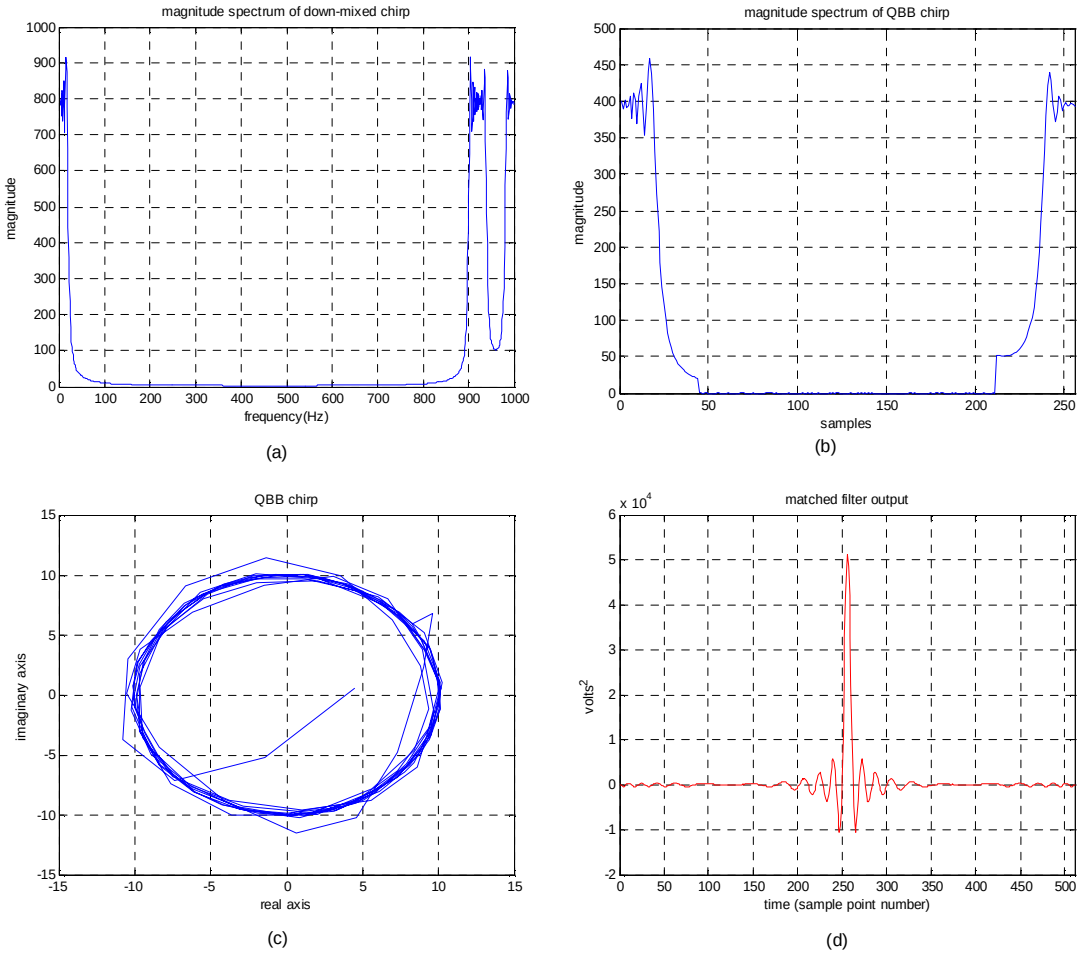

Figure 7.4: *Simulation plots.***(a)** *Magnitude spectrum after down-mixing* **(b)** *After lowpass filtering and downsampling* **(c)** *QBB chirp* **(d)** *Matched filter output.*

The figures on the previous page show the conversion of the chirp to quadrature baseband and the final matched filter detected output shown in Figure 7.4(d). It is seen that downsampling is done at QBB and this reduced the samples by a factor of 4. Thus the point-wise multiplication done by the matched filter takes place on fewer samples and hence the sample processing is expected to be less which should translate to less processing time. The maximum value of the matched filter shifts to the 256^{th} sample point after the downsampling. This presents an advantage of carrying out matched filter detection at QBB compared to doing so at RF.

7.4 RF:- Multipath

The study then looked at a scenario where it was now assumed that the transmission is subjected to multipath effects. This part of the study is relevant in that when applied or related to digital transmissions, we are looking at a case where we have a bit stream transmitted followed by its delayed version. Now in this case, we are considering matched filter detection and seeing how the matched filter output can influence the making of a correct decision during the detection process. Similarly, it is assumed for analytical purposes that we have a noiseless transmission. The parameters of the input chirp used in this simulation remains the same as used for the RF direct path case and this is for purposes of comparing the changes that are brought about by the fact that we now taking into consideration the multipath signal too in the matched filter detection. The figure below shows the block diagram for the multipath analysis simulation. The echo factor 'k' in the multipath signal is assumed to be equal to 1 for simplicity's sake in the analysis process.

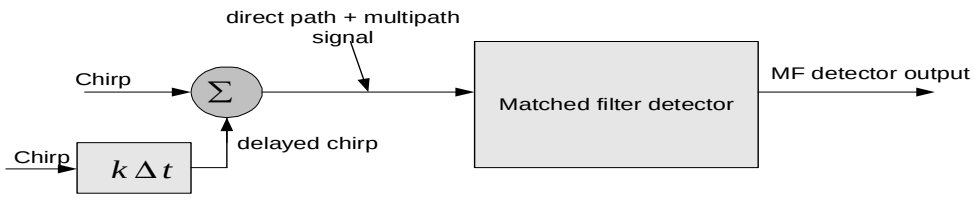

Figure 7.5: *Multipath RF simulation flow.*

The generation of the delayed version of the original chirp is done in the same way as the delayed signals were generated under the previous study on multipath compensation. The figures below show the results obtained from the multipath analysis simulation.

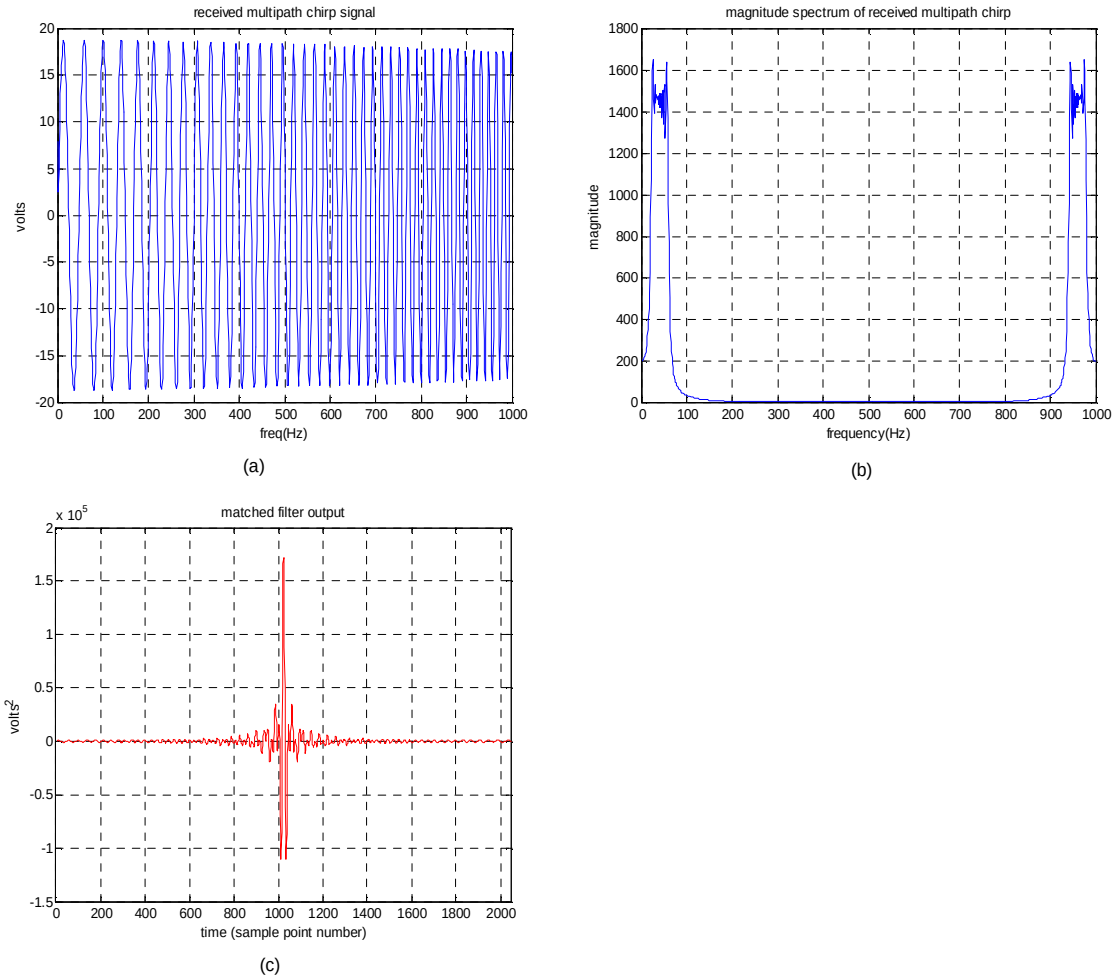

Figure 7.6: (a) *Received multipath chirp* **(b)** *Magnitude spectrum* **(c)** *Matched filter output*.

From Figure 7.6 (a) it is seen that the amplitude of the received signal has increased and the signal amplitude decreases as the frequency approaches 1000Hz. This is due to the phase changes whose effects at higher frequencies result in the decreased amplitude due to the out-of-phase summations of the direct path and time delayed signals taking place as the frequency increases. A look at the magnitude spectrum also shows a considerable increase brought about by the multipath and hence it is expected that the matched filter output will follow suit and indeed it does so as shown in Figure 7.6(c). This result entails that there is increased signal strength at the output of the matched filter and this

energy can be made use of in the detection process.

7.5 QBB:- multipath

The block diagram below illustrates the simulation flow for the analysis carried out at quadrature baseband. The input parameters remain the same as used for the RF simulation.

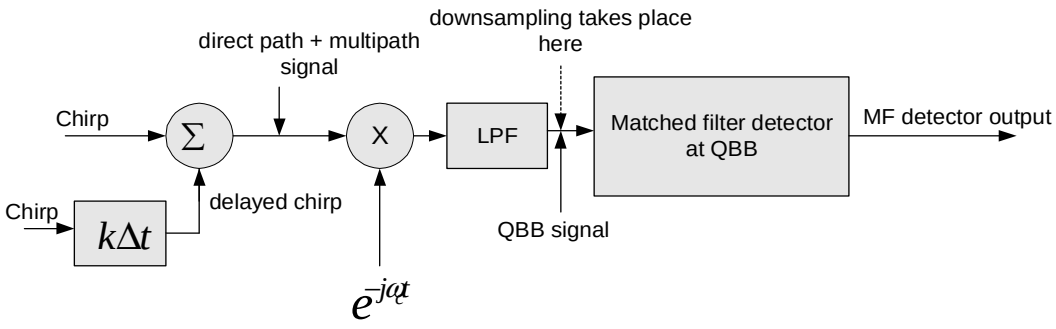

Figure 7.7: *QBB Matlab simulation flow.*

The figure above shows that the received signal is down-mixed and then lowpass filtered down to quadrature baseband before being fed into the matched filter which sits at QBB enabling the detection process to take place at QBB. The simulations results resulting from this simulation are shown in the Figure 7.8 (a), (b), (c) and (d) on the next page. The downsampling reduced the sample point number by a factor of 4. The peak value of the output remains the same as for the RF case entailing that it is equally possible to carry out the matched filter detection at QBB with similar results being obtained. The advantages of this in terms of sample processing and simulation runtime have been discussed earlier.

The spectral changes are notable as was seen under the RF analysis where it was observed that there was an increase in the magnitude of the magnitude spectrum which eventually resulted in increased signal strength at the output of the matched filter and the advantages brought about by this in terms of the detection process in digitals transmissions has been explained. Therefore, it was seen from the results that we can equally carry out matched filter detection at QBB frequencies just as it is done at RF.

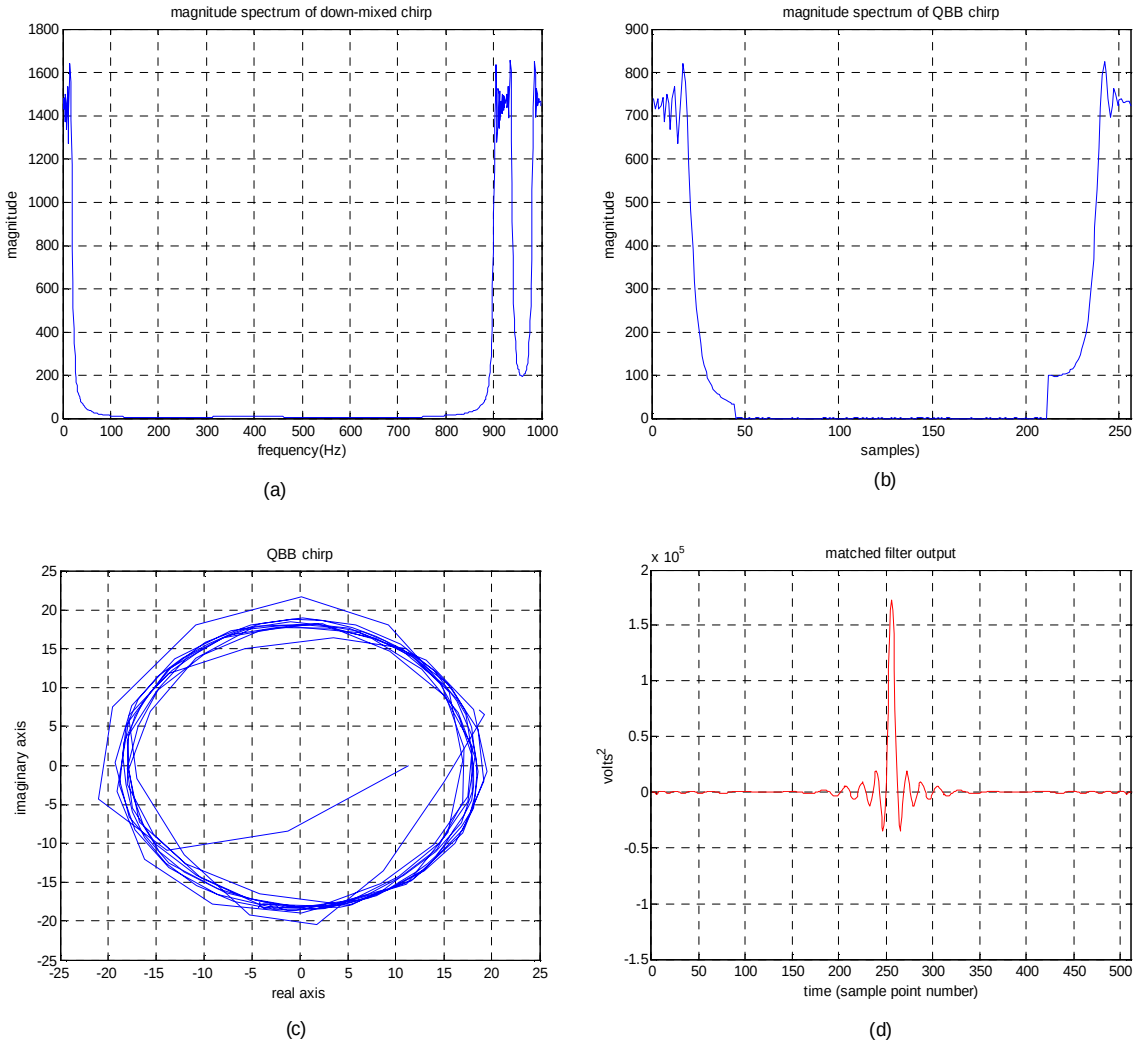

Figure 7.8: *Simulation plots.* **(a)** *Received signal magnitude spectrum* **(b)** *After down-mixing and downsampling* **(c)** *After lowpass filtering* **(d)** *Matched filter output.*

From Figure 7.8(d) it is seen that due to the downsampling, the maximum output of the matched filter now occurs at the 256th sample point. The peak value of the matched filter output for the QBB case is the same as that obtained at RF despite the sample reduction brought about by the downsampling. Overall, it can be concluded for both the RF and QBB cases that the multipath effects actually enhance the signal detection of the matched filter by increasing the signal strength and hence resulting in increased signal strength for the matched filter. Going by the aim of the study, it is seen that indeed we were able to carry out the matched filter detection at lower QBB frequencies and at the same time at lower sampling rates brought about by the further sub-sampling that was carried out.

7.6 RF:-Doppler shift

The simulation moved on to look at the Doppler shift scenario so as to analyze the changes that take place in the matched filter output due to the doppler shifting effects. The block diagram below illustrates the simulation flow.

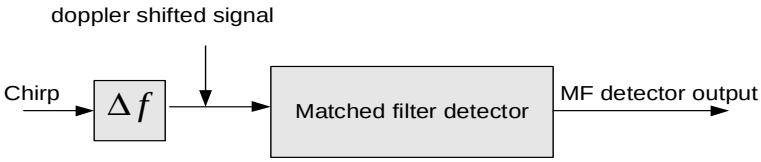

Figure 7.9: *RF simulation flow.*

The generation of the Doppler shifted version of the chirp signal is done in the same way as was done for the Doppler shift compensation analysis. The figures below show the simulation results.

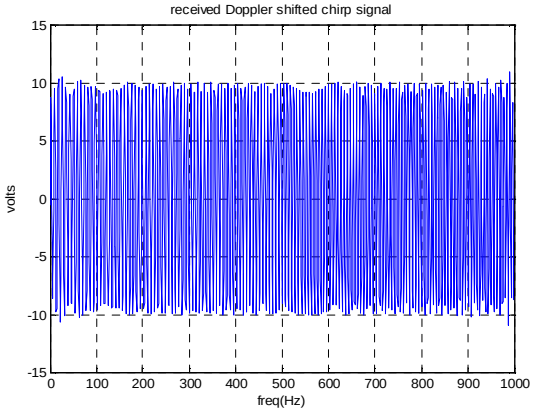

(a)

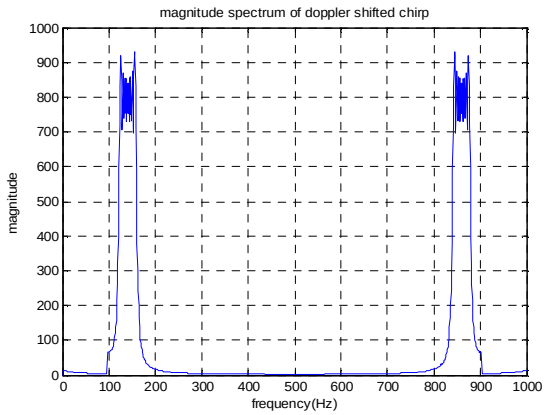

(b)

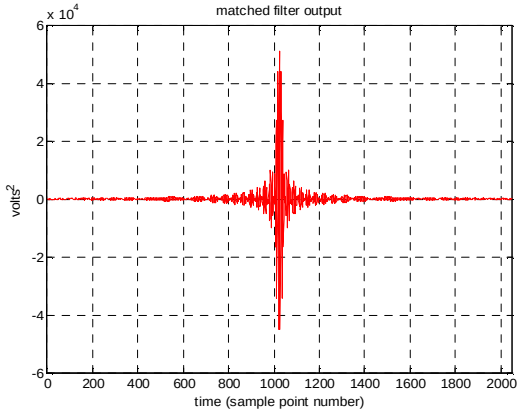

(c)

Figure 7.10: *Simulation plots* **(a)** *Doppler shifted chirp* **(b)** *Magnitude spectrum of MF input signal* **(c)** *MF output.*

The Doppler shifted chirp shown in Figure 7.10(a) shows slight variations in amplitude from the original chirp but with significant changes in the frequency which is seen to be higher due to the positive Doppler shift introduced. This manifests itself in the magnitude spectrum where it seen that there is an upward shift in the frequency components. Looking at the matched filter output, it is seen that the peak output of the MF detector is only slightly affected, having a peak value of approx 5.12e4 which was obtained for the direct path RF analysis. As done in the previous simulations, we move down to quadrature baseband and find out if the scenario changes at QBB.

7.7 QBB:-Doppler shift

Consider the block diagram below showing the simulation flow at QBB.

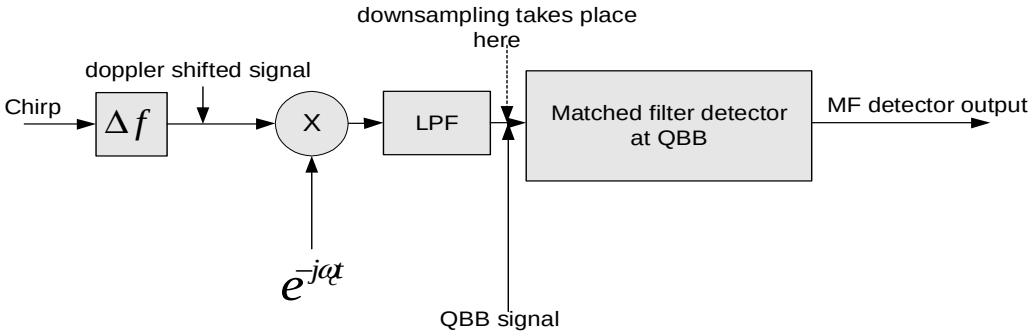

Figure 7.11: *QBB simulation flow diagram.*

By now, we are familiar with the conversion from RF to QBB and hence the earlier explanations given about the spectral changes in previous related analysis do suffice in explaining the current situation. The figures on the next page show the simulation results obtained at QBB.

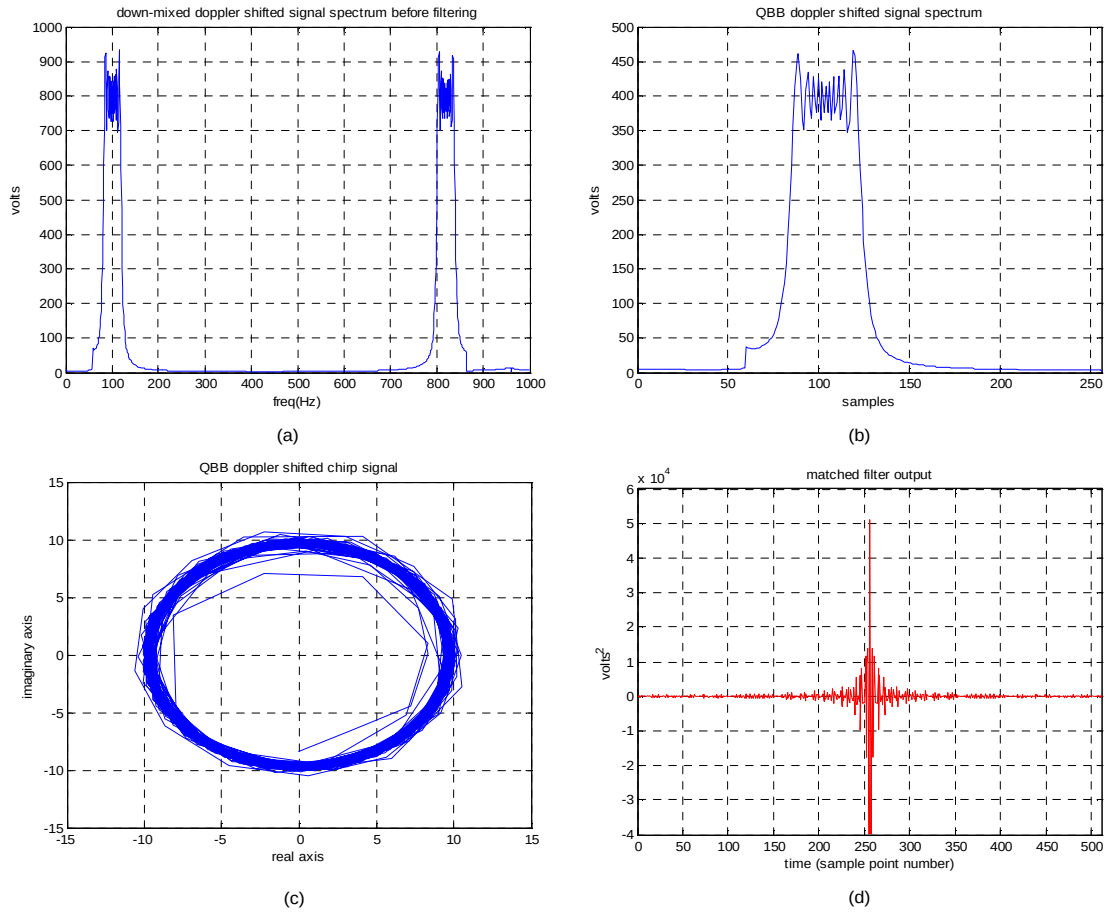

Figure 7.12: *Simulation plots* **(a)** *Magnitude spectrum of down-mixed Doppler shifted chirp* **(b)** *Magnitude spectrum of QBB chirp* **(c)** QBB chirp **(d)** *QBB Doppler shifted signal.*

From Figure 7.12(d) it is seen that the Doppler shift effect on the maximum value of the matched output is minimal. Therefore, it has been shown here that the matched filter detection can take place at QBB and with the further sub-sampling that takes place, it is seen that the processing load reduced which should further translated to a reduction in the simulation processing time. This will be shown in a later part of the chapter.

7.8 Multiple signal reception:- Radio frequency

The block diagram below summarises the simulation flow for the case at hand.

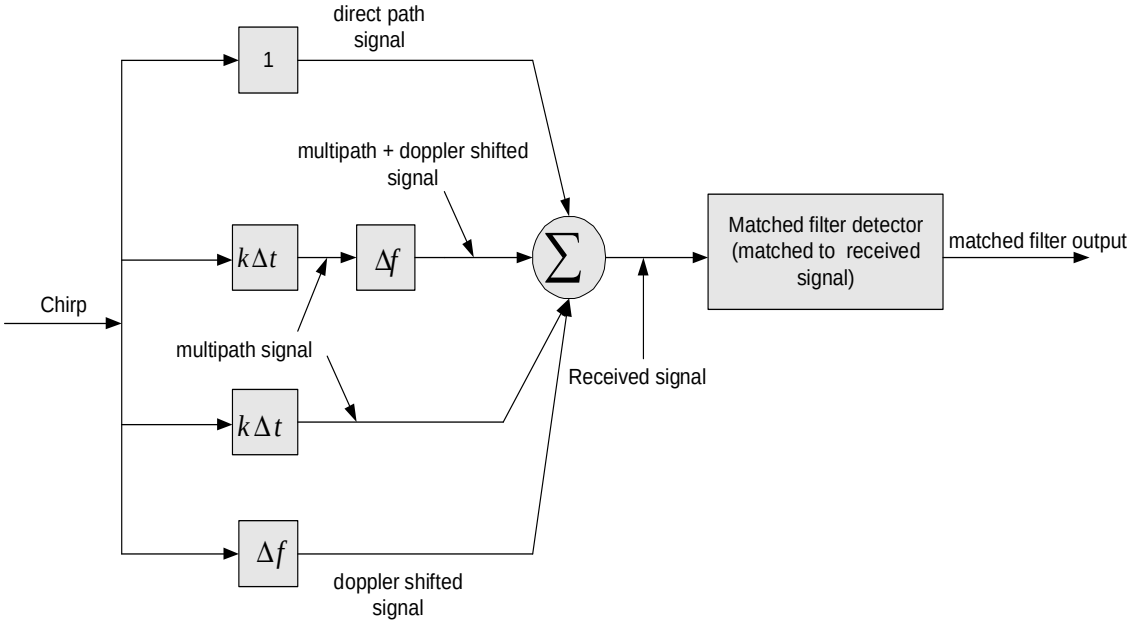

Figure 7.13: *RF simulation flow:- It should be noted that the matched filter is matched to the complex received signal comprising the four input signals summed together.*

The analysis now considers a case of multiple signal reception and investigates the changes observed at the matched filter output due to the multiple signal input to the matched filter. The same mode of generation of the multipath and Doppler shifted signal used for under the compensation analysis is used in the current analysis.

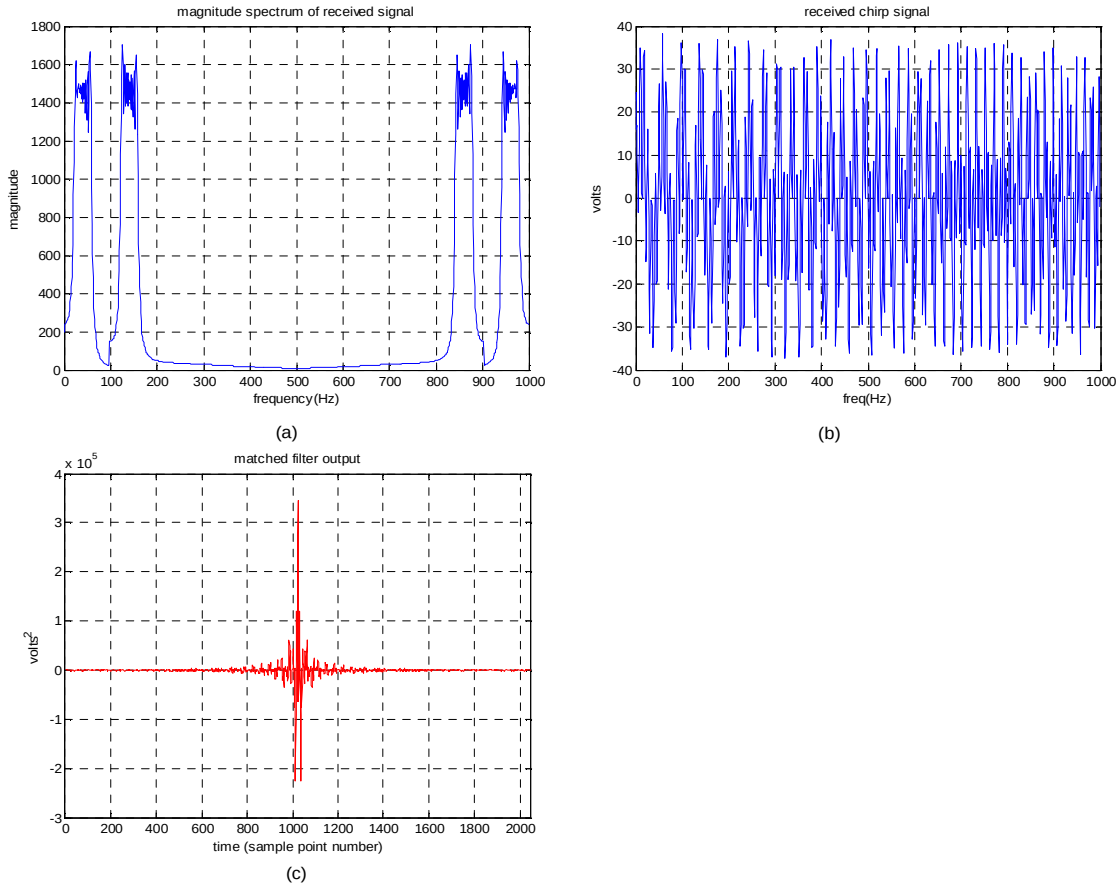

Figure 7.14: *Simulation results.***(a)** *Received signal magnitude spectrum* **(b)** *Received Multipath and Doppler shifted signal* .**(c)** *Matched filter output.*

The magnitude spectrum in Figure 7.14(a) shows the multipath and Doppler shifted components of the received signal. A glance at the spectrum shows that it is a combination of the two spectrums for the separate analysis carried out for multipath and the Doppler shift. The matched filter output is thus expected to have a larger output peak signal strength due to the presence of more signals whose energies are utilised which when added up gave a much stronger signal and this is clearly seen in Figure 7.14(c).

7.9 Multiple signal reception:- Quadrature baseband

The figure below summarizes the simulation flow for the QBB analysis.

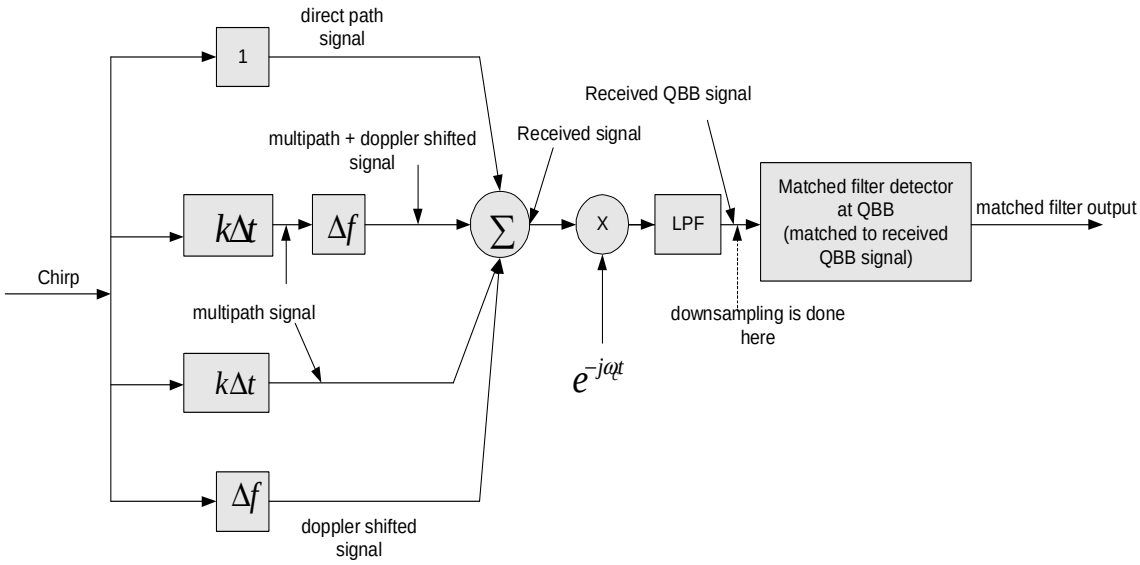

Figure 7.15: *QBB simulation flow:- the figure above clearly shows the 4 input signal paths up to the point of summation. The mixing down follows and lowpass filter moving the process down to QBB and after downsampling the matched filter detection takes place.*

As seen above, the procedure remains the same as in the previous analysis with the same signal parameters being used for the sake of carrying out an effective comparison. The figure on the next page show the simulation results for the QBB analysis.

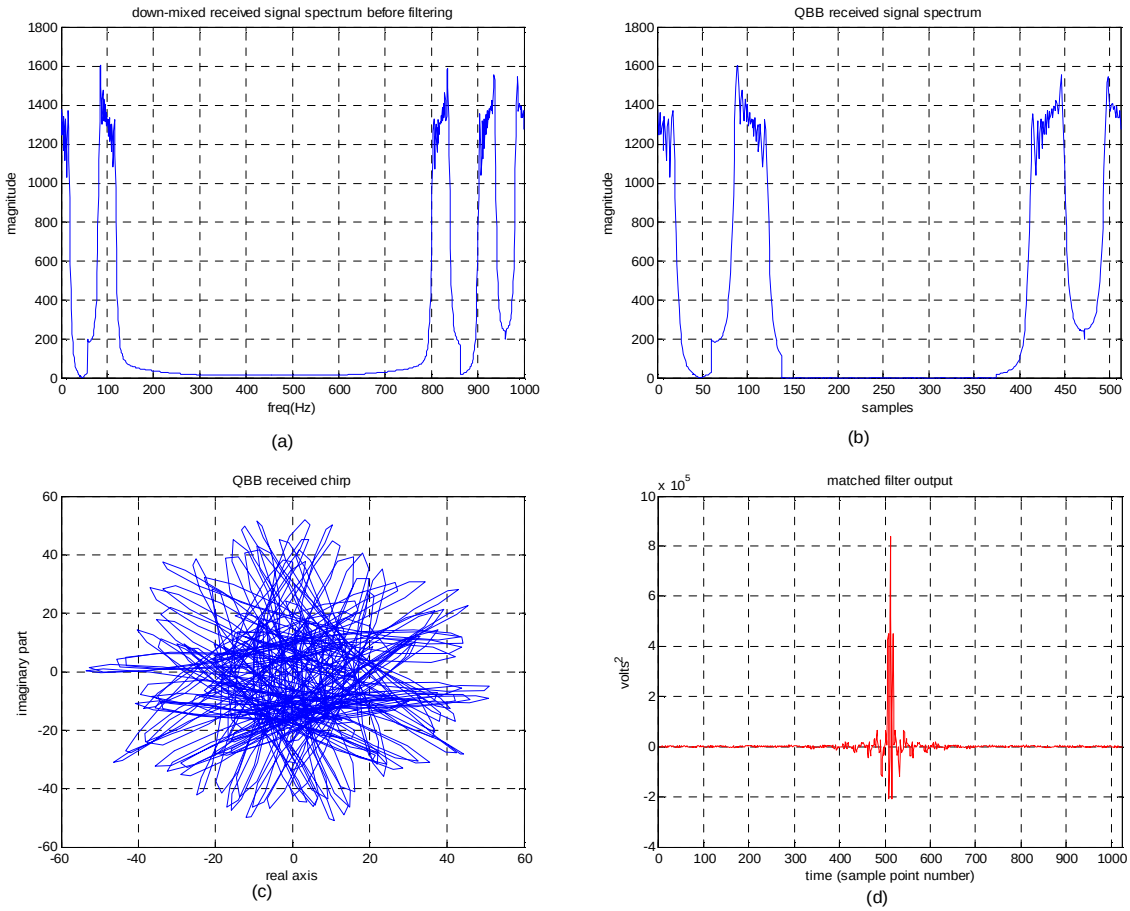

Figure 7.16: *Simulation results* **(a)** *Magnitude spectrum of down-mixed chirp* **(b)** *QBB magnitude spectrum* **(c)** *MF detector output.*

The magnitude spectrum in Figure 7.16(a) shows the direct-path, multipath and Doppler shift components of the received signal. The downsampling factor in this case was 2. A further increase in the factor resulted in aliasing and hence the need to limit the factor to '2'. The matched filter detection which takes place at QBB gives the output shown in Figure 7.16 (d). From the resulting output, it is seen that output signal strength is more than that for the individual direct-path, multipath and Doppler shift cases and thus hence the detection process is more enhanced for the multiple input signal case. Indeed, it has been shown that the matched filter detection could take place at QBB at much lower sampling rates. The comparison in terms of the amount of processing for the RF and QBB cases is given in a later part of the chapter.

7.10 Matched filter detection:-Noisy channel

One common problem in signal processing is that of detecting the presence of a known signal against a background of noise. The main application for matched filtering techniques is in the detection of known deterministic signals in a background of random noise disturbances [4].

7.10.1 Matched Filter Detection- RF

The flow diagram below illustrates the analysis used for the matched filter detection in a noisy channel. It should be noted that the chirp generation remains the same as for the noiseless cases.

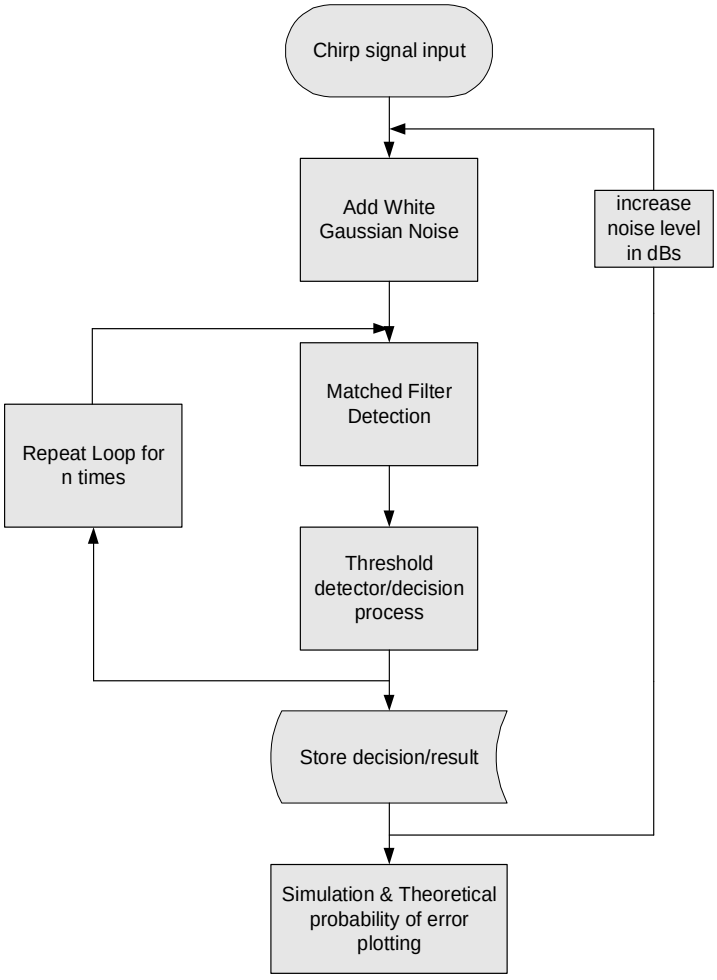

Figure 7.17: *RF simulation flow diagram.*

The Figure on the previous page represents a model used to simulate a matched filter detector in a noisy channel. The Gaussian noise [14, 37] is added to the input chirp and fed to the matched filter detector which has a copy of the original transmitted chirp. The Gaussian noise generated has a normal distribution with a mean = 0 and a standard deviation = 1. This is made possible by use of the MatLab command '*randn*'.

This part of the study considered a noisy channel and it was required to investigate the matched filter output for detection in a Gaussian distributed noise channel at RF and QBB. Appendix B gives more detail about matched filter detection in a noisy channel. The study basically aims to investigate the possibility of carrying out matched filter detection in a noisy channel at QBB and therefore, going into details of the matched filter detection does not serve the main purpose of the study. The results from the simulations carried out at RF and QBB are discussed later in the chapter. In this case, the signal-to-noise ratio factor comes into play and therefore, the simulation needs to be run several times in order to eventually come up with a probability of error plot. In this particular analysis, a positive chirp was generated and transmitted in a noisy channel before the matched filter receives the signal and *convolves* it with a copy of the time reversed original signal. A threshold detector at the output of the matched filter carries out the decision making process. *If the MF output is greater than zero, the decision is '1' and if the output is less than zero, the decision is '0'.* The mathematical derivation for the theoretical probability of error is given in Appendix A. The loop was run 1e6 times in order to achieve the results shown in the graphical plots. It should therefore be noted that the larger the number of runs, the better the matching between the simulation probability of error and the theoretical one. Appendix A also gives the values for the simulation and theoretical probability of error obtained for the direct path case. The noise level in the signal is increased and the loop runs through again and hence the matched filter detection process equally takes place repeatedly. MatLab however only shows the last value of the loop. An extract of part of the MatLab code executing the RF simulation flow illustrated in the previous figure is given on the next page.

```
-------------------------------------------------------------------------------------------------
nch=1e7/sqrt(10.^(dB/10));          %noise power defined with respect
to varying dBs
%-----------------------------------------------------------------
for i=1:1:n
       noise=randn(1,N)*nch;
       xr=x + noise;                % received signal
       y=conv(xr,h);
    p=y(1024);
    if p>0,
        decision(i)=1;              % chirp is detected
    else
        decision(i)=0;              % chirp is not detected
end; end;
    Proberr(dB)=1-(nnz(decision)/n); % calculates the simulated
                                       probability of error.
    M=5.12e4;
    Sigma=nch*sqrt(5.12e4)
    Theor=0.5*qrfc(m./(sqrt(2)*sigma)) % calculates the theoretical
                                         probability of error.
end;
-------------------------------------------------------------
```

The decision is made at the point where y=1024 because the sampling frequency used is 1024 and hence N=1024. The complete MatLab script is can be accessed from the M-Files on the CD in Appendix C. The code therefore shows that for a noise power that has its dB level changing and the simulation runs through from n=1 to n=1e6 and makes a decision n times. This enables and error probability for each dB level to be calculated resulting in a probability of error plot. The in built MatLab function 'nnz' gives the number of non-zero values in a vector and hence is used to give the number of ones from the decision vector which when subtracted from one gives the actual number of zeros (errors). The next section of the chapter gives the simulation results.

7.10.2 Simulation results:- Radio Frequency.

The figures on the next page illustrate the results obtained form the simulation at RF. The first figure shows the received signal for the last value of n which in our case was 1e6 implying that the loop was run 1e6 times. The matched filter convolves the original signal with the received noisy signal and decision is eventually made based on the matched filter output at N=1024. The matched filter output shown in Figure 7.18 (b) on the next page represents the last value of the matched filter and Figure 7.18(c) represents the probability of error plots for both the theoretical and simulation analysis.

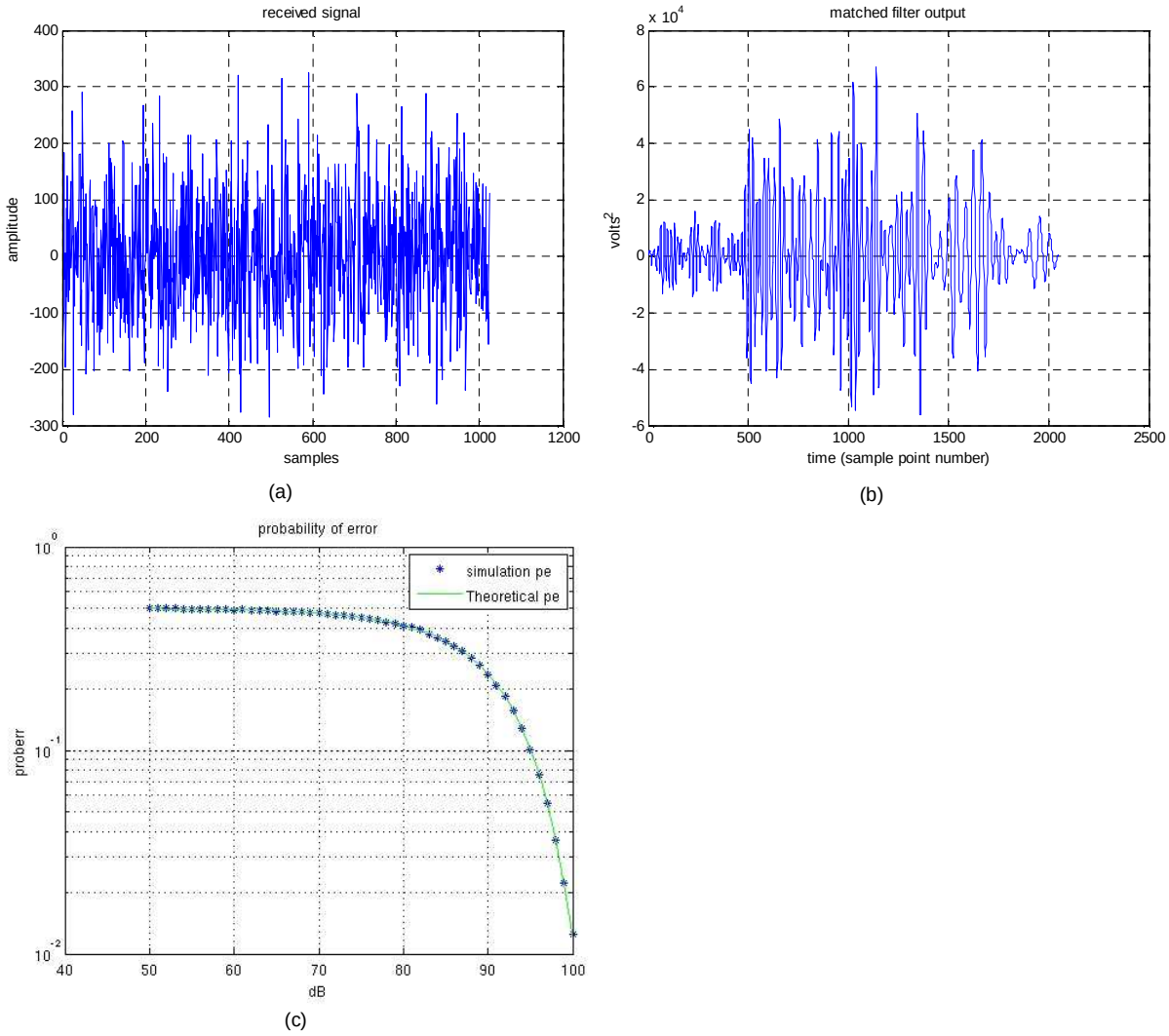

Figure 7.18: *Simulation results.* **(a)** *Received noisy signal:- the last plot of the received signal shows the signal engulfed in noise.* **(b)** *Final plot of matched filter output:-shows that the last value of the matched filter output at t=T is less than the expected value and this due to noise which corresponds to the last plot of the received signal which has a high level of noise.* **(c)** *Probability of error plots: the plots show that the simulation probability of error does match with the calculated theoretical value.*

The simulation moves down to quadrature baseband where received noisy signal now sits at QBB and hence the matched filter detection is expected to take place at QBB too.

7.10.3 Matched Filter Detection- QBB

The simulation flow diagram given below summarizes the QBB analysis.

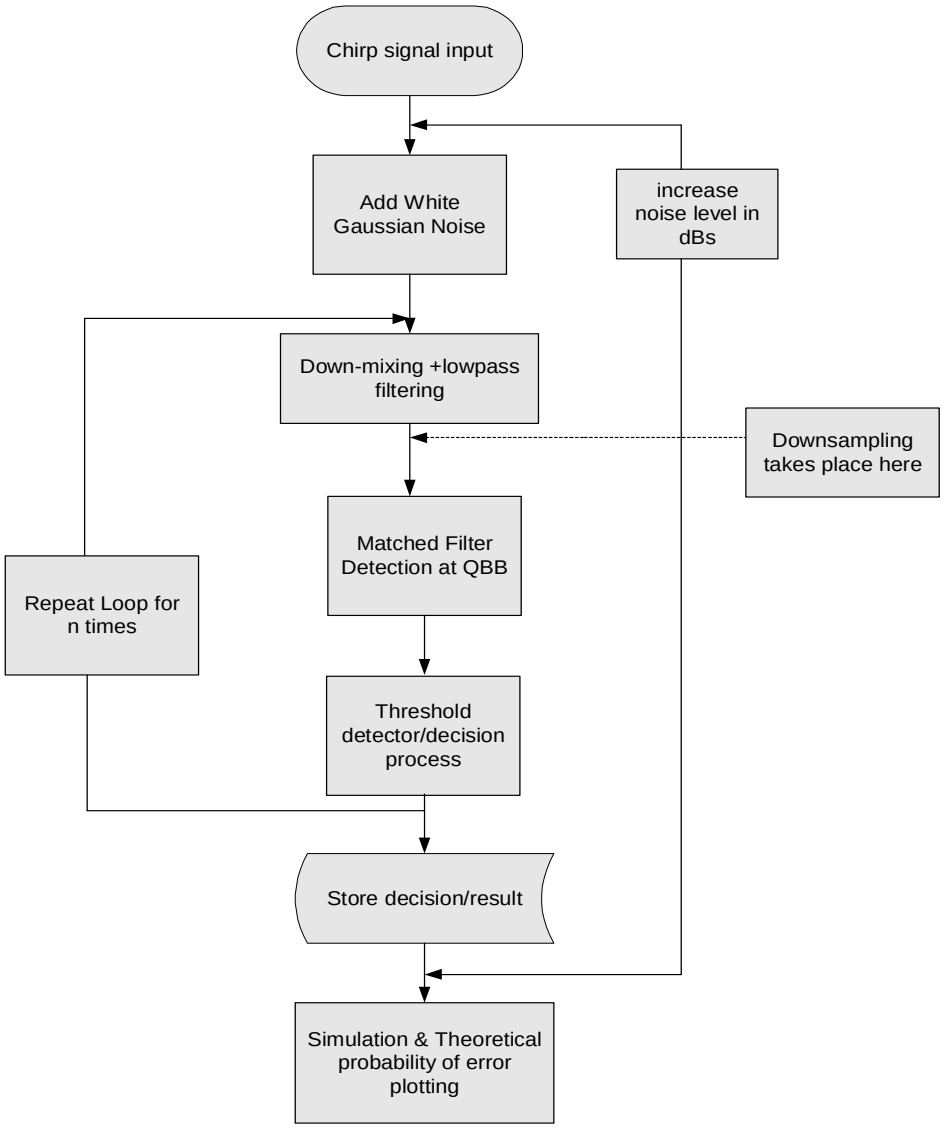

Figure 7.19: *QBB simulation flow diagram.*

The QBB simulation follows a similar looping process to the RF simulation except that after the addition of the Gaussian noise, the signal undergoes conversion to quadrature baseband facilitating for the matched filter detection process to take place at QBB. This is the sole purpose of the study and hence the simulation results should verify the possibility of working at quadrature baseband.

7.10.4 Simulation results:- Quadrature baseband

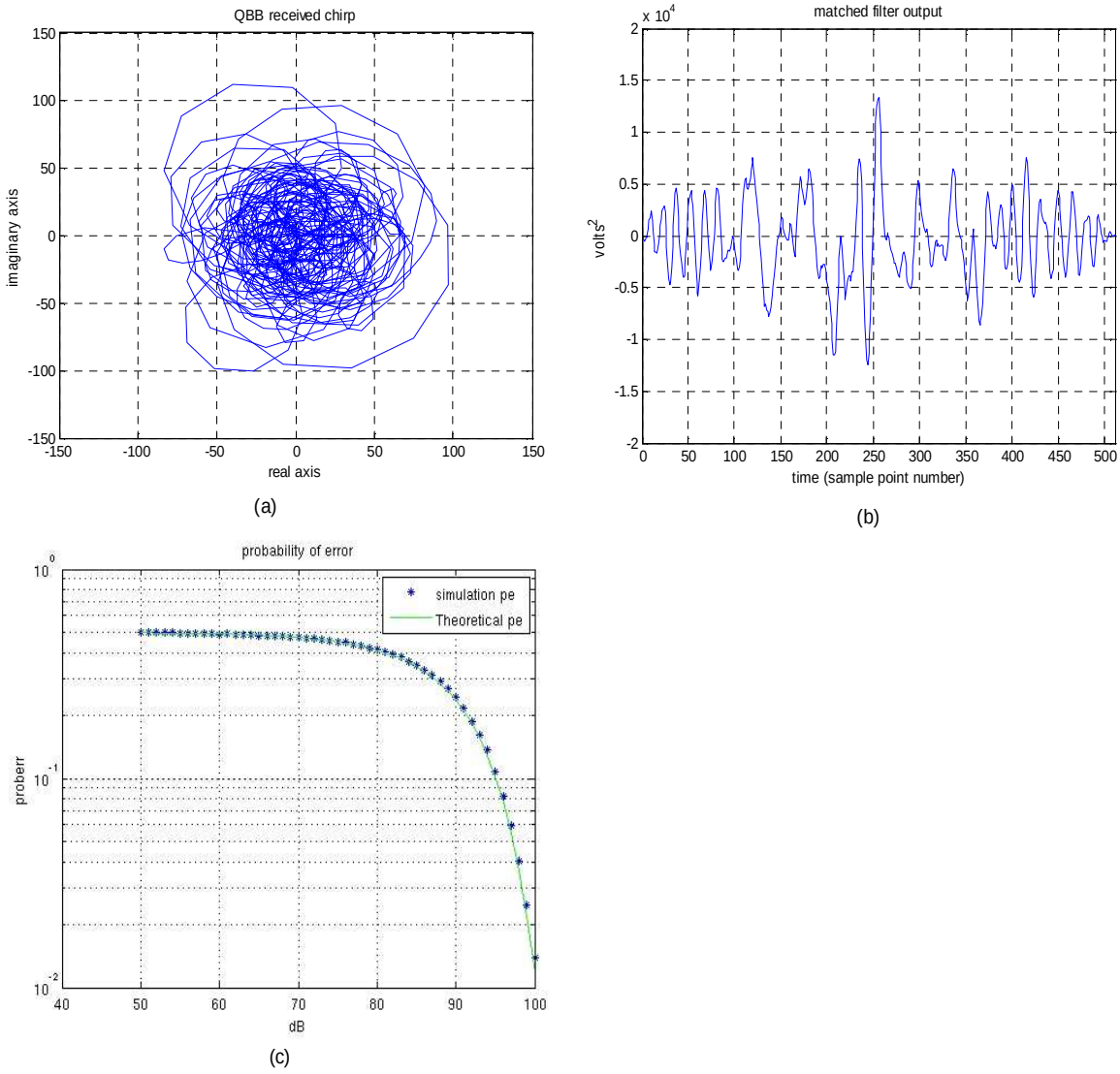

Figure 7.20: (a) *QBB received chirp:-it is seen here that the signal is complex having a real and imaginary part* **(b)** *Matched filter output:- the last value of the matched filter shows that its maximum value at the 256th sample point is above zero which amounts to a decision '1'. However, the intermediate values are present within the simulation.* **(c)** *Probability of error plot:-the plots show that the simulated probability of error does correspond with the theoretical probability of error entailing the correct operation of the simulation. An increase in the number of runs would make the match much more perfect.*

The two curves in Figure 7.20(c) on the previous page show the probability of error plots for the simulation and the theoretical probability calculated. It can be concluded that the Matched filter detection at QBB was successful and that further adjustments in the parameters used can result in better results. The sole purpose of this part of the study has thus been achieved which is to carryout matched filter detection at QBB accompanied with the excepted core benefit of working with at a lower sampling frequency. Having considered the fact that working at QBB is of great benefit in terms of sampling frequency and ultimately bandwidth requirements, the next section of the chapter will consider the case of matched filter detection for multiple reception at QBB whose results will be compared to the RF results through a comparison in terms of probability of error ratios, simulation processing time and sample processing will be made between the RF and QBB multiple signal reception simulations. Having thus far seen the benefits of operating at QBB interms of sample processing reduction, the study concludes by looking at the multiple signal reception case for matched filter detection at RF and QBB.

7.11 Matched filter detection:- Multiple input signal at RF and QBB

The analysis finally looked at the reception of multiple signals. In this case the received signal consists of the direct path chirp, a delayed version or multipath chirp and a Doppler shifted version of the chirp. Noise is then added and then the signal is received by the matched filter where detection takes place. In the QBB case, the signal gets mixed down to quadrature baseband where the matched filter detection takes place. The matched filter is matched to (a) direct path signal, (b) the direct path and multipath and (c) a combination of the three signals, and the output is observed and three probability of error plots are generated for each of the matched filters in both the RF and QBB cases and then compared to the calculated theoretical probability of error plot. Therefore, the generation of the input signals remains as given in an earlier part of the chapter. The figures on the next page summarize the theoretical analysis for the radio frequency and quadrature baseband simulations for the matched filter detection multiple signal reception case. The focus is now on QBB having seen its benefits interms of reduced sample processing.

In the figures that follow, x_d represents the direct-path signal, x_{mp} represents the multipath signal and x_{dp} represents the Doppler shifted signal.

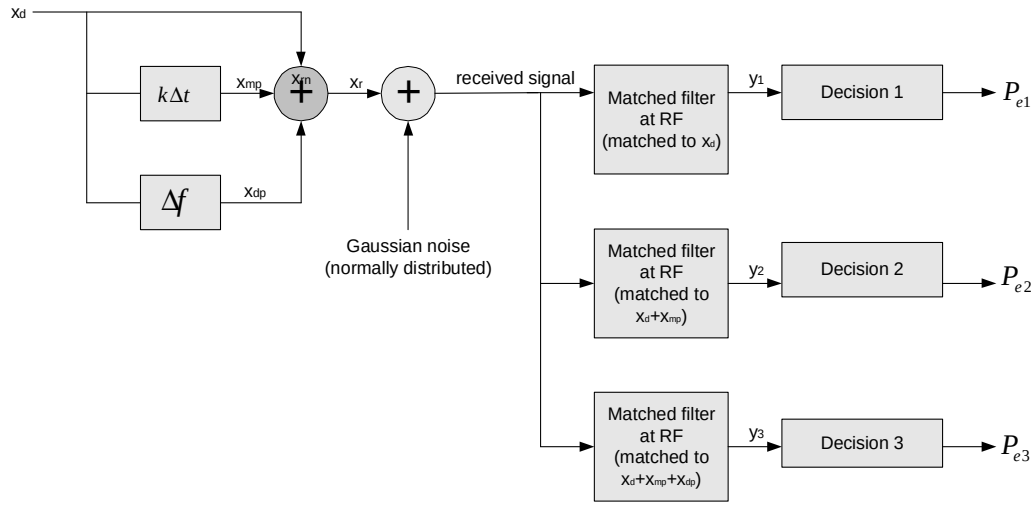

Figure 7.21: *Multiple signal input to matched filter detection at RF:- the 3 matched filters result in 3 different outputs with different strengths.*

The figure below summarises the theoretical analysis at QBB. The three match filters are at QBB and matched to the different components of the multiple input signal.

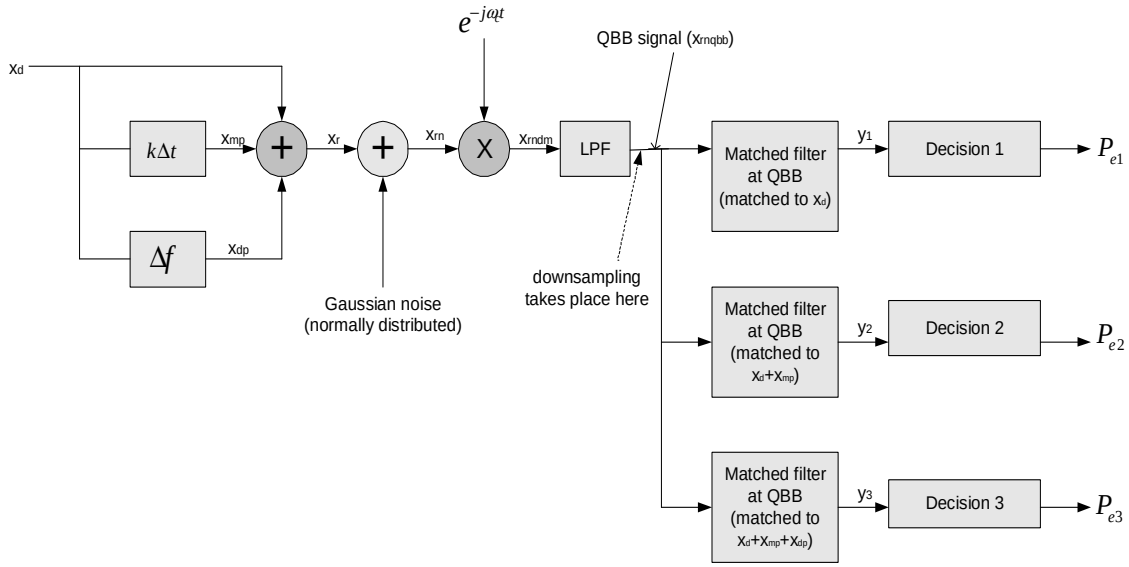

Figure 7.22: *Theoretical flow QBB:-the expected signals at each point are shown in this figure:- the decision is part of the simulation and details can be seen from the simulation code.*

The figure below shows the simulation flow for the matched filter detection analysis at QBB. The RF flow diagram is similar to the QBB one but with the down-mixing, LPF and downsampling stages omitted. The simulation loops are also shown. Each block represents a piece of the overall MatLab code.

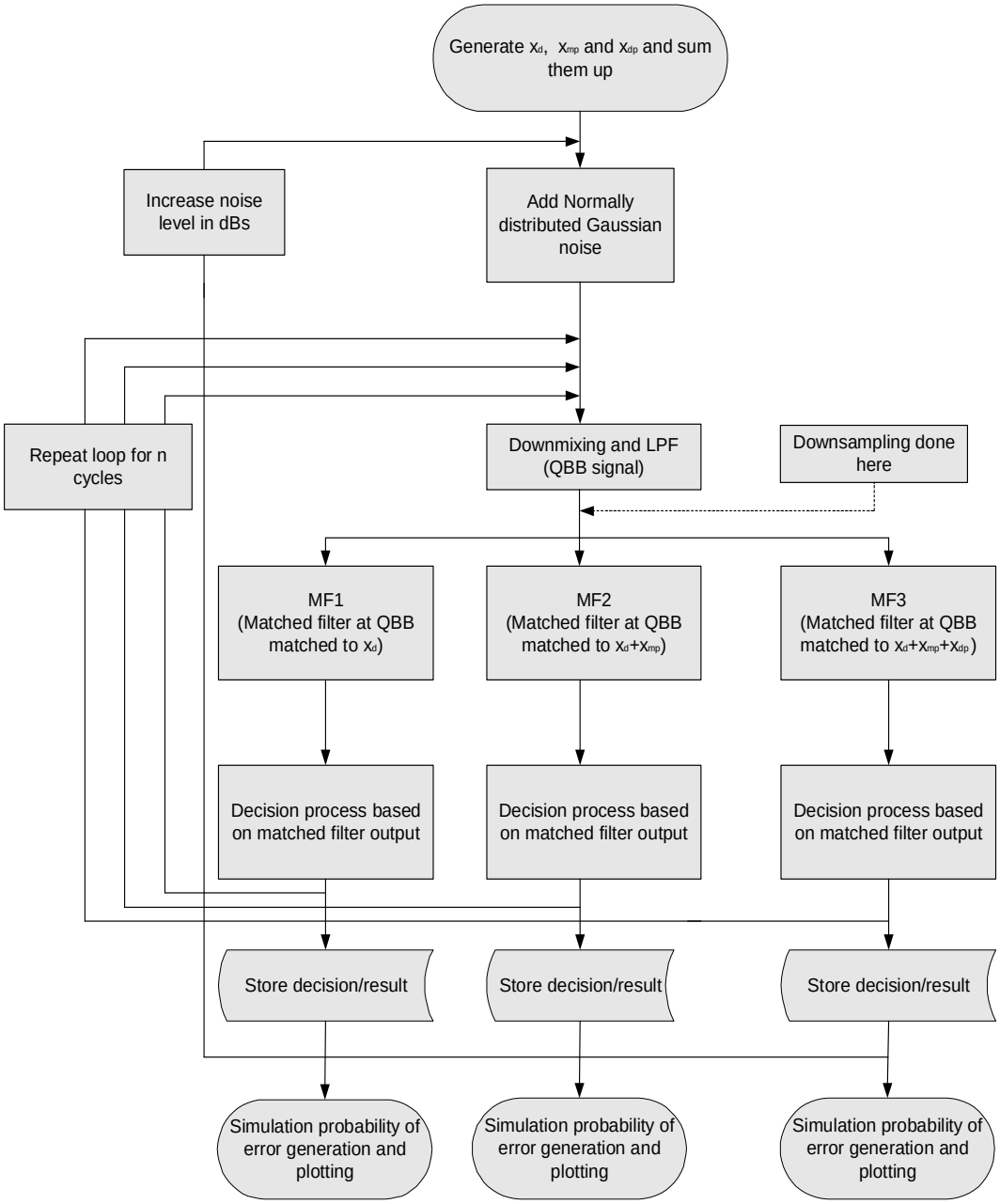

Figure 7.23: *Simulation flow*: *summarizes the flow of the simulation and each block represent a part of the main MatLab code used for the whole process. The first loop shows that the noise is increased in line with the dB range given so as to eventually come up with the probability of error over that dB range for a given number of runs.*

7.11.1 Simulation results:- Matched filter detection at RF

The simulation results are given in the figures below. It should be noted that MatLab only shows the last values of a simulation loop and therefore intermediate values do exist. The resulting probability of error plots are shown on the next page.

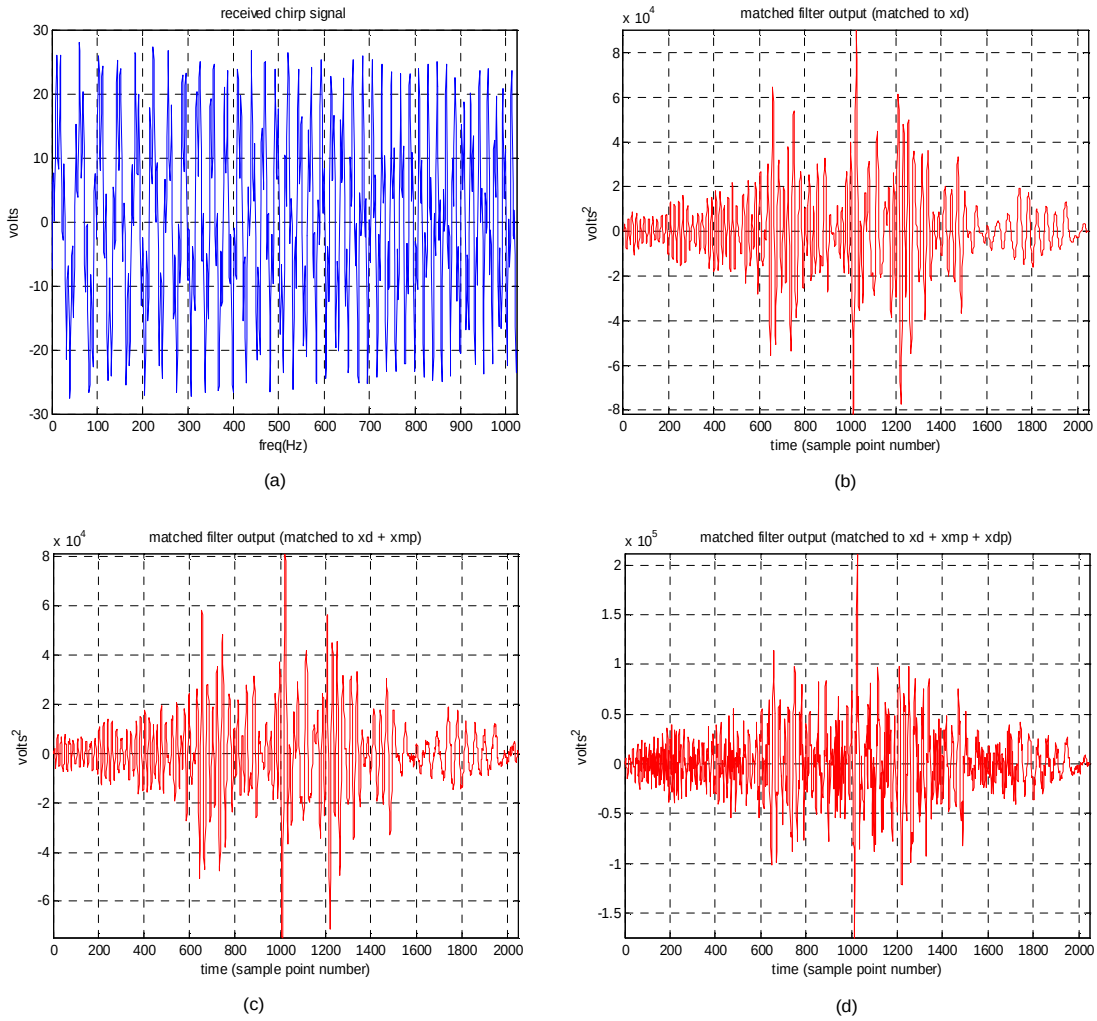

Figure 7.24: (a) *Received summed input signal:- the input to the chirp consists of the three signals which are summed up together.* **(b)** *Matched filter output when matched to* $x_{d.}$ **(c)** *Matched filter output when matched to* $x_d + x_{mp}$ **(d)** *Matched filter output when matched to* $x_d + x_{mp} + x_{dp}$ *:- the last value of the matched filter output which was matched to the direct path signal* x_d*. It is seen that the maximum value of the matched filter output is the largest for this output due to more signal strength brought about by the three input signals.*

The figure below shows the probability of error plots for the different matched filter outputs. It is seen from the plots that the results further verify the matched filter outputs as it can be seen that the probability of error gets smaller as the we move from the 1st matched filter output to the 2nd and 3rd matched filter outputs due to increased signal strength caused by the matched filter locking on to all the available energy in the received signal.

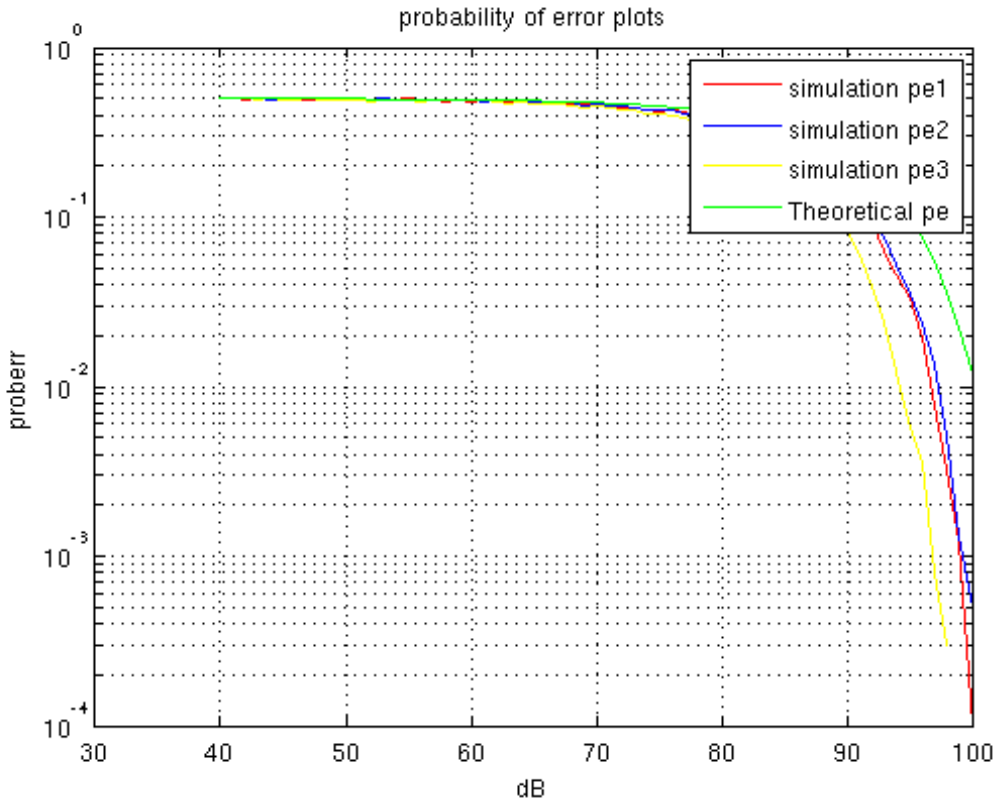

Figure 7.25: *Probability of error plots for multiple input signal matched filter detection at RF.*

7.11.2 Simulation results:- Matched filter detection at QBB

The figures on the next page show the matched filter outputs for the MIMO case at QBB. The parameters used for the RF simulation are the same ones used in the QBB simulation. For the QBB case, the downsampling comes into play and it thus contributes to the reduced sample processing and hence less simulation runtime. In this case, the downsampling factor used was equal to 4. Thus the decision point was made at the 256th sample point of the matched filter output.

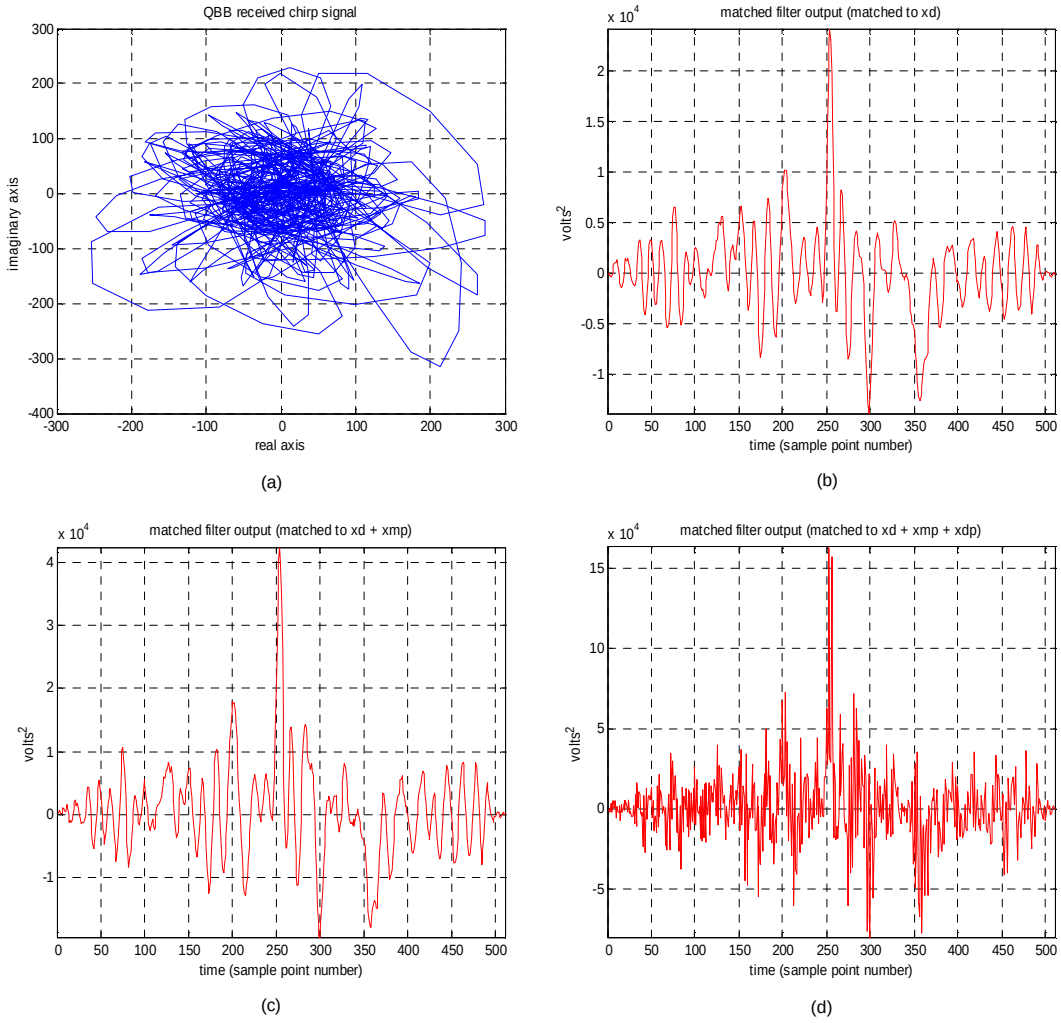

Figure 7.26: (a) *QBB received signal* **(b)** *Matched filter output when matched to* x_d **(c)** *Matched filter output when matched to* $x_d + x_{mp}$ **(d)** *Matched filter output when matched to* $x_d + x_{mp} + x_{dp}$. *The sample reduction in the matched filter outputs can be seen from the figures above.*

From the figures above, it is seen that there is an increase in the matched filter outputs from the one matched to x_d to the one matched to $x_d + x_{mp}$ and the largest output being that of the matched filter that was matched to a $x_d + x_{mp} + x_{dp}$. It should be emphasised again that MatLab plots only the last value of the loop. The figure on the next page shows the probability of error plots for the QBB multiple signal input simulation. The error plots should verify the statement made from the matched filter outputs shown in Figure 7.26 above.

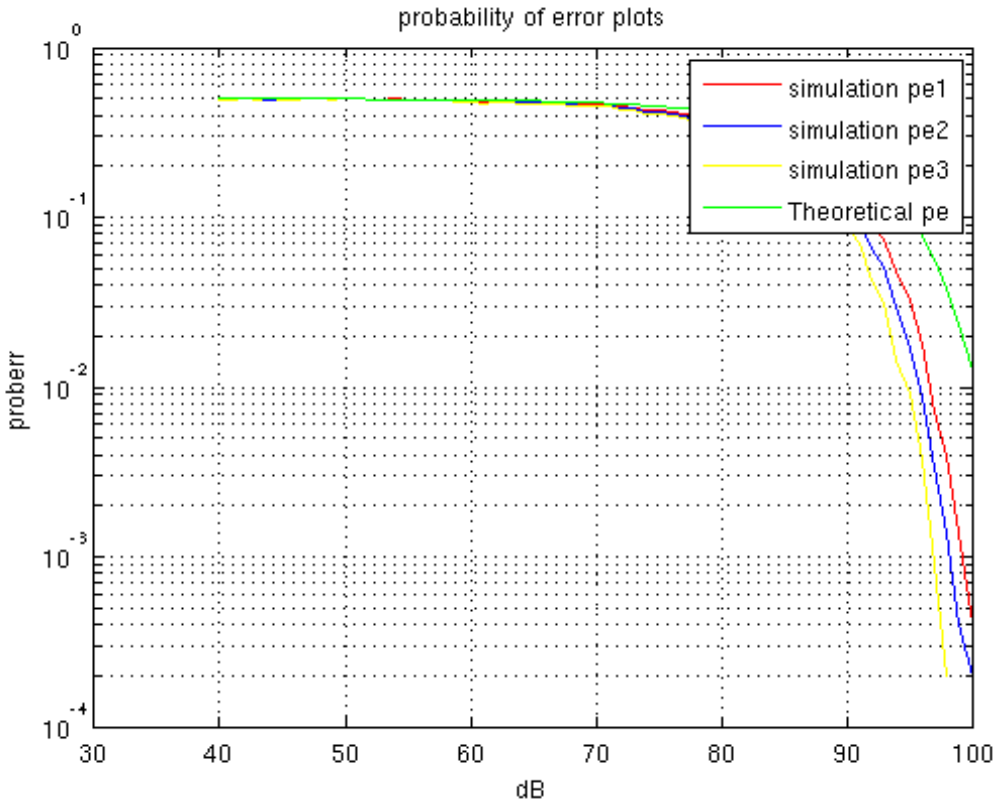

Figure 7.27: *Probability of error plot for multiple signal reception and detection at QBB:- the first plot represents the theoretical probability of error for the direct path case reception and detection whilst the three other plots are for the instances where the matched filter was matched firstly to the direct path and then to the direct path + multi path and finally to the direct path + multipath + doppler shift signal.*

The plots above show the probability of error for the three different matched filter detection conditions and compared with the ideal theoretical case at QBB. Considering Figure 7.27, it can be seen there is a reduction in the probability of error as one move from the direct path matched filter, to the direct path and multipath matched filter and eventually to the direct path, multipath and Doppler shift matched filter. Therefore, the probability of error plots have verified the conclusion made from the matched filter output results. It was thus showing that carrying out matched filter detection in a noisy channel is possible at QBB and with benefits in terms of the processing load expected. The next chapter gives the benefits of working at QBB compared to RF for the simulations carried out under matched filter detection.

7.12 Benefits of carrying out matched filter detection at QBB

By now, from the previous chapters it has been shown how the processing load and runtime for the simulations was measured. It was seen how the ratio of the amount of processing correlated with the runtime ratios with reasonably small discrepancies caused by the variance in the computer processing time. It was also seen that the benefits were more for the real life case where the processing starts from baseband itself. Therefore, for matched filtering case, the measurements for the runtimes and calculations for the QBB case considered the real life scenario. In determining the sample processing for the simulations, *only* the actual matched filtering stage was considered with the signal generation procedures ignored and not being part of the comparison process. The simulation runtime determination followed suit. The table below summarises the outcome of the comparisons.

	RF (t_{rf})	**QBB(t_{qbb})**	**t_{rf}/t_{qbb}**	**N_{rf}**	**N_{qbb}**	**N_{rf}/N_{qbb}**
MF detection:-noiseless channel	Time in seconds		Ratio	Number of calculations		Ratio
1. Direct path	0.01563	0.00372	4.20	2048	512	4.00
2. Multipath	0.01748	0.00461	3.79	2048	512	4.00
3. Doppler shift	0.01735	0.00444	3.91	2048	512	4.00
4. Multiple input	0.02925	0.00651	3.78	2048	512	4.00
MF detection :- noisy channel						
1. Direct path	0.01568	0.00410	3.82	2048	512	4.00
2. Multiple input	0.04546	0.01203	4.11	6144	1536	4.00

Table 7.1: *Simulation runtime and sample processing ratio comparisons. The highest discrepancy between the ratios was about* 5.8% *which is reasonable given the slight variance in the computer processing time. The amount of processing in terms of N for the multiple signal input case for the noisy transmissions is three times more than that for the direct path because of the 3 different matched filters used for the three differently matched signals. The ratio however remains unaffected.*

From the results obtained and shown in the table on the previous page, it does suffice to conclude that matched filter detection at QBB is faster and less bulky in terms of processor load than at RF. There were some limitations in defining some operations in terms of N and therefore relevant assumptions were made so as to best show the comparison between the processing at RF and that at QBB so as to correlate the resulting ratio with that obtained for the simulation runtime. Again it should be noted that the determination of the benefits interms of simulation runtime and sample processing interms of N was just for analysis purposes and so as to see that indeed, working at QBB is more advantageous.

7.13 Conclusion

The chapter looked at matched filter detection for various received signal scenarios and considered noiseless and noisy transmissions. The matched filter output was larger for multiple signal reception due to the matched filter locking on to the energies of the individual input signals. For the detection in a noisy channel, the probability of error plots showed a good correlation between the simulated and the theoretical probability of error. The results obtained showed that working at QBB was not only possible but also reduced the amount of sample processing due to the downsampling carried out. This in turn reduced the simulation runtime. The discrepancies between the calculated and simulated results were within reasonable limits and therefore, it does suffice to make a firm conclusion that the benefits of working at QBB were indeed more than at RF in terms of processing time and processing load.

Chapter 8

Conclusions

This chapter concludes the study and gives an overview of the sample processing and simulation runtime results for the whole study.

8.1 Conclusion

The objectives of the study were achieved and it was verified that beamforming, multipath compensation, Doppler shift compensation and the multiple compensation special case and matched filter detection of a chirp signal (a) could take place at quadrature baseband and (b) processing at quadrature baseband was more numerically efficient which translated to less simulation runtimes. The various algorithms were carried out at both RF and QBB and the results compared. It was seen under beamforming that the results at QBB matched their corresponding RF counterparts and so was the case for the multipath and Doppler shift cases. For the multiple input signal case, there were some limitations in the compensation process but it was shown that compensation was possible under certain conditions which were referred to as the special case. Compensating for multipath and Doppler shift at quadrature baseband did show that working at QBB facilitates sub-sampling which reduces the samples but does not alter the information and hence the compensation process still proved a success. The difference plots given after each of the compensation simulations did further consolidate the effectiveness of the compensation process and thus acting as proof of successful compensation. As already emphasised, working at quadrature baseband does come with the main advantage of lower sampling frequencies which in-turn leads to less complicated equipment and hence reducing operating costs. This study paves way for further research into other signal processing techniques and the possibility of carrying them out at QBB and hence this study is beneficial in that it would facilitate for the enabling of most current signal processing techniques to be carried out at quadrature baseband which comes with its *core advantage* of lower operating frequencies.

8.2 Summary of overall results

The overall results of the simulations carried out for whole study are summarised in the table below. It was seen that operating at QBB did result in an overall improvement in processing speed resulting from the reduction in samples by the downsampling process. This was however not the case for the beamforming as it was seen that the amount of processing required in the QBB case was more. The discrepancy range between the sample processing and the simulation time ratios was from 1.5% to 5.8% and as mentioned earlier, this was due to the variance in the computer processing runtime.

	RF (t_{rf})	QBB(t_{qbb})	t_{rf}/t_{qbb}	N_{rf}	N_{qbb}	N_{rf}/N_{qbb}
Beamforming	Time in seconds		Ratio	Number of Calculations		Ratio
AM DSB-SC	0.36318	0.74992	0.48	11776	25472	0.46
AM DSB-LC	0.35836	0.77418	0.46	11776	25472	0.46
Multipath Compensation						
QAM	0.02715	0.01025	2.65	98304	37632	2.61
Doppler Shift Compensation						
QAM	0.00119	0.00062	1.92	47104	24064	1.96
Multiple input:-Special case						
QAM	0.00122	0.00099	1.23	67584	56832	1.19
Matched Filter(MF) Detection						
Direct path	0.01563	0.00372	4.20	2048	512	4.00
Multipath	0.01748	0.00461	3.79	2048	512	4.00
Doppler shift	0.01735	0.00444	3.91	2048	512	4.00
Multiple input	0.02925	0.00651	3.78	2048	512	4.00
MF detection :-Noisy channel						
Direct path	0.01568	0.00410	3.82	2048	512	4.00
Multiple input	0.04546	0.01203	4.11	6144	1536	4.00

Table 8.1: *Summary of overall simulation results:- RF and QBB.*

Finally, from the results, it was seen that working at lower QBB frequencies coupled with its sub-sampling capabilities did indeed reduce the amount of processing required which in turn led to a reduction in the simulation runtimes.

- For the beamforming case, the benefits of working at QBB were not felt in terms number of calculations for the simulated QBB but when the real life case of processing at baseband was considered the benefits were seen as the ratio of the amount of processing at RF to that at QBB increased considerably by about 31 fold and thus entailing beamforming at QBB being much more efficient.
- For the multipath simulations, the amount of processing reduced by over 2-fold for the simulated case and further reduced by about 9-fold for the real life case showing the immense benefits of processing at QBB as compared to RF.
- For the Doppler shift case, the amount of processing reduced by less almost by 2-fold but upon taking up the processing from baseband itself for the real life case as seen in chapter 5 there was approximately a 31 fold reduction which showed that indeed, QBB does stand out in terms of processing benefits against RF.
- The multiple compensation special case resulted in less reduction in processing by operating at QBB but it still suffices to conclude that working at QBB was more efficient.
- The matched filter detection showed a 4-fold reduction in processing load for the real life QBB case which entails that carrying out the detection process at QBB would result in less processing and hence when applied to real life digital transmissions, it would entail much faster data rates, etc.

8.3 Future work

The continued advancement in software defined radio technology entails the never ending thirst for processing technologies that are compatible with the SDR equipment and that enable more efficient use of available telecommunication resources such as bandwidth. Therefore, this study focused on just a fragment of the many processing techniques that would be required to be done at quadrature baseband considering the benefits that come with it. Therefore, more research can be carried out into the possibility of carrying out other processing techniques at QBB.

Bibliography

[1] J. Kirkhorn. ” *Introduction to IQ demodulation of RF-data,*” pp .4-10, EchoMAT User Manual (FA292640), 15 September 1999.

[2] G-J van Rooyen and J.G**.** Lourens. *”A Quadrature Baseband Approach to Direct Digital FM synthesis*” pp. 228-229, IEEE Transactions on Broadcasting, Vol.46, NO 3 , September 2000.

[3] B.P. Lathi. ”*Communication Systems,*” Wiley and Sons, Inc, 1968.

[4] J.G. Proakis and M. Salehi. ”*Communication Systems Engineering,*” Prentice-Hall International, Inc, 1994.

[5] “*Signal Processing Toolbox User’s Guide-Version 4*” pp 6-122 – 6-126, The Mathworks, Inc, 1998.

[6] G-J van Rooyen. “*Baseband Compensation Principles for Defects in Quadrature Signal Conversion and Processing,*” PhD Thesis, University of Stellenbosch, 2004.

[7] E.P. Cunningham. “*Digital Filtering-An Introduction*, “ John Wiley & Sons, inc, 1995.

[8] “*Communications Toolbox User’s Guide -Version* 1.3,” pp 3-65 – 3-67, The Mathworks, Inc, 1996.

[9] V.K. Madisetti and D.B. Williams, “ *The Digital Signal Processing Handbook,*” 69-1 -69-18, CRC press LCC, 1998.

[10] S. Haykin. “*Adaptive Filter Theory*”,2nd ed, Prentice-Hall, Englewood Cliffs, NJ, 1991.

[11] W.L. Stutzman and G.A. Thiele, “*Antenna Theory and Design,*” John Wiley and Sons, Inc, 1998.

BIBLIOGRAPHY

[12] R. Kwok. " *AM modulation/demodulation*,"
http://foe.mmu.edu.my/course/etm3046/notes/AM(-DSSC)ETM2042.doc

[13] H. Taub and D. L. Schilling. "*Principles of Communication Systems*," pp 87 -131, McGraw-Hill, inc, 1971.

[14] K.S. Shanmugam. "*Digital and Analog Communication systems*," John Wiley and Sons,inc,1979.

[15] http://en.wikipedia.org/wiki/baseband

[16] P.B. Kenington. "*RF and Baseband Techniques for Software Defined Radio*," Artech house, Inc, 2005.

[17] W Tuttlebee. "*Software defined radio*," John Wiley and Sons, Ltd 2002.

[18] C, Langton. "*LTI and Matched Filter*," tutorial 21, 2003. www.complextoreal.com
,
[19] C.A Balanis. "*Antenna theory*," 2nd edition, John Wiley & Sons Inc, 1982, 1997.

[20] 'The digital signal processing handbook',pp 68.2 -68.3,CRC press, LLC, 1992.

[21] www.cisco.com/us/tech/tk722/multipath Document ID:27147

[22] L.R. Rabiner & B. Gold, "*Theory and applications of DSP*," prentice hall, Inc, Bell Telephone laboratories and MIT Lincoln Libraries.1975

[23] J. H. Reed. "*Software Radio-A modern approach to Radio Engineering*" Prentice Hall PTR, 2002.

[24] T . Niesler. "*Digital Signal Processing notes*," SS 414 , slide 1.73 Stellenbosch University, 2001-2008.

[25] http://en.wikipedia.org/wiki/Doppler_effect

BIBLIOGRAPHY

[26] H.L va Trees. "*Detection,estimation and Modulation Theory,*" part 3,Wiley, 2001

[27] S. W. Smith. "*The scientist and Engineer's Guide to Digital Signal Processing*", www.dspguide.com/ch17/2.htm

[28] B, Gorid, R. Rabenstein and A.Stenger. "*Signals and Systems,*" John Wiley & Sons Ltd, 2001.

[29].http://www.cambridge-en.com , Newsletter 5 -March 1999.html

[30] http://en.wikipedia.org/wiki/Chirp

[31] Mahafza, Bassem R. "*Radar Systems Analysis and Design Using Matlab*" ,Chapman &Hall/CRC, 2000.

[32] http://en.wikipedia.org/wiki/downsampling , 11/05/07.

[33] http://en.wikipedia.org/wiki/Envelope_detector , 9/04/07.

[34] http://en.wikipedia.org/wiki/Multiple-input_multiple-output , 6/3/07.

[35] H-S Lim, "*Benefits of FPGAs in Wireless Base Station Baseband Processing Applications*", pp 1-10, XAPP726(v1.0) July,2005. www.xilinx.com

[36] http://www.agilent.com/find/mimo/ ,pp-6-11,application note 1509.

[37] B. Sklar. "*Digital Communications Fundamentals and Applications,*" Prentice Hall, 1988.

[38] S. Haykin, "*An Introduction to Analog and Digital Communications*", John Wiley& Sons, Inc. 1989.

M-FILES

The following M-Files were created.

1. time.m:- This file outlines the MatLab code for carrying out beamforming at RF frequencies.

2. timeqbb.m:- This file outlines the Matlab code for carrying out beamforming in QBB.

3. timebeamcomp.m:- This file compares the RF and QBB beam patterns and gives a numerical average value of the difference between the two normalized beam patterns.

4. **time2.m**:- carries out RF beamforming using the non-coherent method (envelope detection).

5. time2b.m:- Carries out RF beamforming using the coherent detection method.

6. timeqbb2.m:- Carries out QBB beamforming using a coherent method.

7. timebeamcomp2.m :-Carries out a numerical comparison of the three beam patterns.

8. time3.m :- carries out FM RF beamforming .

9. timeqbb3m :- Carries out QBB beamforming .

10. timebeamcomp3.m :-Carries out a numerical comparison of the two beam patterns.

11. mpqamrf.m :- Carries out the multipath compensation analysis at RF for a QAM signal

12. mpqamqbb.m:-Carries out the multipath compensation analysis at QBB for a QAM signal

13. mpfmrf.m :- Carries out the multipath compensation analysis at RF for a FM signal

14. mpfmqbb :- Carries out the multipath compensation analysis at QBB for a FM signal

15. dpqamrf:- simulated the QAM doppler shift compensation at RF.

16. dpqamqbb:-simulated the QAM doppler shift compensation at QBB.

17. dpfmrf:- simulated the FM doppler shift compensation at RF.

18. dpfmqbb:- simulated the FM doppler shift compensation at QBB.

19. mpdpqamrf.m:-Simulates the RF compensation process for the non-special case.

20. mpdpqamrf2.m:-Simulates the RF compensation process for the special case.

21. mpdpqamqbb.m:-Simulates the QBB compensation for the special case

22. chrf.m :- simulates the MF detection for the direct path signal at RF.

23. chqbb.m :- simulates the MF detection for the direct path signal at QBB.

24. chmprf.m :- simulates the MF detection for the multi-path signal at RF.

25. chmpqbb.m :- simulates the MF detection for the multi-path signal at QBB.

26. chdprf.m :- simulates the MF detection for the doppler-shift signal at RF.

27. chdpqbb.m :- simulates the MF detection for the doppler-shift signal at QBB.

28. chmpdprf.m :- simulates the MF detection for the multiple signal reception at RF.

29. chmpdpqbb.m :- simulates the MF detection for the multiple signal reception at QBB.

30. noiserf.m :- simulates the MF detection for the direct path signal at RF for a noisy channel.

31. noiseqbb.m :- simulates the MF detection for the direct path signal at QBB for a noisy channel.

32. mimonoiserf.m:- simulates the MF detection for the MIMO RF case for a noisy channel.

33. mimonoiseqbb.m:- simulates the MF detection for the MIMO QBB case for a noisy channel.

The M-files listed above were also re-run for the simulation time calculations too and the processor load calculations for the simulations are included on the CD in Appendix C.

Appendix A

Theoretical derivation of probability of error

The derivation for the theoretical probability of error is given below. From the mathematical analysis, the expected value of y(T) is 5.12e4 as shown in Chapter 7. We now look at the noise power. In the simulation, the noise was multiplied by a variable nch. Therefore we have:

$$No = \sigma_o{}^2 nch = E\left\{x^2\right\} \tag{A1}$$

The probability density function for a Gaussian distribution is given as

$$f(x) = \frac{1}{\sqrt{2\pi\sigma_o{}^2}} e^{\frac{-(x-m)^2}{2\sigma_o{}^2}} \tag{A2}$$

The expected value 'm' is the average of the value that a random variable takes in a large number of experiments. The noise for the simulation is generated randomly using 'randn' and has a standard deviation of 1 because of the normal distribution [14, 18]. The noise power out numerical value is found using the following equations.

$$p_{noise_{out}} = \int_{-\infty}^{0} N_o nch \,|\, H(f) \,|^2 \, df \tag{A3}$$

which in the discrete domain is given as

$$p_{noise_{out}} = \sum_{n=1}^{N=1024} N_o nch \,|\, H(n) \,|^2 \tag{A4}$$

Inserting the limits of the integration leads us to the following expression in the discrete domain:

$$p_{noise_{out}} = N_o \sum_{n=1}^{N=1024} nch \,|\, H(n) \,|^2 = N_o nch(5.12e4) \tag{A5}$$

The numerical value is substituted for $|H(n)|^2$ because the absolute value of y(n) and $H(n)$ are the same. Referring back to equation A2, we can derive the expression for the theoretical probability of error as follows:

$$Pe = \int_{-\infty}^{0} \frac{1}{\sqrt{2\pi\sigma^2}} e^{\frac{-(x-m)^2}{2\sigma^2}} dx \tag{A6}$$

$$\text{Let } -\left(\frac{x-m}{\sqrt{2}\sigma}\right) = t \text{ then } -dx = \sigma\sqrt{2}dt \tag{A7}$$

The limits are equally changed due to the substitution gas shown below.

$$\begin{aligned} x \to 0, t \to \frac{m}{\sqrt{2}\sigma} \\ x \to -\infty, t \to +\infty \end{aligned} \tag{A8}$$

Equation B6 then reduces to:

$$Pe = -\int_{+\infty}^{\frac{m}{\sqrt{2}\sigma}} \frac{1}{\sqrt{\pi}} e^{-t^2} dt = \frac{1}{\sqrt{\pi}} \int_{\frac{m}{\sqrt{2}\sigma}}^{+\infty} e^{-t^2} dt \tag{A9}$$

Now MatLab does have an inbuilt command ‘erfc’ which executes the integral part of equation B9 with the limits being positive.

$$erfc(x) = \frac{2}{\sqrt{\pi}} \int_{x}^{+\infty} e^{-t^2} dt \tag{A10}$$

The outcome of the execution of this error function should give the same value as the outcome of the same equation if it had its limits changed to negative values.
Therefore, the equation [37] can be re-written as:

$$Pe = \frac{1}{\sqrt{\pi}} \int_{\frac{m}{\sqrt{2}\sigma}}^{+\infty} e^{-t^2} dt \tag{A11}$$

Written in terms of the MatLab error function, let a=$\frac{m}{\sqrt{2}\sigma}$ we have:

$$Pe=\frac{1}{2}erfc(a) \tag{A12}$$

The values of m and σ are given below:

$$\begin{aligned} &m = 5.12e4 \\ &thus \\ &\sigma = nch^{*}|h(n)|^{2} = nch(5.12e4) \end{aligned} \tag{A13}$$

The theoretical *Pe* plot against the noise level in dBs was given earlier in Chapter 7 and compared with the simulation plots. The actual values of the probability of error theoretical and simulation plots obtained for at RF and QBB for the matched filter detection in a noisy channel for the direct path case and multiple signal input case are given in the Appendix C.

Appendix B

Model of a slowly fluctuating target

A slowly fluctuating target model for a radar/slowly fluctuating system is developed as follows;

Assume the sonar/radar system transmits a cosine wave continuously [26]. Thus;

$$s_t(t) = \sqrt{2P_t}\cos(\omega_c t) = \sqrt{2}\,\mathrm{Re}[\sqrt{P_t}e^{j\omega_c t}], -\infty < t > \infty. \quad \text{(B1)}$$

Now we assume a zero velocity target located at some range 'R' from the transmitter, va Trees[26] assumes that the target has a physical structure that includes several reflecting surfaces. Thus the returned signal may be written as;

$$s_r(t) = \sqrt{2}\,\mathrm{Re}\{\sqrt{P_t}\sum_{i=1}^{K} g_i \exp[\, j\omega_c(t-\tau)+\theta_i\,]\} \quad \text{(B2)}$$

The attenuation g_i includes the effects of the transmitting antenna gain. Assuming that the reflection process is frequency-independent; thus if we transmit;

$$s_t(t) = \sqrt{2}\,\mathrm{Re}[\sqrt{P_t}\exp(j\omega_c t + j\omega t)], \quad \text{(B3)}$$

We receive:

$$s_r(t) = \sqrt{2}\,\mathrm{Re}[\sqrt{P_t}b\exp[(\,j(\omega_c+\omega)(t-\tau)]], \quad \text{(B4)}$$

Assume a linear reflection process and considering a target with constant radial velocity v and transmitted energy $E_{t..}$ Further mathematical analysis leads us to the following final expression below.

$$s_r(t) = \sqrt{2}\,\mathrm{Re}[\sqrt{Et}\tilde{b}\tilde{f}(t-\tau+\frac{2v}{c}t)\exp[\, j\omega_c(t+\frac{2v}{c}t)]]. \quad \text{(B5)}$$

It is seen here that the target velocity has two effects which are;

1. A compression or stretching of the time scale of the complex envelope.
2. A shift of the carrier frequency.

In most cases we can ignore this first effect. To demonstrate this, consider the error in plotting $\tilde{f}(t)$ instead of $\tilde{f}(t-(2v/c)t)$. The maximum difference in the arguments occurs at the end of the pulse (say *T*) and equals $2vT/c$. The resulting error in amplitude is a function of the signal bandwidth. If the signal bandwidth is *W*, the signal does not change appreciably in a time equal to W^{-1} [26]. Therefore,

$$\frac{2vt}{c} \ll \frac{1}{W} \tag{B6}$$

Or equivalently,

$$WT \ll \frac{c}{2v}, \tag{B7}$$

Ignoring the time-scale change, the shift in the carrier frequency is called the *Doppler shift*.

$$\omega_D \triangleq \omega_c(\frac{2v}{c}) \tag{B8}$$

It should be noted that there some sonar problems in which Equation C8 is not satisfied. In reality, we know that the speed of propagation of electromagnetic waves is very high (3×10^8) and therefore, the ratio given above will always be true in that the left hand side will always be much greater than the RHS[26]. However, that is not the case for acoustics propagation and therefore, the 1st part of our equation will have to be considered.

Appendix C

Included CD

The CD included with this thesis contains the following

- The MatLab simulations and source code used to get the results in the thesis.
- The source code used in the simulation runtime and sample processing calculations.